Understanding and Describing Muscle Complexity

A Non Invasive Complex Representation of Muscle: A Description through BOLD Fractal Dimension, Phase Space, and Concurrent EMG Metrics

By Joshua E. McGillivray, BEng. Electrical and Biomedical Engineering

A Thesis Submitted to the School of Graduate Studies in the Partial Fulfillment of the Requirements for the Degree Master's of Applied Science in Biomedical Engineering

McMaster University
Master's of Applied Science in Biomedical Engineering (2022)
Hamilton, Ontario (School of Biomedical Engineering)

TITLE: A Non Invasive Complex Representation of Muscle: A Description through BOLD Fractal Dimension, Phase Space, and Concurrent EMG Metrics
AUTHOR: Joshua E. McGillivray (McMaster University)
SUPERVISOR: Dr. Michael D. Noseworthy
EXAMINERS: Dr. Hubert de Bruin and Dr. Dinesh Kumbhare
NUMBER OF PAGES: xiii, 127

Lay Abstract

The human body is complex, and an incredible amount of research has been done to better understand it. Specifically, muscle is built and works in a complex way to allow us to move and perform everyday tasks. There are many diseases that affect how a muscle works, which is why there is a need to describe muscle performance when it is healthy and unhealthy. In this research, muscle behaviour is explored by taking pictures of the leg. From these pictures the blood flow in the calf and shin was measured both when staying still and when performing exercise. Four new techniques were created to describe the blood flow in the leg. The first technique measured how complex the muscle activity is, while staying still. If blood-flow changes a lot in a short amount of time, it is complex. This showed that the different components of muscle, either used for stamina or power, receive blood differently. The second technique used a different way of looking at the muscle to show that there are many different rates and amounts of blood-flow in the muscle. It revealed that muscle has more than the two blood flow options of 1) the normal level when resting and 2) the increased level when exercising. The third technique involved using an image filter to get a clean image of the muscle without the blood vessels affecting or misrepresenting the image. It was able to show what muscle regions were involved in exercise more accurately than before. The final technique involved measuring muscle electricity and blood flow at the same time, to find out when the muscle was exhausted. It demonstrated that muscle, when exhausted, showed larger changes in blood flow when going from resting to exercising. Overall, this research described how muscle performs in healthy individuals using new techniques. These techniques can now be used to compare healthy muscle to damaged/diseased muscle to determine how the muscle is recovering or to diagnose muscular disease.

Abstract

The human body is inherently complex as seen through the structural organization of muscle in terms of its contractile subunit organization and scaling, innervation patterns, and vascular organization. However, the functional complexity of muscle such as its state of oxygenation, metabolism or blood-flow has been less well explored. Thus in an effort to improve our understanding of muscle, blood oxygenation level dependent (BOLD) magnetic resonance imaging of the lower leg, at rest and during a variety of weighted plantar-flexion paradigms, at 40% maximal voluntary contraction, was employed. Prior to experimentation, on 11 healthy subjects, an ergometer and electromyogram (EMG), suitable for use within the MRI, were constructed to allow for concurrent exercise and image acquisition. After collecting muscle BOLD data, four novel techniques were using to describe muscle function. The first technique used the fractal dimension, a measure of complexity, conveying the rate of variation of muscle blood flow at rest. This technique was able to determine differences between the muscles of lower leg, which have varying distributions of muscle fibre types based on function. The second exploratory technique was the use of the phase space, which provides insight into state/state-transitions of a system over time. The phase space representation of the BOLD signal provided novel insight into the muscle activation state. It demonstrated that muscle has more than the two blood flow states of reduced levels at rest and increased levels when exercising. The third technique involved using a signal saturation (SAT) region, proximal to the imaging region, to mitigate the arterial in-flow effects to more accurately represent muscle activation. By observing the correlation between the ideal reference and recorded signal, the acquisition with the arterial suppression improved the assessment of what regions in the muscle were active in the range borderline activation, which has the highest uncertainty. The final outlook on muscle behaviour involved using measures of fatigue from the collected EMG data to develop novel metrics of fatigue based on the BOLD signal. Concurrent BOLD and EMG of the anterior compartment of the lower leg during a plantar-flexion block design, demonstrated that the change in blood-flow between rest and contracted states is an excellent indicator of muscle fatigue. The primary outlook of this thesis is to provide a unique data collection and analytic framework to describe muscle behaviour, which was achieved using non-invasive measures with a complex outlook.

Acknowledgements

Although a Master's Thesis is labeled as an independently driven research project it is anything but that, and I have numerous people to thank. The first person to thank if my supervisor Dr. Noseworthy, none of the work that I have done to date would have been possible without your expertise and guidance. As one of North America's premier MRI researchers I was lucky enough to have you at my disposal throughout the duration of my research project. I would also like to thank Dr. de Bruin and Dr. Kumbhare for their assistance throughout my project. Dr. de Bruin, your wealth of knowledge and willingness to always assist allowed me to overcome many obstacles. Dr. Kumbhare your unique perspective and expertise ensured that my research was not only valid, but also had a clinical outlook, which is arguably the most important piece, as we research to improve society.

Next, I would also like to thank the staff at St. Joseph's Hospital, without their tireless work throughout the pandemic I would not have been able to do any research. To the team of MRI technologists at the Imaging Research Center (IRC) Julie, Carol, Shannon and Suzanne, thank you for the countless hours you put into training and supervising my scanning. The good company made the hours go by faster. And thank you Norm for always being open to answering my many questions and for keeping the IRC running in the midst of difficult times for healthcare.

Additionally, I want to thank all of the students in Dr. Noseworthy's lab for their support throughout my research, whether it was volunteering for experiments or providing me with advice. More specifically, thank you TJ for always being test subject number one and for imparting your circuit knowledge. Thank you Cam for always keeping morale high at the IRC and for being a sounding board. And most of all thank you Alex, I honestly would not have been able to put this thesis together without you. Whether it was volunteering, running the scanner, sitting through my crazy explanations you were always there. I am lucky you decided to come to Canada and will be forever grateful.

Lastly, I would like to thank my support system. A Master's degree throughout the COVID pandemic presents another layer of challenge to stay on track and be constantly motivated to do work. Thank you to my friends Martin, Danny, Aqeel, Evan, and Chen for supporting me through the tougher parts of this journey. To Claire for helping me through the most stressful and challenging points of my thesis. Thank you to my parents Lisa and Marc, and brother Aidan who believed in my ability to complete this thesis more than I did at most times.

I attribute this thesis to everyone I have mentioned, I could not have made it to this point without them. To those I have not directly named you still played a vital role in this process and I will be forever thankful.

Contents

Note: Click on title to go to the page of the desired section

List of Figures

Note: Click on title to go to the page of the desired figure

List of Tables

Note: Click on title to go to the page of the desired table

Acronyms and Abbreviations

Abbreviation	
1H-MRS	*Hydrogen Spectroscopy*
ALS	*Amyotrophic Lateral Sclerosis*
ANC	*Adaptive Noise Cancelling*
AUC	*Area Under the Curve*
BOLD	*Blood Oxygen Level Dependent*
EPI	*Echo-planar Imaging*
EMG	*Electromyography*
FD	*Fractal Dimension*
fMRI	*Functional Magnetic Resonance Imaging*
FT	*Fast-twitch*
GE	*Gradient Echo*
HRF	*Hemodynamic Response Function*
IEMG	*Integrated Root Mean Squared EMG*
mBOLD	*Muscle BOLD*
MRI	*Magnetic Resonance Imaging*
mfMRI	*muscle functional MRI*
MS	*Multiple Sclerosis*
MVC	*Maximal Voluntary Contraction*
PCr	*Phosocreatine*
POAD	*Peripheral Arterial Occlusive Disease*
QA	*Quality Assurance*
RF	*Radio-Frequency*
RMS	*Root Mean Squared*
ROI	*Region of Interest*
RPM	*Revolutions Per Minute*
SAR	*Specific Absorption Rate*
SE	*Spin Echo*
SNR	*Signal to Noise Ratio*
ST	*Slow-twitch*
TE	*Echo Time*
TR	*Repetition Time*
TTP	*Time to Peak*
VOI	*Voxel of Interest*

Declaration of Authorship

I, Joshua E. McGillivray, declare that this thesis titled, "A Non Invasive Complex Representation of Muscle: A Description through BOLD Fractal Dimension, Phase Space, and Concurrent EMG Metrics" and the work presented in it are my own. I confirm that:

Chapter 1

- All content in this section was written by Joshua E. McGillivray.
- Sections 1.2 and 1.2.1 have direct excerpts from my published work:
  McGillivray et al. (2021) Crit. Rev. Biomed. Eng. 43:236-260

Chapter 2 - 4

- All content in this section was written by and figures created by Joshua E. McGillivray.

Chapter 5

- This chapter was written for publication intent by first author, Joshua E. McGillivray.
- Alejandro Amador is responsible for the spectroscopy data collection/analysis portion of this pilot study.

Chapter 6 - 12

- All content in this section was written by and figures created by Joshua E. McGillivray.

Appendix

- All analysis scripts were written by Joshua E. McGillivray, apart from the eventTable.m function which was written by Alex Amador and modified for use by Joshua E. McGillivray.

Chapter 1

Introduction

1.1 Declaration

Please note italicized text has been taken word for word from my published work:
McGillivray et al. (2021) Crit. Rev. Biomed. Eng. 43:236-260

1.2 Thesis Structure

The specific coverage and positioning of each section can be found in the table of contents above. But for the reader who chooses to read the thesis in its entirety, the general overview of the flow is as follows. The introduction section will serve to set the stage for the importance of the research contained within the thesis and to provide relevance to the more technical details that follow. The background section will provide an overview of the fundamental anatomy, magnetic resonance imaging (MRI) knowledge and the basics of the methods to describe systems in a complex manner. This is followed by a comprehensive literature review of the current research landscape of skeletal muscle imaging in MRI, with a specific focus on blood oxygenation level dependent (BOLD) MRI imaging in skeletal muscle, in isolation and in combination with electromyography (EMG). The research objective, hypothesis and aims will then be described. The next point of coverage is on the pilot study, which informed the final data acquisition for this thesis. This will be followed by the developmental phase section, where the development of the ergometer and EMG are covered. The data acquisition and general preprocessing that is common to all analysis techniques is then outlined. From there the four major analytical investigations into the functional behaviour are covered which each having their own brief methods, results, and discussion. To conclude the thesis, an overarching discussion which ties in all the analytical techniques, some limitations and areas of future work are outlined.

1.3 The Societal Need for Exercise

The importance of physical exercise is impressed upon us from a very young age, as it has been shown to improve physical and mental health, as well as cognition. Despite the apparent benefits of physical exercise, it is still not uniformly practiced across society.

Although exercise benefits all populations, its effects on populations with disease and or disorder can sometimes be more profound. One such population is individuals with Alzheimer's, which effects 13% and 43% of those above the age of 65 and 85 respectively. [1] The 10 million people across the globe who suffer from Parkinson's disease also benefit from exercise. [2]

Parkinson's disease like Alzheimer's is a devastating disease, which burdens the US healthcare system with yearly costs of $52 billion and $536 billion, respectively.[2], [3]

Notably, levodopa, a dopamine precursor, is used to treat the Parkinson's disease dopamine associated deficiency, yet exercise can be used to naturally increase dopamine levels within the brain.[4] The increase in dopamine affects the motor initiation pathway and has been linked to symptom mitigation.[4] Likewise, exercise can benefit the 15 million individuals globally affected by stroke, 5 million of which experience permanent disability, such as hemiparesis. [5] Physical exercise has shown to mitigate hemiparesis, thus improving motor function and consequently quality of life. [6] Remarkably, 85% of strokes worldwide are caused by high blood pressure, which is more prevalent due to the global obesity crisis. [5] Thus, physical exercise is imperative to save the lives of the 1.9 billion overweight individuals, who are at risk of stroke, as it reduces hypertension and body fat. [7], [8] Furthermore, it is essential to relieve this corresponding healthcare burden, which conservatively costs the American healthcare system 150 billion dollars annually.[9]

Similarly, the treatment of mental health disorders is a major contributor to the healthcare burden, with an estimated cost of $201 billion in the USA in 2013.[10] Physical exercise reduces rate and symptom severity of depression and anxiety, which effect 264 and 284 million worldwide respectively, lessening this burden.[11] Additionally, exercise serves to benefit the portion of the population with ADHD which is 2.2% of adolescents (<18 years) and 2.8% of adults (18-44 years) worldwide.[12] Exercise induced increases of dopamine and brain-derived neurotrophic factor counter the typical deficiency seen in the ADHD population, improving impulse control, working memory and executive function. [13] Similarly, exercise is known to improve cognition and promote structural and functional brain changes, thus acting as a protective factor against neurodegeneration. [14] Finally, research has shown that physical exercise reduces the risk of developing cardiovascular disease, type II diabetes, some cancers in the bladder, breast, kidney and lung, and of falling in the elderly.[15]

Physical exercise serves to benefit the general population, to mitigate disease, reduce symptom severity and improve cognition, amongst numerous other things. [4], [5], [11], [13] Although the cognitive and physical benefits of exercise have been explored, muscle activity during exercise and rest and its relation to muscular health and performance remains not well characterized. To fill this gap MRI researchers are seeking unique methods to examine muscular health and function. Muscle is structurally and functionally complex and could benefit from a complex representation. An improved representation and understanding of the complex nature of muscle, in conjunction with how exercise modulates health and disease symptoms, will allow society to attain the maximal benefits from physical exercise.

1.3.1 Exercise Forms and Benefits

Simply stated, physical exercise is any form of movement that actively works the muscles and requires more energy consumption than if one were resting.[16] The four generally agreed upon types of exercise are aerobic/endurance, strength/muscle strengthening, balance, and flexibility/stretching. [8], [17], [18] Although exercise can be categorized into these four groups some physical activity can fit the criteria for multiple groups, but primarily belong to one.

The first type of exercise to discuss is strength/muscle strengthening exercise, which works a specific muscle or grouping of muscles. Strength exercises serve to build muscle mass, which

improves posture, regulates body weight and blood sugar, and reduces elderly fall rates.[8] Strength exercises are performed against resistance, and can be performed statically, such that there is no change in muscle length or dynamically, which requires muscle shortening and/or lengthening. Examples include squats, push-ups, lunges, chin-ups and dips.

The second exercise type is flexibility/stretching, where one actively attempts to improve their range of motion through contorting the body in specific positions. Stretching acts to lengthen muscles and tendons to maintain their flexibility and length. [8] Stretching increases mobility, which reduces falling rates, joint pain and the risk of muscle cramps and strains. [8] Stretches can be static or dynamic and be held for varying time durations.

The third exercise type is balance, which involves muscle control and environmental perception to stabilize the body and control its positioning.[17] Impaired balance is attributed to loss of muscle tone, increased joint rigidity and losses in vision and hearing. [8] Regular practice of balance reduces the onset of its inevitable decline and reduces elderly fall risk. Balance exercises can be performed with eyes open or closed, to increase difficulty, and include standing on one foot or the heal-to-toe walk. [18]

The final exercise type that will be discussed is aerobic exercise, which places higher metabolic demands on the body, thus increasing cardiovascular and respiratory workload. It promotes blood vessel relaxation, decreases blood pressure and sugar levels, reduces inflammation and body fat, and improves mood and cognition. [8] A sample of aerobic exercise forms include brisk walking, swimming, running, cycling, tennis and basketball. [8], [18]

Furthermore, exercise can be less conventionally grouped into either open skill or closed skill forms. The grouping of open versus closed skill exercise was made because exercise environment can impact cognition.[19] Accordingly, open skill exercise is performed in a dynamic and changing environment, whereas the closed skill exercise environment is static and predictable.[19] open skill exercise requires adaptability, continuous decision making and is often driven by an external stimulus, [19] examples include tennis, squash, basketball, and boxing. In contrast, closed skill exercise is more self-paced, requires less decision making and has a smaller cognitive demand than open skill exercise. [19] closed skill exercise include swimming, golfing, running and archery. Most aerobic exercise studies examined in this review are closed skill exercise in the form of cycling, running or brisk walking, reducing exercise environment induced variation.

1.4 The Need to Improve Muscular Disease/Disorder Diagnosis

Neuromuscular disorders can have a profound and devastating effect, as they can inhibit movement, speech, vision, respiration, and various other functions, severely reducing quality of life. Some common neuromuscular disorders include amyotrophic lateral sclerosis (ALS), multiple sclerosis (MS), muscular dystrophy, and myopathy. [20] ALS and MS pertain to dysfunction in the central and peripheral nervous system respectively, whereas muscular dystrophy and myopathy relate to dysfunction on the muscle fibre level.[20] Remarkably, the global prevalence of neuromuscular disease is estimated to be 0.1 – 0.3%, which is comparable to that of Parkinson's.[21] Diagnosis and treatment are highly dependent on the specific neuromuscular disorder. One such subset are muscular dystrophies whose prevalence is 25/100,000 person-years.[22] With no known cure for muscular dystrophies early diagnosis is essential to delay muscle wasting and preserve quality of life. The diagnostic pathways include testing for gene

mutations, blood creatine kinase levels to indicate muscle leakage, electromyography (EMG) to detect abnormal muscle electricity profiles, and biopsy to examine muscle fibre ratio, volume, and the prevalence of necrotic tissue.[23] However, the gold-standard for neuromuscular disorder diagnosis is muscle biopsy, as it identifies fibre type ratios, allowing for comparison to known muscle norms.[24] The non-invasive clinical alternative of surface EMG does not provide fibre specific information as surface electrodes only provide information on general muscle behaviour.[24] In invasive EMG the small surface area of penetrating electrodes reduces the generalizability of the reading over the entire muscle, but provides information on fibre level muscle function.[24] Biopsy and EMG can also be complementary in neuromuscular disorder diagnosis by detailing muscle structural and functional abnormalities, respectively, which can lead to a more complete diagnosis.

1.4.1 The Need for Improved Muscle Biopsy

To have the ability to non-invasively characterise skeletal muscle fibre composition, would be clinically valuable to those with neuromuscular disease, as it would alleviate patient pain and further damage of the already deteriorating muscles, associated with biopsy.[25] It could also improve on the non-fibre specific electromyography, which showed diagnostic accuracy on the order of 70% in comparison to 90% for biopsy.[25] Not only this, but it could address some of the short comings of muscle biopsy associated with sampling region and accuracy. The deltoid, biceps, and quadriceps muscles are typically chosen for biopsy due to their ease of access, sufficiently large fibre size, and regular fibre type distribution.[24] Sampling solely in these regions inherently limits the diagnostic ability if the abnormality is present in a region other than those listed above. To overcome the limitation of biopsy sampling region, MR images present an alternative as they can examine entire cross sections of muscles other than those listed above. Furthermore, biopsy assumes that the tissue subsamples are an accurate representation of the entire muscle. While this assumption is necessary to ensure that we do not extensively damage the muscle through sampling, this can lead to false negative results. If patients go undiagnosed the damage associated with a second biopsy and disease progression could cause irreversible damage that was preventable. Minimally invasive alternatives to biopsy such as the use of fibre-optic probes, to measure changes in muscle sarcomere length, have been proposed. [26] Through using reflection spectroscopy and probes on the order of 250 micrometers wide, one could observe nanoscale muscle movements providing insight into muscle dysfunction. [26] This technique shows promise but has not been well refined to define twitch fibre behaviour and muscle composition. The primary focus in the direction of non-invasive biopsy alternatives is in MR based solutions. As previously stated, MR imaging would allow for entire muscle cross sections to be examined, which removes the inaccuracy of the chosen biopsy samples and provides a larger distribution of muscle fibres. This would not only remove the element of muscular damage associated with biopsy, but could characterize specific muscles to provide more informed diagnostics. Researchers have attempted to address the problem of developing a non-invasive biopsy replacement using MRI, but have had little success. The primary current non-invasive MR alternatives are either using muscle carnosine levels measured via hydrogen spectroscopy (1H-MRS), [27] or using MR muscle volume estimates with measures of maximum muscle contractile force and strength to estimate muscle composition [28]. The current methods require anatomically informed voxel placement, so this only alleviates the variance caused by biopsy muscle subsampling, [27] and an extensive data and clinically infeasible collection procedure,

requiring a dynamometer for force measurement and a reflective marker camera system to determine ankle orientation [28]. Consequently, there is still a need for a non-invasive muscle biopsy alternative that is not dependent on regional selection, like the 1H-MRS technique, and does not require extensive set-up and time, like the forced based technique.

1.5 The Need to Understand and Classify Muscle Injury

Skeletal muscle by mass is the most prominent tissue in the body, accounting for approximately 45% of body weight.[29] It is the voluntary contractile unit of the body connected to bone through fibrous tendons, which allows for posture maintenance, heat generation, movement, and various other functions. Muscle injury is highly prevalent due to its high presentation throughout the body and our dependence on locomotion in daily life. Although more associated with sport, the conduction of physical work can lead to skeletal muscle strain, which can be accompanied by subsequent loss in muscle performance, increased inflammation, tissue edema, and if the injury is sustained long term muscle degeneration. [30] Specifically, in amateur and professional sports it is estimated that 30 to 50% of all injuries are caused by soft-tissue lesions.[29] Although nonsurgical treatment of muscle injury, such as rehabilitation plans, have a good prognosis for most athletes any treatment failure can postpone the return to physical activity for weeks or even months. Absence of physical activity can have negative implications on physical and mental health, which signifies the importance of understanding muscle and how it is affected by injury. [8], [11] Although muscle injury to the athlete demographic is a substantial problem, an arguably larger demographic suffering from this is the elderly. It is estimated that by 2050 a quarter of the global population will be older than 65 years old. [30] This vast population will experience the age induced decline in muscle tone and overall mobility, leaving them vulnerable to experience muscle injury. The increased latency associated with the restoration of muscle performance and muscle regeneration in the elderly leaves them particularly vulnerable as well.[31] Interestingly immobility, which is associated with dysfunction of the musculoskeletal system, is a predictor for poor health outcomes, such as mortality. [31] Therefore an improved understanding of muscle function and dysfunction, associated with injury, would be beneficial for the elderly not only to inform rehabilitation decisions and routes of origin, but for its role as a health prognostic.

In addition to the diagnosis of muscle injury the severity of the injury must also be assessed. Classically muscle injury is characterized into three groupings based on signs and symptoms; grade I (edema and discomfort), grade II (impaired function and possibly ecchymosis), and grade III (rupture and extensive hematoma). [29] Ultrasound is commonly used to verify diagnosis due to its ability to image in "real-time" and its good soft tissue contrast. [29] Operator dependence, such as variation in transducer angle and applied pressure, makes diagnostic repeatability a point of concern. To mitigate operator dependence MRI is also used as a diagnostic due to its excellent soft-tissue contrast. Although the anatomical clarity is improved with MRI by using static images it comes at the cost of dynamic imaging, which could present valuable insights. [29] An ideal combination of functional and structural MR would provide the benefits of improved ability to grade muscle injury. With structural MR to assess muscle damage readily developed, the primary interest in research is to look for functional MR metrics to understand the complex behaviour of healthy and damaged muscle. Functional magnetic resonance imaging (fMRI) is being used to bridge this gap as it non-invasively provides insight into the blood flow and metabolic profiles of tissues, such as muscle.[32] Additionally, it also has shown utility

in characterising skeletal muscle physiology in healthy and diseased populations.[33] But the complex structural and functional organization of muscle is yet to be well defined. An improved understanding of muscle function using complex MRI metrics can provide the novel insight required to accurately describe muscle health. This would improve diagnosis and reduce the duration of rehabilitation, which is essential with aging population worldwide.

1.6 The Intended Implications of This Work

This master's thesis was undertaken to perform research that would hold clinical importance. The intent of this work was to address the need to understand and promote the effects of exercise, to aid in muscular diagnosis, and to use a unique representation to describe muscle in the hopes of providing novel discriminators to determine differences between healthy and diseased muscle. The work is intended to address the major needs in the areas discussed above.

To address the first issue of understanding the benefits of exercise, functional imaging was performed at rest and during contraction using an in-house built MRI compatible ergometer. Concurrent EMG was also recorded during some exercise stints. The intent of this was to compare muscle activation at rest to during exercise of healthy patients. By using the muscle BOLD and EMG signal the relationship between the blood flow and electrical activation could be explored to understand muscle activation. This relationship although previously explored could benefit from novel complex metrics, such as the fractal dimension or phase space representations, as muscle is structurally and functionally complex and should be described as such.

In an effort to improve muscular disease and diagnosis a non-invasive biopsy alternative could be developed using the knowledge of perfusion based differences in muscle. With the rationale that relative differences in muscle perfusion between slow and fast-twitch muscle fibers could be isolated using BOLD imaging an exploration into techniques that could identify muscle differences was undertaken. With the ability to identify muscle specific differences related to perfusion, as different muscle groups will have varying fiber type ratios, this could provide the foundation for a non-invasive biopsy replacement. A non-invasive biopsy replacement would change the landscape of current muscle disease/disorder diagnosis. Additionally, it could be incorporated into rehabilitation plans to assess muscle fiber dynamics throughout the course of rehabilitation without the worry of causing harm to already damaged muscle.

The final area of major need that was of focus was to improve fundamental knowledge of muscle activation using MRI. This would help to address the shortcoming of MRI compared to ultrasound in grading muscle injury. If MRI had the combination of improved resolution and soft tissue contrast, paired with the ability to assess muscle functionally, as is done with ultrasound, it would become the gold standard for grading muscle injury. By using conventional activation metrics in combination with novel complexity based metrics the goal was to quantify muscle activation as a gradient, as opposed to a binary on/off representation. An activation gradient would more accurately describe muscle function allowing one to determine relative functional deficits as a result of injury. Likewise, an activation gradient would also allow for rehabilitation progression assessment. Specifically, a phase space representation of the muscle BOLD signal is used to determine this activation gradient and is explored in the thesis. The novel complex outlook of muscle through using the non-invasive techniques of MRI and EMG proposed in this thesis although exploratory was informed with clinical implications. The work

must be read not only for curiosity in scientific discovery, but with a clinical eye and the goal of translating findings to the clinic.

Chapter 2

Background

2.1 Anatomy

2.1.1 Skeletal Muscle

The three types of muscle found in the human body are smooth, cardiac and skeletal. Each has distinct structural differences that allow for the performance of specific functions. Since this study is primarily focused on assessing muscle during exercise and at rest, skeletal muscle will primarily be explored.

A basic knowledge of skeletal muscle anatomy, innervation, and perfusion is necessary prior to attempting to characterise muscle health and function. Skeletal muscle is the voluntary contractile unit of the body connected to bone through fibrous tendons, which allows for posture maintenance, heat generation, movement, and various other functions. To enable control of muscle its fibres are innervated, perfused by blood vessels to meet metabolic demands, and structurally organised with connective tissue boundaries, which allow for load bearing. The outermost connective tissue layer of each skeletal muscle is the epimysium, which allows for structural organisation and containment of contractile subunits to facilitate coherent contraction.[34] Relative to the muscle body the lower-level contractile unit are the muscle fibres, bundled in groups called fascicles which are covered in a perimysium connective tissue layer.[34] Each respective muscle fibre within a fascicle is encased in an endomysium collagen rich connective tissue layer.[34] Muscle fibres mirror the structural organisation of skeletal muscle with somatic motor neuron innervation, perfusion via capillaries, and contractile units called myofibrils.[34] The self-similar nature of the skeletal muscle composition is seemingly fractal like, with the numerous sarcomere contractile units contributing to the large forces generated by skeletal muscles.

The fundamental contractile unit in skeletal muscle is a sarcomere, composed of actin and myosin filaments, whose interaction generates tension and a resulting contractile force.[34] Groupings of sarcomeres, surrounded by the sarcolemma, make up individual muscle fibres.[34] It is important to note that any given muscle fibre is innervated by a single motor neuron, but one motor neuron may innervate multiple muscle fibers.[35] A motor unit is all the muscle fibres innervated by an alpha motor neuron.[35] The number of muscle fibres in a motor unit varies; for instance, the motor units consist of 100 and 1000 muscle fibres for the muscles of the hand and lower leg respectively.[35] The size of a motor unit determines its functionality, as smaller units achieve fine precision motion, in contrast to the gross motion initiated by larger units.[34] The size, rate of firing and number of recruited of motor units all contribute to muscle

contractile force.[34] Intuitively, to generate a greater force more motor units are recruited and they will fire at a faster rate. In saying this, to prevent motor fatigue motor units are selectively recruited such that only the minimum amount needed to achieve the task are recruited. [34]

More generally, muscle fibres can be broadly grouped into three types; type I (slow-twitch oxidative (STO)), type IIA (fast-twitch oxidative (FTO)) and type IIB (fast-twitch glycolytic (FTG)).[36] They are classified based on their rate of shortening, which is directly correlated with myosin ATPase activity, perfusion, and primary metabolic pathway.[36] Generally, type I fibres rely on aerobic/oxidative metabolism, type IIB on anaerobic/glycolytic metabolism and type IIA falls in the middle of this spectrum.[36] Thus, intuitively type I fibres lend themselves to endurance-based tasks and type II to power activities, as they will fatigue more quickly. Along the same lines, postural muscles should contain a higher density of type I fibres and movement driven muscles with a higher type II fibre density. For instance, in the lower leg the soleus is considered to be postural and gastrocnemius as movement driven. The percentage proportion of slow-twitch muscle found in the soleus and gastrocnemius respectively was 70% and 50%, illustrating how muscle body fibre profiles are dependent on function.[37]

Skeletal muscle cells like neurons, are excitable and this property is leveraged to facilitate contraction via excitation-contraction coupling.[34] The broad steps that are required to allow for muscle contraction to occur are detailed below. First, contraction must be initiated either in the region of the cortical homunculus corresponding to the muscle of interest, or at the specific spinal level. This signal is sent, via an action potential, to the specific muscular site. This facilitates the release of the neurotransmitter acetylcholine from the presynaptic membrane of the neuro-muscular junction.[34] The acetylcholine receptors sitting at the motor endplate then allow for the action potential to propagate to the muscle fibre through the opening of sodium ions channels resulting in depolarization.[34] The neuro-muscular junction cannot stay in an acetylcholine saturated state indefinitely, thus acetylcholine concentration in the synaptic cleft is regulated by the enzyme acetylcholinesterase.[34] The action potential has now propagated to the motor plate and continues down the transverse tubules to initiate the release of Ca2+ from the sarcoplasmic reticulum.[34] This causes local Ca2+ release from the sarcoplasm to cause contraction on the cellular level of the sarcomere.[34] Contraction is regulated by the release of calcium from the sarcoplasmic reticulum. Through having a fundamental understanding of muscle contraction at the cellular level the recording of muscular activation via EMG can be better interpreted.

Furthermore, the focus of this experiment is to look at overall muscle function during different rest and during exercise paradigms. Skeletal muscle contraction can be divided into two categories isometric contraction and isotonic contraction.[34] The less common of the two is isometric contraction, which is when the muscle produces tensile forces without a corresponding change in muscle length.[34] Isotonic contraction on the contrary is when joint angle changes due to the lengthening or shortening of the muscle.[34] It can be further divided into concentric and eccentric contraction, which involve muscles shortening and lengthening respectively to move a load.[34] The primary mode of contraction employed was isometric contraction as this reduces motion artifact when performing simultaneous muscular imaging and exercise paradigms.

2.1.2 The Circulatory System

The circulatory system, through its complex network of blood vessels, performs the essential role of providing blood to cells to facilitate the exchange of nutrients (i.e. oxygen) and removal of waste (i.e. carbon dioxide).[38] Vascular perfusion responds to the metabolic needs of tissues by changing blood pressure and flow to the region of interest.[39] Tissues in metabolic need will receive more blood and thus more oxygen, whereas blood will be shunted from regions that are relatively inactive. The muscle layer within the vascular wall is responsible for the shunting of blood, but also modulates blood pressure through vasodilation and vasoconstriction. There is an interplay between blood pressure, blood flow, and nutrient exchange to achieve optimal vascular perfusion. This is controlled by brain regions such as the cerebellum and the brain stem as they regulate breathing, heartbeat, body temperature, and blood pressure.[40]

The physiological needs associated with skeletal muscle during aerobic exercise, such as cycling, can cause a contradictory change in blood pressure and flow.[39] What is meant by this is the increased metabolic demands of contracting muscles cause an increase in blood flow along with a vasodilation.[39] This allows for the exchange of oxygen, carbon-dioxide and other waste products, such as lactic acid, from the muscle to the blood at a more rapid rate. But vasodilation causes a corresponding decrease in blood pressure, which can decrease cardiac output and reduce the amount of blood received at the muscle's vascular bed. This problem is resolved through an interplay between the local and systemic responses of the circulatory system.[39] Vasoconstriction is maintained in larger vessels feeding the muscle, whereas vasodilation occurs at the arterial level.[39] This provides an optimal balance between having a high enough blood pressure to achieve a high cardiac output and enough vascular perfusion to meet the metabolic needs of the muscle tissue.

Additionally, exercise causes alterations to the partial pressure of carbon dioxide and oxygen, cardiac output, and glucose and lactic acid levels in the blood.[41] These factors will affect regional blood flow within the muscle in terms of its volume, but also in its distribution. With a finite amount of blood volume it must be preferentially distributed based on metabolic need. To facilitate locomotion, blood will be preferentially shunted to the muscle agonist (which are involved in contraction) versus the antagonist (which relax to enable contraction) due to differing metabolic demands. The associated regional changes in blood flow can be correlated with regions of activation and can set the foundation for the use of changes in blood flow to investigate regional muscle activation.

2.2 Electromyography

Electromyography (EMG) is a means of measuring muscle activation, as muscle contraction generates a measurable electrical signal. [42] EMG can be performed invasively, with penetrating needle-based electrodes, or non-invasively, with surface electrodes.[43] The cost of the non-invasive technique is a lower spatial resolution, as the muscle activation cannot be characterized at the fibre level, but rather at the level of motor units. In saying this, when one is looking at gross muscle function the functional unit of contraction is the motor unit, so surface EMG does provide an adequate spatial resolution in these studies.

Surface EMG measures the activation of motors units which are "comprised of a single alpha motor neuron and all the fibres it enervates".[42] The action potential signals for the fibres

innervated by the motor neuron to contract and cause a local depolarization in the muscle tissue, inducing a muscle action potential, which varies from the characteristic action potentials seen in the nervous system.[42] Thus, a motor unit action potential is a summation of muscle fibre action potentials that align both temporally and spatially.[42] The EMG surface electrodes do not pick up the activation of a single motor unit, but rather groupings of motor units contributing to the same task.[42] It is also infeasible for a surface electrode to only detect the activity of one motor unit, as muscle fibres can lay tangent to each other but be innervated by different motor units.[42] It has even been found that "any portion of the muscle may contain fibers belonging to as many as 20-50 motor units".[42]

Surface EMG recordings are used primarily to characterize superficial muscle contraction temporally and in terms of its magnitude.[43] EMG signals are a vital electrophysiological measure to clinicians and researchers in the field of medicine due to their relatively high amplitude, ease of capture, and use in pathological versus normal comparative studies.[43] However, EMG data is not easy to analyze as it is contaminated with physiological and electronic noise. Also, since EMG is recorded during muscle contraction, the movement of the recording electrodes and leads is inevitable and will correspondingly cause motion artifact. Wavelet decomposition, independent component analysis and empirical mode decomposition are some of a few methods to clean the noise contaminated signals.[43] The EMG data can then be analyzed for its activation time, amplitude, duration, time to peak contract, and contraction frequency among other measures depending on the application. [43] In this study, EMG is an optimal modality to look at site-specific measures based on electrode placement and muscle activation, with a high degree of temporal resolution.

2.3 BOLD MRI

2.3.1 Biological Basis

The blood oxygenation level-dependent (BOLD) effect was discovered in the early 1990s and since then has been utilized in functional magnetic resonance imaging (fMRI) studies. [32] fMRI employs the BOLD effect to non-invasively provide insight into the blood flow and metabolic profiles of tissues, such as brain and skeletal muscle, in both healthy and diseased populations. [32], [44]–[46] The muscle BOLD signal is hypothesized to originate from the microvasculature. [45] The physiologic parameters that have been hypothesized to influence the muscle BOLD signal include muscle blood volume, perfusion, metabolic factors, and vascular architecture.[45] Since fibre types, have differing perfusion demands and muscles having varying ratios of fibre types, depending on the muscle's function, BOLD could characterize functional differences on the fibre type or global muscle level.[47] Muscle being a profoundly metabolically active tissue means paradigms that will vary muscular activation can be used to elicit functional differences. These functional differences can be non-invasively observed through the BOLD signal in a given volume of interest (on the fibre type or entire muscle level). A task related change in blood flow can either be characterized by an increase or decrease in regional vascular perfusion, since the body has a limited supply of blood, which will modulate the BOLD signal within the volume of interest.

In MRI the signal characteristics are dependent on the magnetic properties of the spin environment and spin interaction, with hydrogen spins being of interest due to the bodies large water content. Blood has a high water content, but also contains molecules such as hemoglobin,

which is imperative to BOLD imaging.[48][34] The magnetic properties of hemoglobin are dependent on its oxygenation state either in its oxygenated (oxyhemoglobin) or deoxygenated (deoxyhemoglobin) form.[48] Oxyhemoglobin behaves as a diamagnetic substance and has a weak negative susceptibility to magnetic fields. [48], [49] Deoxyhemoglobin in contrast behaves as a paramagnetic substance and has a positive susceptibility that is weaker than diamagnetic substances.[48], [49] Thus, within any particular imaging volume the relative amount of oxy- and deoxy-hemoglobin will affect the susceptibility of the local water molecules through modulating their rate of dephasing.[48] The rate of spin dephasing is related to the signal amplitude and the corresponding image contrast.[48] More specifically, regions with highly deoxygenated blood will be characterized by a decreased signal intensity due to the signal loss associated with paramagnetic induced spin dephasing.[48] Furthermore, since metabolic activity is related to the oxy- deoxy- blood fraction the MR signal intensity will dynamically change based on metabolic need.[48]

Physiologically, the basis for the BOLD effect is that increased metabolic activity is accompanied by an increased regional supply of blood and oxyhemoglobin.[48] This at face value is counter intuitive as one would believe an increased metabolic need would decrease oxyhemoglobin tissue concentration.[48] But, to ensure the tissue is highly perfused with oxygenated blood a pressure gradient to promote local cell oxygen uptake is established. Specifically, to increase the pressure gradient to transport oxygen from the blood into the cell an increased blood oxygen concentration is required.[48] Therefore, the activated region will receive more blood flow, but the amount of oxygen extracted will be less than the amount delivered, causing a relative decrease in the local concentration of deoxyhemoglobin and a corresponding increase in signal intensity.[48]

The BOLD effect is often described as an increased MR signal intensity, in an active metabolic region, due to an increased regional oxyhemoglobin concentration, but this description lacks in detail. A more detailed characterization of the BOLD response over time, in the two highly metabolically active tissues of brain and muscle, is outlined through the hemodynamic response function (HRF), as detailed in Fig. 2.1. It must be noted that the BOLD signal timecourse detailed in Fig. 2.1 is an approximation and the signal amplitude and latency is approximate and is dependent on exercise intensity. The more commonly modeled HRF is for neural activation. It is first characterized by an initial dip due to a small increase in deoxyhemoglobin accompanied with stimulus processing.[48] Next the increase in neuronal activity is shown through the rapid increase in BOLD intensity that is due to greater regional supply of blood and oxyhemoglobin.[48] The intensity will rise to a peak of 2-10% change in signal, at 3T, and can plateau if the stimulus is continually presented.[48] When the stimulus is no longer present the MR signal returns to the baseline but will undershoot it.[48] The undershoot is caused by the rapid decrease in regional blood flow and a delayed normalization in hemoglobin levels causing an increase in the local deoxyhemoglobin concentration.[48] Eventually, the undershoot is corrected and a hemostatic norm is reached. The HRF of muscle has been less readily characterized due to large variation in the response based on specific muscle site and demand inducing variation. Instead the muscle BOLD response is characterized by its time to peak (time to peak BOLD response), hyperemic peak value (maximum BOLD response value), peak area, and peak width. [46], [50], [51] Some general observations when comparing the HRF of the respective tissues is the lack of initial dip and more rapid time to peak with muscle. This can be attributed to reduced latency required to vasodilate in the less restricted vascular framework in muscle

compared to brain. Both will display the signal undershoot due to a rapid decrease in regional blood flow and a delayed normalization in hemoglobin levels causing an increase in the local deoxyhemoglobin concentration. [51]. This will be followed by a return to equilibrium that would be expected to be more rapid for muscle due to less regulated vascular constriction and dilation compared to the highly regulated cerebral blood flow in the brain.

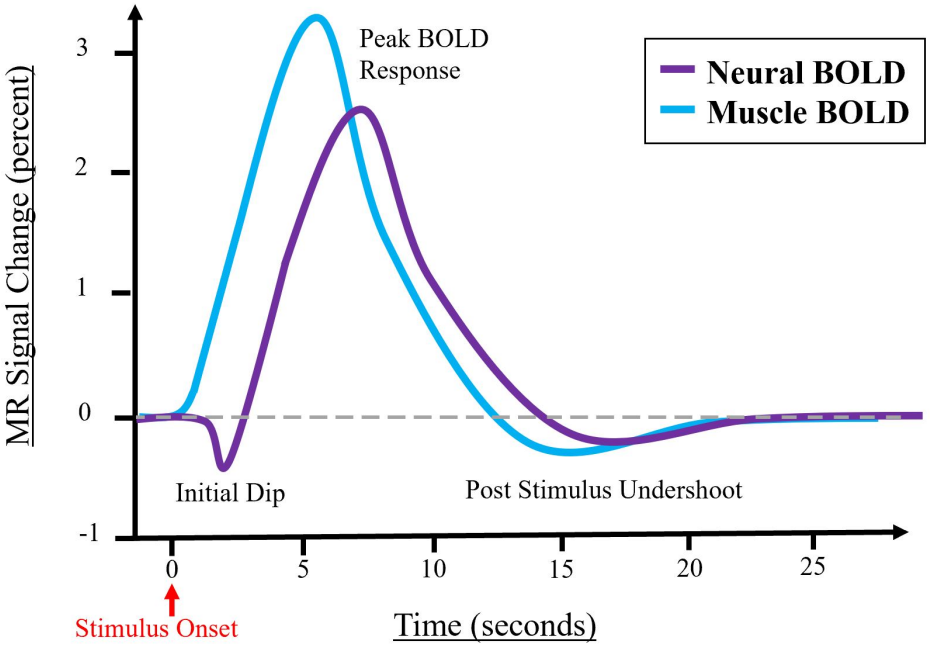

FIGURE 2.1: Sketch of the temporal BOLD response in the brain and muscle. Note the signal amplitude is approximate and is dependent on exercise intensity.

2.3.2 Image Acquisition Techniques

The imaging sequence must meet two essential criteria to perform functional imaging through the use of a BOLD technique. Firstly, it must accentuate the BOLD effect, which as previously outlined relies on the hemoglobin susceptibility based on oxygenation state. Secondly, it must acquire images at a temporal resolution captured fast enough to characterize the active tissue's changing hemodynamic state.

Using the fact that differences in susceptibility will cause a difference in the spin dephasing, we can satisfy the first criteria.[52] The relative increase in the fraction of oxygenated hemoglobin in active muscle tissue will reduce spin dephasing, relative to areas of inactivity, which will cause an increase in the transverse relaxation time known as T2*.[52] Therefore by employing a sequence with a T2* weighting this will promote image contrast through the BOLD effect. An image weighting is determined by two major factors, echo time (TE) and repetition time (TR). A T2* weighted image is achieved by having a relatively long TR and long TE. For BOLD muscle imaging, TE values are typically between 30-120ms.[53] This study uses a TE=35ms, which falls into this range. The TR value chosen is dependent on the specific image sequence used, such as echo-planar imaging (EPI) or fast gradient/spin echo.

The second condition of having sufficient temporal resolution is met using high speed imaging sequences. One such is EPI, as it can acquire a single image in 20ms. This is possible because it only uses one radio-frequency (RF) excitation pulse to obtain all of the spatial-encoding information.[54] Furthermore, EPI is intrinsically T2* weighted as uses only one RF excitation, unlike a conventional sequence which has many, therefore there is no repetition time and thus an infinitely long TR.[54] The major variation in EPI sequences in BOLD studies, aside from the TE value, is the method of RF excitation either through gradient echo (GE) or spin echo (SE). The most popular is GE-EPI as it can achieve a high functional contrast to noise ratio while still maintaining high temporal resolution. [55] Typically SE-EPI is not as commonly used as the rephasing accentuates the static dephasing effects in the field inhomogeneities around larger vessels.[55] But, at higher field strengths this effect is reduced and SE-EPI can have a better spatial specificity in comparison to GE-EPI.[55]

2.4 Complex Representation

2.4.1 The Fractal Dimension

Definition

Many objects in nature possess complexity in either their structural organization or in how they operate functionally. This extends to the human body which is known to be an inherently complex system structurally and functionally. Interestingly complexity which remains constant over differing scale is seen in pathology, such is in tumor boundaries or their vascular patterns. [56] One such metric used to describe this behaviour is the fractal dimension (FD), which is a measure of the self-similarity and complexity of a system in either the spatial or temporal domain.[56]–[59]

Fractal geometry described by Mandelbrot improved the characterization of natural structures and shapes, which contributed to our improved understanding of complex systems and chaos in nature. [57] The fractal geometry is different from the conventional euclidean geometry that we use to describe space, as unlike the Euclidean dimension, objects are no longer required to have an integer spatial dimension. [57] This non-integer dimension characterization is obtained by using a "self-similarity" outlook. For instance a fractal object is self-similar as it would have the same geometric properties when examined at any level of magnification/scale. [57] If self-similarity is preserved over a changing scale then an object can be quantified as more complex. For instance the koch snowflake, which shows iterative addition of symmetrical edges, demonstrates the self-similarity and complexity relation as a function of scale, as shown in Fig. 2.2. With in increase in the number of edges the perimeter of the shape (a one dimensional measure) gets more complex, and since the edges are symmetrical in appearance, the self-similarity is preserved. Therefore the fractal dimension will scale from 1 to 2 as perimeter is a 1D measure of geometry.

Another way to interpret the self-similarity complexity relation is looking at information gained over variable measurement scale. If we take the edge length of the single line in Fig. 2.2 to be L when measuring the perimeter depending on the length of the ruler whether it is greater than or less than L we will get the same measurement for the line. This also holds for the first snow flake in Fig. 2.2. Whereas in the second snow flake in Fig. 2.2 if the ruler is of length L we will not be able to actually measure the length of the edges which are L/4. Therefore

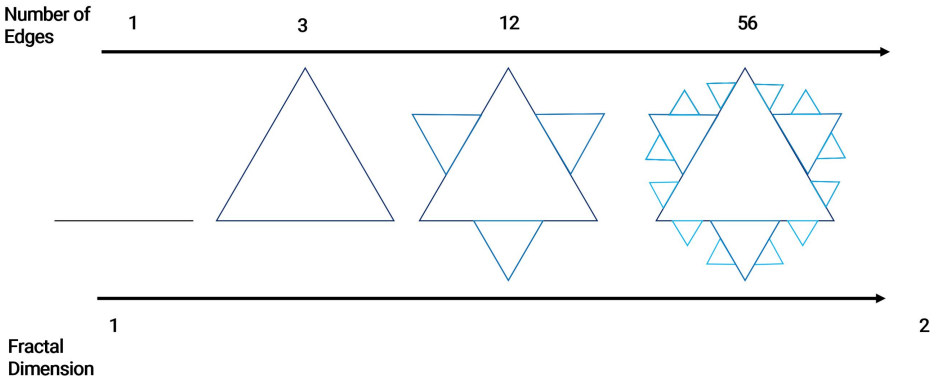

FIGURE 2.2: Demonstration of relationship between complexity and self-similarity using a Koch snowflake example.

we are gaining more information the system as the measurement unit gets smaller, meaning we require more information to accurately represent the system, implying it is complex. The complexity between snow-flake one and two vastly different yet the self-similarity is maintained while changing scale, indicating how we can use self-similarity on a changing scale to provide insight into complexity.

This can also be used in the time domain to describe the signal complexity. Instead of using a length metric to understand the fractal dimension described through a "self-similarity" outlook, in the time domain we can use the metric of variance. If the variance of a signal changes as a function of scale then we can model it as a complex signal. For instance, if complexity increases as the scale gets smaller then we get more information about a signal as the scale decreases and it requires finer measurement windows to be accurately represented and is thus complex. A self-similar time series over changing scale will require finer measurement windows to be more accurately represented, so it also encompasses complexity measures in the time series. Some other key features of fractal time series are encompassed in its statistical properties as it may have a skewed probability distribution. Its complexity can also be demonstrated through a frequency representation with a power spectrum with a baseline of 1/frequency. [60] Additionally, the time series can be locally or globally self-similar and may show statistical dependence over a short or long range. [60]

Basis for Use

The human body is an inherently complex system in terms of both its organization and operation, so it is best to describe it through a complex metric, such as the FD. Geometrically, the human circulatory system shows scale independent self-similarity in its branching patterns from arteries, to arterioles, to microvasculature, and through the venous system. Additionally, the FD has been used to describe the complexity of both healthy and diseased vascular geometry. One such instance is where patients with cerebral arteriovenous malformations showed an increased FD in their affected hemisphere.[59] Furthermore, the temporal complexity of the circulatory system has been investigated through fractal characterization of the arterial time series waveform. The arterial waveform has been shown to be complex, displaying self-similarity, and its fractal description having clinical utility.[61] For instance, cardiovascular disorders can

be identified through arterial stiffening and hypertension, which have been related to changes in central pulse pressure. [61] Interestingly, decreases in arterial time series FD correlated with increased central pulse pressure, providing a powerful diagnostic measure.[61] Likewise, the BOLD signal, which is a relative temporal measure of perfusion and metabolism, via the ratio of deoxy- to oxy-hemoglobin, has been readily characterized via the FD metric. fMRI BOLD signal complexity has been used to differentiate healthy subjects from those with Alzheimer's disease [62] and mild traumatic brain injury [63], and the level of consciousness in those with disorders of consciousness [64]. In addition, geometrically the muscle fibre also shows a degree of power-scaled self similarity when scaling down the levels from the muscle belly, to muscle fascicle, to muscle fibre, to myofibril. The fractal organization of both the muscle and circulatory system and its prominent use of FD in the fMRI literature suggests a plausible relevance in describing the differing vascular profiles of muscle fibres through the skeletal muscle BOLD signal. This rationale is why it was chosen to be employed as a means to describe muscle in the work contained in this thesis.

2.4.2 The Phase Space

Definition

The phase space is a method to describe non-linear systems and it is particularly of interest in describing the muscle activation, which it why it has been used in EMG studies. [65] More specifically, it it known that muscle operation is non-linear as its activation threshold is non-linear due to variable discharge threshold depending on specific motor neuron, and since the recruitment of motor units is non-linearly related to force output. [65], [66] The phase space reconstruction technique is well described by EMG researchers Chen and Wang and is as follows: *"The basic idea of phase space reconstruction is that evolution of any state component of a system depends on other interacting components within the same system so the information of these related components is hidden under the evolution of the component. In order to reconstruct a "equivalent" high dimensional space that the system embeds in, we need only to investigate the component by utilizing some time-delay data of observed time series as new coordinate for the phase space. By repeating the process, the "equivalent" phase space can be obtained. The process is called time-delay embedding."* [65]

The phase space is then created by plotting the temporal function against its delay. The phase space time-delay can be found using the C-C method, using principle component analysis, or the method of delays to select components in a joint or independent approach, . [67] Alternatively, the phase space can be represented by using the temporal derivative to represent the system delay. When performing a voxel-wise analysis the embedding dimension computed may vary at each voxel, therefore the temporal derivative computation of the phase space would present more stability and it is the method used in this work.

Basis for Use

The muscle BOLD phase space describes muscle activity state/state-transitions over time. If the phase space is examined at rest the expectation is that the temporal signal would oscillate/revolve around a single state, the null state, which is theoretically shown in Fig. 2.3. Using this inference one can characterize the oscillation around the stable rest-state to describe biological factors such as stability or activity distribution. For instance, variability of deviation from the

oscillatory path would provide insight into muscular stability which could be hypothesized to show twitches or muscular activation at rest. The spread/distribution of the oscillation from the zero point would provide insight on range of activity or perfusion to the muscle at rest. The phase space is more conventionally used to examine state/state-changes, with a theoretical muscle BOLD phase space when transitioning from rest to contraction shown in Fig. 2.4. Here a change in amplitude in the BOLD time-series indicating muscle activation would be illustrated by a new state in the phase plane (i.e. oscillation around a new center). Now conventional muscle BOLD measures such as time to peak and hyperemic peak value would be conveyed in the phase space as relative difference in state location and center point of active state respectively. Therefore the phase space conveys the conventional measures of the time-domain analysis of the muscle BOLD signal while also presenting novel insights. Through performing a block design paradigm, alternating between rest and active states, the phase space could provide novel insight into state transitions and fatigue over time. Most importantly it could provide insight into an activation gradient of muscle, as if more than two states are observed in the phase plane, then this suggests activation is not a binary process. Thus, the complex representation of muscle BOLD through using the phase space could more readily characterize the signal compared to conventional time-domain analysis.

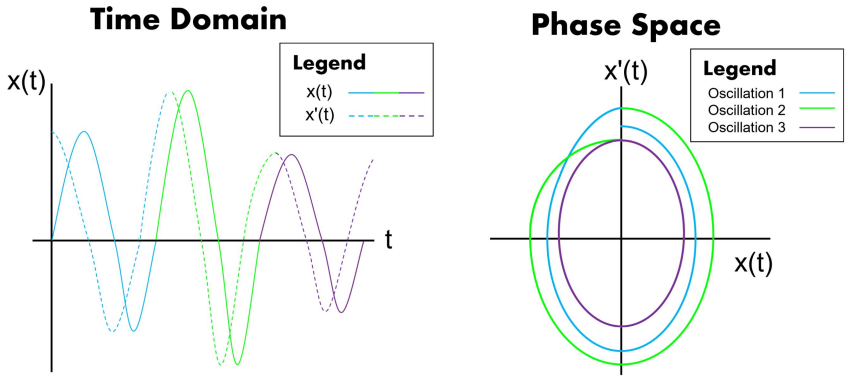

FIGURE 2.3: Theoretical Phase Space of a muscle at rest.

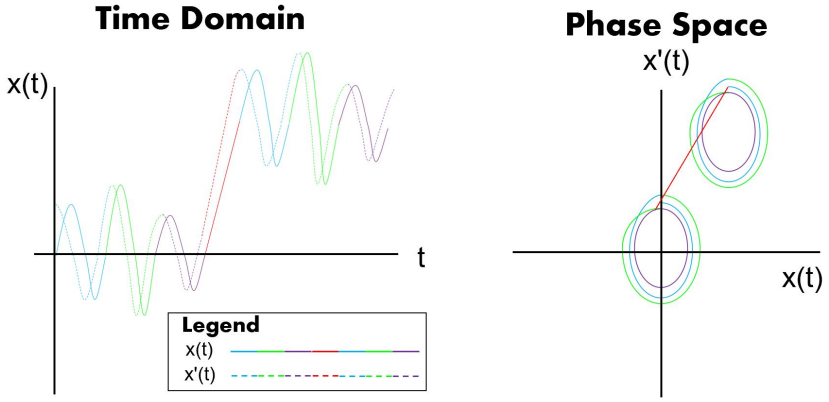

FIGURE 2.4: Theoretical Phase Space of a muscle during activity when transition between rest to active during one example contraction.

Chapter 3

Literature Review

3.1 Muscle BOLD Studies

As the primary method of non-invasive assessment of muscle function in the thesis it is imperative to review the existing literature on muscle BOLD (mBOLD). To limit the scope the Boolean search term was used in PubMed to return relevant studies ("muscle BOLD" OR " mBOLD") NOT ("rat" OR "animal"). Scope was focused on human muscle BOLD investigations through the above term.

Although muscle BOLD studies specify that they used mBOLD they do not use the conventional BOLD examination seen in neural activation studies where the BOLD time course is correlated with an ideal hemodyanmic response function (HRF) based on the paradigm block length. Some studies which use mBOLD employ a framework similar to what is described as muscle functional MRI (mfMRI). mfMRI examines differing transverse relaxation times at the pre- versus post- state as a function of changing stimuli (i.e. exercise or proximal vessel occlusion). The transverse relaxation time T2* can be found from using multi-echo echo planar imaging sequence. Then relaxation times can be found foe a particular voxel by performing a least-square fit of mono-exponential decay of the signal intensities as a function of the increasing echo time, S=I0*exp(TE/T2*).[45] This technique does not require concurrent exercise to be performed, which can mitigate the affect of motion artifact. Additionally, the muscle BOLD response is characterized by its time to peak (time to peak BOLD response), hyperemic peak value (maximum BOLD response value), peak area, and peak width. [46], [50], [51] This analysis requires concurrent exercise and BOLD imaging, which is more reflective of the muscle's functional state during exercise, as opposed to the previous analysis which uses a pre and post muscle assessment to provide outlook. In saying this, the correlation with the ideal HRF for muscle BOLD in the instance of a block design is still a valid measure of activation, but it presents the drawback of requiring multiple exercise blocks to be performed during concurrent MRI, whereas the previous techniques could be performed with one stint of high intensity exercise. As such, the described mBOLD studies must be looked at with a different lens then the conventional neural BOLD/fMRI studies that predominate the literature. For a very comprehensive review of mBOLD in terms of paradigm best practices, metrics to describe BOLD time courses, and confounding factors of the mBOLD signal such as age, relative fitness, fibre type and drug ingestion, the following should be referenced [45]. For instance differences due to age have be linked to increased vascular rigidity, and muscle differences (which vary in their fibre type ratios) due to perfusion, oxygenation uptake and capillary density variations.[45] Another review, that has more of a clinical outlook, describes the usefulness of mBOLD in

examining vascular diseases, such as peripheral arterial occlusive disease, diabetes mellitus, and chronic compartment syndrome. [33] To examine blood-flow affects due to disease/disorder it is conventional to use ischemia and/or reactive hyperemia paradigms, which involves occluding blood-flow to a proximal artery to the imaging slice (conventionally with a pressure cuff) then observing the return to normal blood flow. One work that employed this framework revealed diabetic and obese individual's had an altered blood-volume status. [33]

Similar to the previously discussed reviews, one study on mBOLD investigated a multitude of factors that affect vasomodulation such as varying oxygenation induced state, exercise induced changes, and the ingestion of vaso-dilating/constricting supplements. [68] To test these factors a combination of 6 scanning acquisitions were used that were pre- or post exercise with either ingesting nothing, caffeine, or an antihistamine. [68] The mBOLD scans were collected with 4 90s cycles of normoxia then 45s with hyperoxia in order to modulate the BOLD amplitude while in a resting-state. [68] As an overarching review the BOLD signal was modulated at rest via partial oxygenation pressure changes, with exercise producing a significant increase in the absolute BOLD signal in the soleus and gastrocnemius with no substance ingested. [68] Finally, a differing relation was seen in the gastrocnemius and soleus due to substance ingestion, with caffeine increasing gastrocnemius BOLD amplitude, with no soleus change, and the antihistamine decreased soleus BOLD amplitude, but did not affect the gastrocnemius. [68] This work has set the foundation for substance regulation before experimentation and suggests fibre type differences in the muscle can contribute differences in the BOLD signal, which is also explored in Chapter 8.

Some foundational work in mBOLD during hyperemia and ischemia, was explored at different field strengths and was attempted to be automated due to its vast use throughout the mBOLD literature. One study examined the validity of using paradigms that induce ischemia/hyperemia and the corresponding change in muscle recorded via mBOLD at differing field strengths.[69] Eight healthy volunteers experienced temporary vascular occlusion at the thigh, using a compression cuff, and fat-saturated multi-echo gradient-echo EPI images were taken prior to and post occlusion using a 1.5T and 3T magnet.[69] The differences in relaxation time quantified via R2 measures were assessed for all participants in the gastrocnemius and soleus muscles.[69] The change in relaxation time increased, in both muscles and -emia conditions, at higher field strength and ranged from 1.6 to 2.2 greater at 3T.[69] Therefore, this work suggests higher field strength magnets should be used for exploratory muscle studies that require improved pre and post hyperemia/ischemia state discrepancy. The concern of higher field strengths causing significant extravascular BOLD effects, that would affect skeletal muscle transverse relaxation time computation, was proven to be a non-concern [70], indicating higher field strengths are ideal. Due to the vast effort of examining state induced differences in muscle relaxation using multi-echo mBOLD one group tried to make an automated framework to examine reactive hyperemia. [71] Using a multi-echo EPI mBOLD acquisition the ROIs of the soleus, gastrocnemius and tibialis anterior muscles were examined. [71] A gamma-variate sigmoidal function was fitted to derive the time to peak, hyperemic peak value, peak area, and peak width metrics. [71] The derived values based off the model versus the actual data were highly correlated, but presented the benefit of removing the operator dependence which was observed. [71] This study shows the possibility of an automated, and hence scalable, assessment of functional muscle behaviour.

Some studies focused on the effects of occlusion on muscle perfusion/metabolism as characterized through the mBOLD signal while operating at high field strengths, due to the foundational

work in [69]. One group used 8 participants where thigh-specific vascular cuff was used to induce hyperenemia prior to imaging of the calf muscle with a 3T or 7T magnetic respectively.[72] They employed a change in relaxation time framework to facilitate comparisons between field strengths R2* rate constants were calculated as R2* = 1/T2*. [72] Notably, mean preocclusion R2* and the change in R2* value was greater at 7T. [72] With the added benefit of 7T magnets already providing improved SNR this study demonstrated the feasibility of performing muscle investigations at high field strengths, which is conventionally used for neural imaging. Another study which performed high field muscle imaging examined maximal plantar-flexion contraction and its corresponding change in signal amplitude in the soleus.[73] The maximal amplitude was found by fitting a ninth order polynomial to derive a line of best fit, time-to-peak signal was determined by identifying the inflection in the derivative of the line of best fit.[73] The results demonstrated increased pre-contractile signal amplitude from 0.3–7.0%, with heterogenity across the seven subjects.[73] This work had the contribution of showing difference in mBOLD signal amplitude at high field strength and the variance contribution that can be expected from participant biological variability.

Furthermore, the use of mBOLD to examine skeletal muscle micro-circulation abnormalities has been translated to the clinical population who experience systemic sclerosis. Using a multi-echo mBOLD acquisition in calf, metrics of minimal and maximal hemoglobin oxygen saturation and time to peak (TTP), were derived after cuff-induced ischemia followed by reactive hyperemia. [74] The result showed when comparing patients to healthy controls that there were functional deficits in the calf, that were more pronounced in the gastrocnemius, as demonstrated through increased oxygenation desaturaion during ischemia and impaired oxygenation during hyperemia in patients. [74] The work demonstrates the utility in the mBOLD signal in examining microcirculation abnormalities, which is its hypothesized point of origin. This research group further continued their exploration into systemic sclerosis by trying to correlate their previous impactful mBOLD findings with transcutaneous oxygen pressure measures.[75] To measure transcutaneous oxygen pressure an electrode was placed on the skin adjacent to the upper portion of the lateral gastrocnemius ensuring scars and veins were avoided. [75] The high correlation between the transcutaneous oxygen pressure and T2* decay curve demonstrated the ability of the metrics to convey similar information. [75] The same group using the same research subjects examined mBOLD and skin laser Doppler flowmetry (LDF) relationship for those with systemic sclerosis. [76] LDF operates on the principle of the moving blood inducing a doppler frequency shift and was measured in the same location as the MR images. [76] The metrics from the mBOLD and LDF were 93% and 94% correlated for the healthy and patient groups respectively, demonstrating how it is a comparable measure to mBOLD and transcutaneous oxygen pressure.[76]

Additionally, mBOLD was used to examine skeletal muscle micro-circulation abnormalities another clinical population of those experiencing peripheral arterial occlusive disease (POAD). One study used mBOLD to examine the use of percutaneous transluminal angioplasty of the superficial femoral artery to improve blood-flow in the calf. [77] Notably post procedure the maximum T2* was increased, time-to-peak was decreased and T2* end value was decreased. [77] These results in combination suggest increased perfusion, with more rapid onset, and less residual blood remaining after hyperemia, which are all beneficial, demonstrating the validity of the technique. Another group took this work in a different direction and examined POAD patients compared to healthy age matched controls.[78] Using the conventional single-shot multi-echo

planar imaging of the calf with pressure cuff induced ischemia, they observed group differences in transverse relaxation value. [78]

Reactive hypermia was also used to explore age induced differences in muscle function.[79] Once again a multi-echo T2*-weighted single-shot multi-echo EPI sequence was used used for imaging, with metrics such as hyperemia peak value and time to peak being quantified, this time in a healthy versus elderly comparison.[79] Temporary vascular occlusion was induced at the level of the thigh with imaging performed in the calf of the 11 elderly and 17 younger volunteers.[79] The functional recovery of muscle was impaired in the elderly with a faster ascension to a lower peak blood flow, and delayed return to equilibrium compared to the younger population. [79] The impact on age and muscle function was also explored using maximal plantar flexion exercise induced hyperemia. [80] Functional images were acquired continuously for 4 min, where once every 30s 1s maximal voluntary contraction dorsiflexion was performed.[80] BOLD amplitude was negatively correlated to age and the longer time to peak BOLD amplitude was inferred to be due to impaired blood flow kinetics. [80] Additionally, using hyperemia provoked by a cuff-compression technique and recording multi-echo mBOLD in the calf, smokers were also seen to have impaired muscle blood flow response. [81]

Some studies go one step further than solely mBOLD and are multi-technique studies. One such variation is when studies combine blood flow related measures via mBOLD and metabolic profiles via muscle spectroscopy. One study examined the metabolic profile of the gastrocnemius and soleus muscle by observing the phosphocreatine (PCr) spectral peak roll off, and the difference in perfusion by using change in T2 * maps, from mBOLD acquisitions.[82] 15 Fontaine stage II patients, and 18 healthy controls performed a plantar-flexion paradigm at a rate of 1Hz and data were acquired in synchrony with motion.[82] Notably, gastrocnemius and soleus R2* at end-recovery was not significantly different from one another or between groups, but gastrocnemius had increased hyperemic BOLD amplitude and slower PCr recovery in patients. [82] This study contributed insight into the mitochondrial energy profile with BOLD measures in a relatively concurrent approach, demonstrating the necessity for multi-technique MRI studies. Another study that investigated the muscle BOLD/PCr relationship instead focused on the effect of electrical muscular stimulation on their interconnection. [83] Electrodes for stimulation were placed at the motor points of the superior and inferior heads of the medial gastrocnemius muscles and stimulation functional and spectral data were compared to rest. [83] Stimulation increased the BOLD signal amplitude in the gastrocnemius and soleus during EMS but did not significantly affect the PCr peak. [83] These results indicate that the regularity of contraction induced by stimulation has a greater affect on the perfusion profile of muscle and less of an effect on the mitochondrial metabolic profile. Another group has looked at the effect of muscle activation during plantar-flexion of varying weight, using the multi-modal approach of muscle BOLD and near infrared spectroscopy (NIRS).[84] During a 14-min period MRI EPI single acquisitions for 789ms while resting were followed by a delay of 2211ms where plantar-flexion was performed, with a similarly employed paradigm for NIRS acquisition.[84] Interestingly the BOLD signal amplitude and oxygen saturation measured from NIRS decreased with the onset of 2kg exercise, even more so when the weight was increased to 6kg.[84] This observation of decreased BOLD signal amplitude has not been commonly observed in the literature, so the results must be taken with caution.

3.2 Non-invasive MR Biopsy Studies

To have the ability to non-invasively characterise skeletal muscle fibre composition would be clinically valuable to those with neuromuscular disease in order to address two of the major draw-backs with biopsy. The first is it would alleviate patient pain and further damage of the already deteriorating muscles, associated with biopsy.[25] The second, which can be addressed with MRI as it allows for entire muscle cross sections to be examined, is the subsampling inaccuracy of the chosen biopsy samples. As such, researchers have attempted to address the problem of developing a non-invasive biopsy replacement using MRI, but have had little success.

The current non-invasive MR alternative is using muscle carnosine levels measured in the gastrocnemius via hydrogen spectroscopy (1H-MRS), where increased levels were found in the FT fibres of young, experienced, and ex-athletes.[27] The study consisted of 83 controls, 15 young track-and-field athletes, 51 elite athletes and 14 ex-athletes. The results showed that compared to the reference population power athletes had approximately 30% higher and endurance athletes had approximately 20% lower carnosine levels. [27] Although this result is encouraging, 1H-MRS is highly sensitive to B0 field homogeneity and lipids, as inhomogeneities can lead to spectral broadening that can obscure metabolites such as carnosine. Therefore, the results are highly dependent on voxel placement and require previous anatomical knowledge to properly avoid fat in voxel selection. Thus, the dependence on voxel placement only mitigates the variance caused by biopsy muscle subsampling. Furthermore, some muscular disorders cause fat to replace wasting muscle tissue, so the findings on the ideal athlete population may not transition well to the clinical population.[20]

Another proposed MR method used measures of maximum muscle contractile force, strength, and volume to estimate muscle composition.[28] This is proposed with the ideology that the relative power of fast-twitch fibres would be greater than that of slow-twitch for a given cross-sectional area. The maximal contractile force and contractile strength was measured by performing plantar flexion.[28] The estimate of muscle volume for the gastrocnemius and soleus was found through obtaining structural, T1-weighted, MR images and segmenting compartments based on tissue boundaries.[28] Soleus biopsy was followed by staining of histological samples, with anti-MHC II to isolate fast versus slow twitch fibres, the percent area of type-II fibres in the histological sample was used as an estimate the relative percent area for the entire muscle body.[28] The results showed that maximum contractile force normalised by soleus muscle volume and strength correlated with percentage area of type-II fibres, indicating that the normalised force metric could serve as a histology replacement.[28] This result is very encouraging, but the question must be asked about validity of using a force metric normalization as there is a contribution from other muscles in the triceps surae during muscle contraction. In addition, it has the draw back of the extensive data collection procedure requiring a dynamometer for force measurement, and a reflective marker camera system to determine ankle orientation.[28] With three maximum voluntary contractions as specific joint angles, followed by three isokinetic contractions at seven different angular velocities respectively the detailed set up and long protocol make it infeasible to replace biopsy.

Consequently, there is still a need for a non-invasive muscle biopsy alternative that is not dependent on regional selection, like the 1H-MRS technique, and does not require extensive set-up and time, like the forced based technique. The previous two MR techniques attempt to differentiate between muscle fibre type by leveraging metabolic differences between fibre types

[27] and their differences in contractile unit strength/rate of firing [28]. This still leaves the differences in perfusion, which come as a consequence of the spectrum of anaerobic to aerobic metabolism of muscle fibres, as a viable differentiator. The current work employs the metric of temporal fractal dimension, to detail BOLD signal complexity, to provide insight on the impact of the differing vascular organisation and perfusion for respective fibre types, as detailed in Chapter5 and Chapter 8.

3.3 BOLD and Phase Space Studies

The phase space is a method to describe non-linear systems and it is particularly of interest in describing the muscle activation, which it why it has been used in EMG studies. To the author's knowledge it has yet to be used to describe muscle activity state/state-transitions over time through the BOLD signal. In saying this, it has been used in a limited capacity to assess the non-linearity of neural activity via the BOLD imaging acquisitions, which is the closest parallel that can be used as reference in the present work. Here the distinction between muscle BOLD and neural BOLD studies signified by using the convention to call neural BOLD studies functional (fMRI).

Currently the use of fMRI and the phase space is limited to healthy cohorts, with the majority of the literature focusing on exploratory science and not to clinical translation. One study has focused on examining the non-linearity of the resting-state fMRI signal [85]. The spatiotemporal lyapunov exponent, which is a metric to describe the chaotic nature of a system, was calculated for resting-state fMRI and pure correlated noise to estimate system non-linearity. The results demonstrated that resting-state fMRI does not fully resemble noise, so the fMRI flucations may be an inherent model of basal neural activation. [85]. Additionally, the phase space representation of fMRI was used to as demonstrate how activation is achieved by transition from the resting-state critical point via a cascade process. [86] This was achieved through examining phase space transitions of resting-state fMRI data. [86] The phase space has also been used to examine the resting-state with the outlook of examining the connectivity of resting-state networks. [87] This study instead of using the conventional linear correlation technique to examine network connectivity, used phase synchronization between brain regions as characterized by a new metric "correlation between probabilities of recurrence". Notably phase synchronization was decreased between networks when comparing resting to an anesthetized state, indicating the validity of this metric and the phase space to examine neural deficiencies. [87] Similarly, resting-state fMRI phase space has been able to differentiate neural deficits in concussed compared to healthy children through investigating neural activity dispersion. The observed increase in resting-state neural activity dispersion in healthy compared to concussed brain, with a regional dependency, suggests healthy children could have an improved ability to transition from dispersed to focused neural activity during tasks. This work at the time of this thesis is currently being prepared for publication. Interestingly, another group has created a metric which they term, temporal coherence mapping, by correlating the transition states of the fMRI resting-state phase space.[88] This metric is used to understand how the brain activity in the present will affect future activity. [88] The final study of note was an exploratory analysis of the fMRI phase space during a simple fingering tapping motor task paradigm as opposed to at rest. [89] This work showed that the phase space where the active and resting states could be readily separated was a more functionally active region, which was validated through comparison with the activation shown via correlation with the ideal hemodynamic response function.

Additionally, the work showed how the phase space separability is sensitive to hand-dominance and thus could quantify brain state organization as an activation metric, as opposed to pure amplitude metrics. This work informed the exploration into muscle activation during a simple ankle flexion paradigm as detailed in Chapter9.

3.4 Muscle MRI and EMG Studies

Their have been numerous investigations of muscle using MRI and EMG due to their complementary pairing, as MRI has high spatial resolution and EMG high temporal resolution. As such, muscle MRI is often used to collect spatial information regarding muscle architecture and EMG used to collected functional information through the electrical activation profile during contraction. This thesis uses both EMG and rapid muscle BOLD imaging, which has good temporal resolution with at TR=110ms, to gain simultaneous functional information on muscle, as opposed to complementary spatial and functional information conventionally explored. Despite the difference in utility in the MRI acquisition to the existing literature, a coverage of muscle MRI, primarily used for static information, and EMG still provides relevant backing of this work. To limit scope animal and infant studies are excluded from discussion. The coverage is roughly broken down by anatomical location.

To begin muscle MRI and EMG has been used to assess muscle function and its innervation in the upper limb. One study explored the use of EMG and T2-mapping of the biceps brachii to examine muscle fatigue.[90] They used the metric of integrated root mean squared EMG (IEMG), and the increase in IEMG as the fatigue metric.[90] IEMG was determined by taking the l-s integral of the EMG and multiplying by the square root of 2. Mirroring the IEMG measure, T2 increased as a function of relative resistance when either concentric or eccentric actions were performed, indicating that T2 value could be used to indicate muscle fatigue. [90] More recently, the technique of graphical signal processing was extended to similar investigation of the biceps while measuring surface EMG and using MRI to examine changes in T2 time as a function of exercise. [91] Using a novel approach to define EMG origins, the muscle activation patterns of four subjects performing four isometric tasks are estimated using a resistive network for the given MRI morphology. [91] Without going into much detail, 90% the activation of the surface EMG was able to be explained by the muscle models derived through solving an inverse problem. [91] Additionally, MRI and EMG have been paired to examine the effects of deinnervation on muscle.[92] In this study population the primary point of affliction was impairment to the upper limb with 30% of subjects having upper extremity peripheral nerve injury, 20% in the lower limb and 44% having lumbar radiculopathy.[92] Notably an increase in spontaneous EMG activity directly correlated with increased signal on STIR MRI, which indicates deinnervation.[92] This showed the utility in using STIR to assess deinnervation in the muscle.[92] Another study also was in agreement with the secondary findings in this study in regards to the usefulness of MRI and EMG to assess radiculopathy. [93] Muscle deinnervation assessment through MRI and EMG is not of primary interest of the current study, but if further information is desired these additional sources can be referenced [94]–[96] .

The next region to be discussed is the core/back. One study examined muscle functional MRI (mfMRI), which is the difference in T2 value when comparing prior to post exercise state, and EMG of the lumbar back muscles.[97] This work demonstrated that there is a linear relationship between increase in exercise intensity and T2 value increase, which also held for

increased EMG amplitude, as a function of exercise. [97] This work has the primary contribution of demonstrating the linear relationship of mfMRI and EMG with exercise intensity and the validity of accessing lumbar activity using each technique in isolation. [97] Furthermore, one study used structural MRI to investigate cross-sectional area increases in core muscle tone and the corresponding EMG response after a 4 week exercise paradigm. [98] The EMG activity increased in the rectus abdominis, which correlated with the increases in muscle tone in the core muscles, indicating the strengthening paradigm increased muscle functional output. [98]

The final area of discussion, which is of utmost relevance to this thesis is EMG and MRI studies that focus on the lower limb. The first study of note is one that investigated the activation of triceps surae, consisting of the soleus and two gastrocnemius muscle bellies, using mfMRI and EMG. [99] The study consisted of 6 males and used mfMRI to examine the differences in the T2 transverse relaxation times at rest and immediately after exercise, while EMG was recorded during exercise. [99] EMG was recorded from the middle of the gastrocnemius medialis and lateralus, soleus and tibialis anterior muscle bellies, with the reference on the thigh bone. [99] The exercise consisted of three separate trials which increased in weighting of, bilateral, unilateral and unilateral with an additional 15% of body weight standing calf-raises. [99] The results showed that mfMRI signals and integrated EMG activity correlate with workload in individual triceps surae muscles, but less so in the lateral gastrocnemius. [99] This work although with non-concurrent MRI/EMG demonstrates the utility of functional muscular imaging in the leg. Another study also used mfMRI and EMG to examine the lower leg, but instead investigated the effect of knee angle upon plantar flexion. [100] This study used two separate groups who were height and weight matched who performed identical protocols while assessing muscle activation with MRI or EMG respectively. [100] The exercise paradigm consisted of dynamic plantar flexion at 25% maximal voluntary contraction for 2 minutes while the knee was extended (0° flexion), flexed (90°), and partially flexed (45°).[100] The EMG electrodes were placed on the two gastrocnemius bellies, soleus, and tibilias anterior, with comparison of T2 changes from the MRI also in these muscles. [100] The muscles groups with significant increases in T2 after exercise corresponded with the EMG increases in mean amplitude and were, the medial/lateral gastrocnemius (0° flexion), soleus (90° flexion), soleus and lateral gastrocnemius (45° flexion). [100] [100] This work signified the dependence of subject leg orientation during functional imaging of the lower leg when examining regional activation.

Furthermore, the mfMRI and EMG has been used to examine leg function in elite cyclists, with the intended outlook of examining muscle activation homogeneity. [101] 8 professional cyclists performed cycling on an electrically braked cycle ergometer with concurrent EMG, in eight muscles of the right lower limb (i.e. hamstrings, quadriceps, gastrocnemius and tibialis anterior), and respiration measurement.[101] Before cycling with constant workload increases or after 3 hours of recovery, an MRI session was used to examine differences in transverse relaxation times of muscles in the quadriceps. [101] Interestingly, the study showed that the EMG activation patterns and T2 value increases across muscles were varied based on cyclist even with similar maximal oxygen consumption and training volume. [101] This work demonstrates the heterogeneity of muscle recruitment among subjects in a uniform subject group, so multi-subject studies such as this one will be heavily affected by subject biological variability. Another study of interest, is one that examined hamstring function during hip extension using not only the combination of mfMRI and EMG, but also muscle cross sectional area measures through MRI. [102] MRI and EMG tests were performed separately with MRI acquisitions occurring at

rest, immediately after, 2 and 7 days after the exercise. [102] Six males underwent the exercise protocol consisting of 5 sets of 10 repetitions of the hip extension while EMG was recorded for the biceps femoris long head, semitendinosus, and semimembranosus muscles. [102] The results showed that the the integrated EMG values, normalized by MVC iEMG, increased in the biceps femoris long head and semimembranosus, and were significantly higher than in the semitendinosus. [102] Additionally, immediately post exercise the semimembranosus showed increases in T2 value and cross sectional area. [102] This work was the first to investigation hip flexion using this novel technique and showed how the cross sectional area of muscle changes after exercise. Similarly, another study examined hamstring function, but with the use of a knee flexion instead of hip extension exercise paradigm. [103] In order to investigate fatigue effects, EMG of the hamstring was recorded for 7 males who performed eccentric knee flexion exercise. [103] Prior to and post exercise mfMRI images and the maximum isometric knee flexion torque was captured.[103] As expected based on previous literature the T2 values when comparing pre to post exercise were significantly increased in the bicep femoris, semitendinosus, and semimembranosus muscles. [103] But interestingly, post exercise the circumferences of bicep femoris, semitendinosus, and semimembranosus muscles increased showing similar results to [102]. Additionally, the average EMG decreased in all muscle groups from the first to fifth set of exercise, which could suggest extreme neuromuscular fatigue. [103] This work provided novel insight into the EMG at extreme fatigue compared to minimal fatigue where the correlation with mfMRI T2 value increases goes from being positively correlated to negatively correlated.

The final study of note, that may be arguably the most important is the work performed in a Master's thesis exploring the use of concurrent BOLD and EMG. [104] This work demonstrated the feasibility of collecting concurrent muscle BOLD and EMG of the lower leg, which set the foundation for the work explored in this thesis in Chapter 11. This focus of the previous work was on the feasibility of the development of the MRI compatible EMG and denoising architecture. [104] The exercise was performed in two stints with either 30% or 50% MVC and consisted of plantar flexion during simultaneous EMG acquisition, which was not performed by other studies. Two EMG electrodes were placed on the right medial gastrocnemius and reference on the ankle. In addition to demonstrating concurrent muscle BOLD/EMG feasibility, the work performed a small investigation into the relation of muscle contractile strength and BOLD time to return to rest. It showed a correlation between increased relative muscle effort and an increase in time to return to rest. These results although profound are extended upon in this work. The true novelty in this work is providing non-static functional information about muscle with concurrent EMG measures, as opposed to the static measures used in the mfMRI studies. Additionally these mfMRI studies only occur pre and post exercise providing little to no dynamic information about the muscle behaviour.

Chapter 4

Research Hypothesis, Objective and Aims

4.1 General Objective

Use a novel complex representation of muscle BOLD and EMG to understand and quantify muscle behaviour during rest and simple lower limb exercise paradigms.

4.2 General Hypothesis

If muscle at rest and during activation is described through the complex metrics of the fractal dimension and phase space organization, then this will lead to novel insights on muscle structure and will more accurately describe the process of muscle activation gradient.

4.3 Specific Objectives

The general objective can be broken down into three major objectives:

1. Use the fractal dimension to differentiate between muscles in the lower leg
    - This objective would inform the development of a non-invasive biopsy alternative
2. Use the phase space to gain insight into muscle activation state
    - This objective would describe muscle activation using a gradient, which is important in describing muscle function in healthy versus diseased populations
3. Use a saturation band to gain insight into arterial inflow effects
    - This objective would describe how a saturation band could be relevant in noise suppression, which is important to more accurately describe muscle activation
4. Use the concurrent EMG and BOLD signal to relate perfusion and electrical activation
    - This objective would show the importance to MRI compatible EMG systems and if it is worth developing for clinical use

4.4 Specific Hypotheses

1. *Use the fractal dimension to differentiate between muscles in the lower leg*
   If a bi-fractal representation of the temporal BOLD signal is used to describe muscles with varying twitch fibre profiles then the gastrocnemius, soleus, and anterior group will show differing fractal dimensions, due to muscle fibre dependent perfusion differences.
2. *Use the phase space to gain insight into muscle activation state*
   If the phase space is used to examine muscle during a lower limb exercise paradigm then it will demonstrate that muscle activation is a gradient by identifying more than two states.
3. *Use a saturation band to gain insight into arterial inflow effects*
   If a saturation band is placed superior to the imaging slices then the effect of arterial in-flow will be reduced, leading to less noise in the data and improved muscle activation assessment.
4. *Use the concurrent EMG and BOLD signal to relate perfusion and electrical activation*
   If muscle fatigue is observed with EMG then the BOLD centroid, describing perfusion rate, and the BOLD area under the curve, describing perfusion magnitude, will increase.

4.5 Specific Aims

1. General Development
   - Design and construct a MRI compatible ankle flexion ergometer to allow for simple lower leg exercise paradigms
   - Design and build a MRI compatible EMG circuit that will interface with the MR compatible ECG leads and record data for later analysis
2. Protocol
   - Implement an optimal bracing technique to reduce head, torso and excess lower limb motion to limit motion artifact
   - Design a protocol to allow for the use of an MRI compatible ankle flexion ergometer while restricting EMG lead motion and subsequent noise effects
3. Data Collection/Analysis
   - Record concurrent EMG and muscle BOLD to achieve high spatial and temporal resolution of muscular activity
   - Reduce the distortion effects of EMG on MR images, that cannot be addressed by the study protocol, with post-processing noise reduction algorithms
   - Improve the quality of the EMG data, which is degraded due to the eddy currents caused by the static magnetic field, with noise reduction algorithms
4. Physiological Measures
   - Determine the spatial temporal muscle activation characteristics using the high temporal and spatial resolution of EMG and BOLD MRI respectively

- Determine the effect of muscle fatigue during exercise on EMG and muscle BOLD recordings
- Determine muscle differences based on perfusion
- Describe muscle activation patterns using complex measures to provide novel insight relative to the binary active/in-active representation

Chapter 5

Pilot Study

5.1 Declaration

Please note that this section was written by Joshua Ethan McGillivray (JEM) with intent to publish. As such, there was collaboration with Alejandro Amador (AA). This work will be used for a first author publication for JEM with AA as a secondary author. AA is responsible for the spectroscopy data collection/analysis portion of this pilot study. This included writing the spectroscopy data collection/analysis/results section and generating the spectroscopy figure 5.1.

5.2 Abstract

5.2.1 Background

Magnetic resonance imaging (MRI) solutions to replace muscle biopsy have had limited success. They attempt to differentiate fibre type by metabolism and contractile unit firing strength/rate differences, leaving perfusion differences as an unexplored viable differentiator. The prominent use of the fractal dimension in the functional MRI literature suggests its potential to isolate fibre types based on the differing vascular profiles.

5.2.2 Purpose

To investigate the use of non-invasive magnetic resonance imaging techniques via metrics of metabolism and blood flow to characterize muscle fibre profiles.

5.2.3 Methods

Eight male subjects (4 endurance/slow-twitch: 4 power/fast-twitch athletes), were grouped based on their physical activity habits. Activity groupings were confirmed using proton magnetic resonance spectroscopy to determine the tibialis anterior carnosine metabolic profile. Resting-state muscle blood oxygen level-dependent (BOLD) images were collected, and soleus, gastrocnemius, and anterior muscles were manually segmented for their differing fibre type profiles. Voxel-wise normalized and segmented BOLD time-series bifractal dimension was computed using the scaled windowed variance approach, with linear detrending. The bifractal dimension was computed by estimating the slope by fitting two lines, components 1 and 2, to the non-saturated portion of the log-log plot for a given voxel and segment, then averaging across segments.

5.2.4 Results

Higher relative carnosine levels were observed in fast-twitch compared to slow-twitch participants, confirming predicted activity-induced fibre differentiation. The median bifractal dimension followed the trend of soleus > gastrocnemius > anterior muscles. Across subjects, the bifractal dimension for each muscle was significantly different with component 1 and 2 p-values of 5.43e-7 and 1.41e-5. Regardless of muscle or component, significant differences, all p values $p<0.01$, were seen when comparing between groups for each muscle respectively. Variable component discriminability was observed with component 1 being influenced by fast-twitch and component 2 by slow-twitch fibres.

5.2.5 Conclusion

Median voxel bifractal dimension differentiated soleus, gastrocnemius, and anterior muscles within subjects, and based on activity groupings, with a larger fractal dimension indicating a higher slow-twitch fibre density.

5.3 Introduction

Research in sport has allowed humans to push the boundaries of possibility by developing optimal training paradigms by investigating factors that affect muscle such as nutrition, metabolism, and mechanics.[105], [106] The fundamental contractile unit of muscle, muscle fibres, can be broadly grouped into three types: type I (slow-twitch oxidative (STO)), type IIA (fast-twitch oxidative (FTO)) and type IIB (fast-twitch glycolytic (FTG)). They are classified based on their rate of shortening, which is directly correlated with myosin ATPase activity, perfusion, and primary metabolic pathway [36]. Research shows that habitual endurance exercise training reduces the volume of fast-twitch fibres and increases slow-twitch fibre volume on the order of 20% [107]. These findings were enabled by performing, muscle biopsies, which identifies fibre type ratios, provides insight into muscle health and performance by allowing for comparison to known muscle norms [24]. Biopsy, although useful, is invasive and leads to muscle damage that stunts training, thus preventing its adoption despite its benefit of dynamic muscle fibre profile assessment as a function of training.

Currently, magnetic resonance imaging (MRI) has provided preliminary solutions to replace muscle biopsy. Through using MRI, entire muscle cross-sections can be non-invasively examined, which removes the inaccuracy of the subsampling error due to the chosen biopsy samples by providing a larger distribution of muscle fibres. One MRI alternative uses muscle carnosine levels, heavily involved in muscle cell homeostasis during contraction [108], measured via hydrogen magnetic resonance spectroscopy (1H-MRS), where increased levels were found in the fast-twitch fibres of young, experienced, and ex-athletes in the gastrocnemius muscle [27]. Although this result is encouraging, 1H-MRS is highly sensitive to B0 field homogeneity and lipids, leading to results that are variable and highly dependent on voxel placement. Another proposed biopsy replacement uses measures of maximum muscle contractile force and strength during plantar flexion and structural MR images to estimate muscle volume [28]. The results showed that maximum contractile force normalized by soleus muscle volume and strength correlated with the percentage area of type-II fibres, indicating that the normalized force metric

could serve as a histology replacement [28]. Regrettably, the extensive data collection procedure requiring a dynamometer for force measurement, and a reflective marker camera system to determine ankle orientation limits the technique's reproducibility and consequent adoption [28].

The previous two MR techniques differentiate between muscle fibre types by leveraging differences in metabolism [27], [109] and in contractile unit firing strength/rate [28], leaving perfusion differences as an unexplored viable differentiator. Functional magnetic resonance imaging (fMRI) employs the blood oxygenation level-dependent (BOLD) effect to non-invasively provide insight into the blood flow and metabolic profiles of tissues, such as brain and skeletal muscle, in both healthy and diseased populations [24], [32], [45]. Furthermore, fMRI BOLD signal complexity has been used to differentiate healthy subjects from those with Alzheimer's disease [62] and mild traumatic brain injury [63]. In both instances the differentiating metric is the fractal dimension (FD), which is a measure of the self-similarity and complexity of a system in either the spatial or temporal domain [58], [59]. Since muscle BOLD signal is hypothesized to originate from the microvasculature and it is known that type I and II fibres have differing perfusion demands, this suggests that the muscle BOLD signal could characterize muscle fibre profiles [24], [47]. The fractal organization and scale-independent self-similarity of both the muscle and circulatory system, and the prominent use of FD in the fMRI literature and in neural imaging research suggest that the temporal FD of the skeletal muscle BOLD signal could isolate for fibre type based on the differing vascular profiles. This non-invasive MRI-based metric could monitor the dynamic changes in fibre type as a function of training, which could revolutionize the development of training plans for power/endurance athletes alike, pushing the boundaries of sport.

5.4 Methods

5.4.1 Subjects

Eight athletic male subjects (n=8, age 26±2.4yr, height 178±5.6cm, weight 71±9.2kg) were recruited and consented to participation in the HREB-approved research protocol. Recruitment numbers and population were limited due to compliance with hospital COVID-19 safety protocols. All subjects were preliminarily grouped into endurance and power sport groupings. The four endurance athletes were all long-distance runners, and power athletes participated in weightlifting, hockey, soccer, and fencing based on recommendations from the literature [110]. Preliminary groupings were made on the basis of fibre profile differentiation due to habitual activity performance [107]. Therefore, endurance compared to power athletes should show a greater relative amount of STO fibres. Similar to the work in [27], where increased levels of carnosine were correlated with higher fast-twitch fibre density, the relative carnosine concentration in participant's tibialis anterior served as a quantitative confirmation of the hypothesized activity-based groupings. After performing this combination of quantitative and qualitative assessments on all participants, four showed fast-twitch characteristics and four slow-twitch, which is summarized in Tab. 5.1.

TABLE 5.1: Summary of participant muscle composition classification. Classification decisions made based on the agreement of the activity grouping and relative tibialis anterior carnosine concentration. The eight preliminary participants were grouped into two groups of four for subsequent analysis.

Subject	Primary Exercise	Activity Group	Relative Carnosine Concentration	Primary Muscle Fibre Type Estimate
1	Distance Running	Endurance	0.0035	Slow-twitch
2	Weightlifting	Power	0.0145	Fast-twitch
3	Hockey	Power	0.0145	Fast-twitch
4	Distance Running	Endurance	0.0047	Slow-twitch
5	Soccer	Power	0.0080	Fast-twitch
6	Distance Running	Endurance	0.0077	Slow-twitch
7	Distance Running	Endurance	0.0070	Slow-twitch
8	Fencing	Power	0.0113	Fast-twitch

5.4.2 Functional and Spectroscopy Data Acquisition

Participants lay on the scanner bed for 30min prior to collecting images of the right lower leg. This allowed for the normalization of muscle compartment size, which changes with contraction and blood flow in the legs, shown to affect the skeletal muscle BOLD signal and metabolism, which significantly differs during rest [111], [112]. A 16-channel transmit/receive extremity coil and GE Discovery MR750 3T MRI scanner were used. Padding was positioned under the legs and feet, and a Velcro strap was positioned across the scanning bed to brace the legs and limit movement, which can profoundly affect relatively lower resolution functional images and lead to poor MRS spectra quality due to inhomogeneous excitation. An anatomic reference was collected from proton density-weighted, fat-suppressed images (0.625x0.625x4mm, 15 slices, 1mm spacing, TE/TR/flip=30/3000ms/111deg). The anatomic reference was used to guide the voxel of interest (VOI) positioning to avoid large fat septa or other muscle groups. 1H-MRS (PRESS sequence, VOI=20x20x20mm3, TE/TR=30/1500ms, 256 averages, CHESS water suppression) data from a VOI in the tibialis anterior muscle were acquired. For functional image collection (2.5x2.5x10mm, no slice spacing, TE/TR/flip=35/109ms/70deg, 2434 volumes) two thick slices were collected to adequately sample the muscle while minimizing the repetition time (TR). Minimizing TR was essential to improve temporal resolution. If the sampling rate is too low there will be temporal smoothing of a possibly highly variable signal, thus masking its fractal complexity.

5.4.3 Spectroscopy

Data Preprocessing

1H-MRS raw data were preprocessed using the Tarquin software package [113]. Data was transient averaged, eddy-current corrected using an unsuppressed water acquisition, and frequency and phase-corrected with reference to the water peak located at 4.65ppm, followed by a 2x zero-filling and Fourier transformed. Finally, preprocessed data were exported for an in-house carnosine quantification analysis.

Data Analysis and Statistics

The carnosine proton MRS peaks are located on the higher side of the spectrum, giving rise to two resonance peaks at 8ppm (C2) and 7ppm (C4), which come from the imidazole protons of the carnosine molecule. The unpopulated higher side of the proton spectrum isolates the carnosine peaks from most of the peaks often present in 1H-MRS of skeletal muscle, such as lipids or creatine, showing little to no overlap with other metabolites as seen in the 1H-MRS sample spectrum in Fig. 5.1(top). This feature makes metabolite integration, followed by a metabolite ratio computation, a reliable and straightforward quantification method [114], using the water peak at 4.65ppm as an internal concentration reference. 1H-MRS quantification analysis was performed with an in-house program using MATLAB. First, the carnosine (at 8ppm) and water (at 4.65ppm) peaks were extracted from each participant's spectrum with a frequency window, centered at the corresponding frequency shift, with $\pm$0.3ppm and $\pm$0.2ppm, respectively, corresponding to twice the average FWHM of each peak[115]. The carnosine spectral window was detrended to account for the macromolecules and baseline of the spectra [116]. Finally, the absolute proton spectroscopy spectra of carnosine and water were integrated within the frequency window to account for baseline correction inaccuracy, followed by a ratio of carnosine vs. water for each participant. A t-test statistical analysis was performed, grouping the carnosine metabolite ratio by type of muscle fibres.

5.4.4 Functional

Data Preprocessing

Using the FMRIB Software Library, resting-state functional images were motion corrected, and the gastrocnemius [slow-twitch/fast-twitch dense], soleus [slow-twitch dense] and anterior muscles (tibialis anterior, peroneus and extensor longus groups) [fast-twitch dense] were manually segmented, using the high-resolution anatomical reference, for their differing twitch fibre profiles[117]. The first and last 193 volumes were truncated due to the short repetition time not satisfying the Ernst angle condition and motion considerations respectively [118]. BOLD time series were normalized by dividing by the first time point, to account for coil sensitivity and proximity signal amplitude dependence. The remaining normalized 2048 volumes were segmented into four 512-point windows, which provided an ideal base for fractal computation.

Data Analysis and Statistics

The temporal fractal dimension of the BOLD signal analysis, was modeled based on previous explorations of characterizing the temporal fractal signal through scaled windowed variance methods with detrending [119]. To facilitate computation of how the variance changes as a function of window size on a log-based scale the fractal time series is truncated to be of length of base two, 2n. Iteratively the signal is segmented into w windows of varying length where w = (2n/2m) for integer values of m such that m greater than or equal to 1 and less than or equal to n-1. For each window the baseline is corrected by fitting the slope of a line from the window start to end point and subtracting it from the given windowed time course [119]. Baseline correction is required due to BOLD time series baseline drift caused by gradient mechanical vibrations and heating, which affect shim quality and the effective voxel specific resonant frequency in echo planar imaging acquisitions [63]. For all w windows for a given window size 2m, the standard deviation for the given baseline corrected window is computed. The mean standard deviation

of all w windows for a window size of 2m is computed and stored. This is performed iteratively for all window sizes. To characterize the hypothesized exponential change in variability as a function of window size the average standard deviation is plotted against an increasing window size on a log-log scale. The fitted slope of this plot yields an estimate of the hurst exponential [119], which is related to the temporal fractal dimension (FD) through FD+H=1. To estimate these slopes, first the non-saturated portion of the plot was identified. We expect the slope of the log-log plot of variability as a function of window size to saturate as temporal variability appears invariable at large window sizes [120]. To employ a bi-fractal representation the slope estimates for each component are made by performing a linear fitting in the non-saturated portion of the plot between the smallest window size to the midpoint for component one and from the window midpoint to endpoint for component two. The decision to employ a bi-fractal representation was based on the original hypothesis of slow and fast twitch fibres having differing blood-flow complexity and some preliminary observations of two differing slopes during mono-fractal dimension fitting.

Analysis was performed on a voxel-wise basis due to the concern of significant effects being obscured by averaging. If the BOLD time series of all voxels within a given muscle of interest were averaged this would reduce the variance in the temporal signal. The reduced variance could limit the discrimination power of the temporal FD metric, which describes signal variance as a function of time scale. Consequently, as specifically detailed above, the voxel-wise BOLD time-series bi-fractal dimension was computed using the scaled windowed variance approach, with linear detrending, removing scanner-induced low-frequency variations [119]. For each voxel the segment-wise FD was computed over each of the four respective 512-point windows, then averaged across segments. Averaging the four FD measures across four-time windows improved voxel FD measure reliability, as the error associated with each linear slope FD estimate is reduced through the average. The alternative of averaging the four temporal windows and then computing the FD was undesirable as it would reduce temporal variation and the power of the FD metric. Furthermore, since temporal variability appears invariable at large window sizes, FD measures would be unreliable without segmentation [120]. A window size of 512 points was chosen to strike a balance between having a long enough window to have a sufficient number of points for linear fitting and enough statistical points for averaging.

Prior to performing any statistical analysis all bi-FD distributions for a given participant, component and muscle were tested for normality. All bi-FD voxel distributions were negatively skewed. Temporal complexity FD increases from one (non-complex) to two (purely complex) are non-linear, which could lead to the observed non-normal FD distribution. Post log transform correction distributions still failed Jarque-Bera normality tests, therefore Wilcoxon rank sum tests were used to examine within participant differences and Kruskal-Wallis to test within and between group differences.

5.5 Results

5.5.1 Spectroscopy Data - Metabolic Differences

The primary interest of this study was to examine the use of a bifractal model of the BOLD signal to characterize muscle twitch fibre profiles, which was achieved by comparing the soleus [slow-twitch], gastrocnemius [mixed-twitch], and anterior muscles of the lower leg [fast-twitch]. Muscle differences were examined on a participant level, but also through primary fibre type groupings.

These groupings can aid in removing the biological variability contributions through using the knowledge that performing endurance/power activities habitually will lead to predicted changes in muscle fibre type distributions.. A total of eight proton spectra were collected, showing an average linewidth quality of 14.5±1.7Hz. To ensure that the ratio reflects solely the behaviour of carnosine, a t-test was performed on the water peak integration between FT and ST groups, showing no statistical difference (p=0.09) between them. The power/fast-twitch compared to the endurance/slow-twitch groupings had significantly higher relative carnosine levels ($p < 0.05$) as seen in Fig. 5.1(bottom).

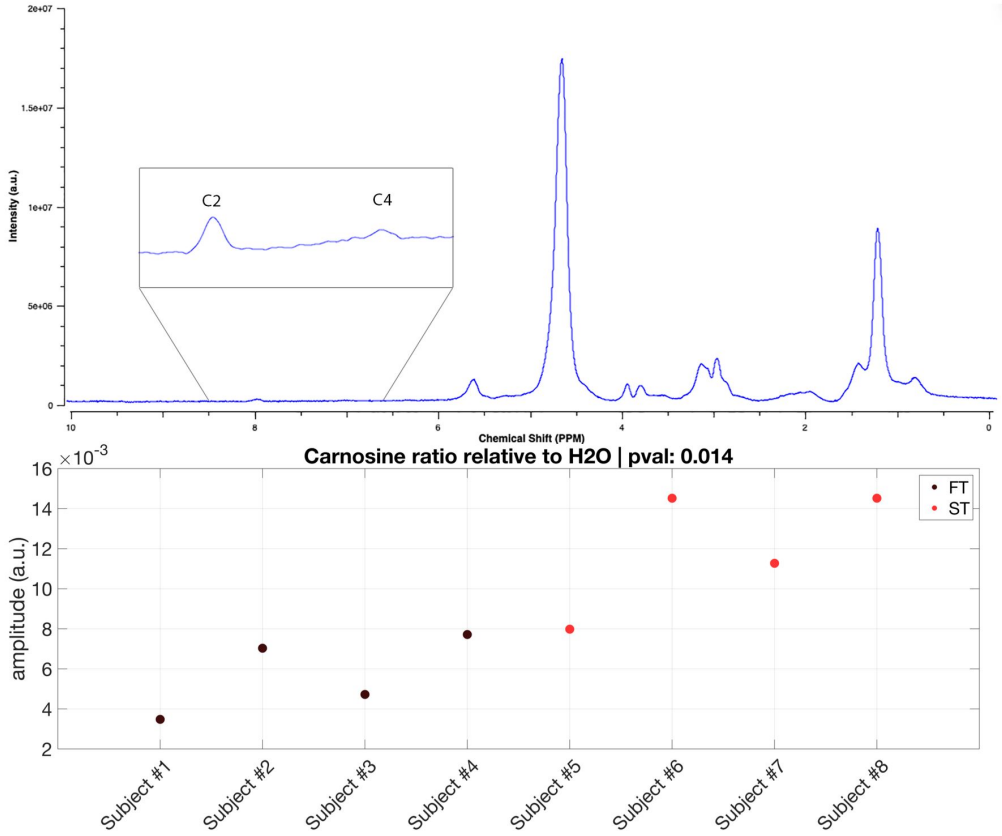

FIGURE 5.1: Illustration of the pathway from spectral data acquisition to relative carnosine estimate. The top image shows a sample hydrogen magnetic resonance spectrum after preliminary processing with no water suppression and labeled the creatine peaks (C2,C4). The bottom image shows resulting creatine approximation through an integration of the detrended spectrum while using water as a reference. The plot shows clear separation between predicted fast and slow twitch dominant participants from original activity grouping.

5.5.2 Functional Data - Perfusion Differences

Between Subject Analysis

When comparing across all subjects, there was a significant difference in the complexity of blood-flow depending on the muscle group. When comparing across muscles, significance levels were of similar order for both components, component 1 $p < 0.0001$ and component 2 $p < 0.0001$

Tab. 5.3. Furthermore, the median bifractal dimension was used, due to the non-normality of the fractal distributions, to assess if there was a trend with fractal dimension and density of particular fibre type. For both components the median FD across all subjects showed a trend of soleus > gastrocnemius > anterior muscles, as seen in Fig. 5.2. With significant differences between muscles across the entire subject cohort, further investigation for differences between activity groupings, within activity groupings and on a single participant basis were performed.

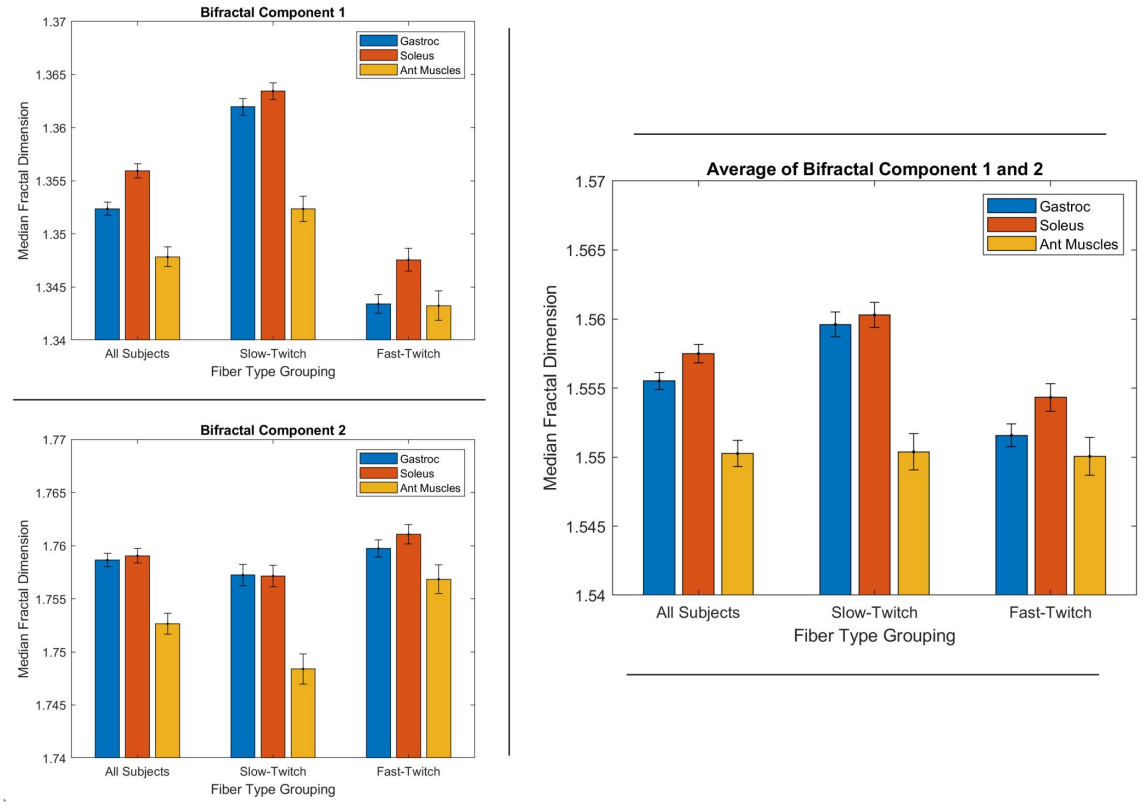

FIGURE 5.2: Comparison of median fractal dimension (FD) and median average deviation scaled by the square root of the sample number. Comparisons separated by component and activity grouping. Within activity grouping the FD trend is soleus > gastrocnemius > anterior group.

Between Activity Group Analysis

Comparisons were performed between the endurance/slow-twitch and power/fast-twitch grouped for each muscle respectively. Since habitual exercise induces fibre type differentiation, the same muscle would have different fibre type ratios for each group. Comparisons were performed by using ranked sum tests for each component of the fractal dimension for each muscle individually, and are summarized in Tab. 5.2. Significant differences are seen when comparing muscles between groups for all muscles and both components. Notably, component 1 relative to 2 shows greater differences between the groups in gastrocnemius and soleus and a smaller difference in the anterior muscle. The soleus and gastrocnemius containing more slow-twitch fibres than the anterior group suggests that the components' difference in discrimination could be related to fibre type, but this observation needs to be further explored.

TABLE 5.2: Summary of participant muscle blood-flow complexity differences. Comparisons were performed by testing differences between muscles for each component respectively, using different sets of participants. Kruskal-Wallis classification was employed due to skewed distribution of fractal dimension data. Across all participants there are differences between muscles. More significant differences are seen when examining the slow-twitch participants relative to the fast-twitch participants regardless of component.

Comparisons Bi-fractal Dimension Component 1		P Value (Ranked Sum Test)
Group Differences (Fast vs. Slow Twitch)	Gastrocnemius	6.655e-40
	Soleus	1.812e-28
	Anterior Group	4.404e-5
Comparisons Bi-fractal Dimension Component 2		**P Value (Prob. >Chi-sq)**
Group Differences (Fast vs. Slow Twitch)	Gastrocnemius	0.0126
	Soleus	0.00995
	Anterior Group	2.584e-5

Interestingly, for component 1 the FD of endurance/slow-twitch > power/fast-twitch group, but for component 2 the trend was reversed. This in combination with the variable muscle discriminability depending on component suggests a sensitivity to fibre type and/or particular activity grouping. Therefore, to remove the component sensitivity effect, the average of the two components was taken. This showed not only that the complexity was soleus > gastrocnemius > anterior muscles but also endurance/slow-twitch > power/fast-twitch group. The observations based on the activity groupings suggest a larger median fractal dimension corresponds to a higher slow-twitch fibre density and variable component fibre type sensitivity.

Within Activity Group Analysis

Since significant differences were found between muscles and there were differences between the muscles depending on the activity the participant performed, the next level of comparison was finding differences within a group of athletes who perform similar exercise. Differences between muscles were then assessed for participants in each activity grouping, and are summarized in Tab. 5.3. Endurance athletes had significant differences between their gastrocnemius, soleus and anterior grouping, whereas power athletes only showed marginally or non-significant differences. This suggests a greater variability in fast-twitch athlete fibre type distributions leading to less significant group-based conclusions.

Median muscle fractal dimensions were computed for each activity grouping for each component separately and are shown in in Fig. 5.2. When looking within a particular activity grouping the FD showed a trend of soleus > gastrocnemius > anterior muscles (in Fig. 5.2). This is in line with the behaviour observed across all subjects and suggests a larger median fractal dimension corresponds to a higher slow-twitch fibre density.

TABLE 5.3: Summary of participant muscle blood-flow complexity differences. Comparisons were performed by testing differences between muscles for each component respectively, using different sets of participants. Kruskal-Wallis classification was employed due to skewed distribution of fractal dimension data. Across all participants there are differences between muscles. More significant differences are seen when examining the slow-twitch participants relative to the fast-twitch participants regardless of component.

Comparisons Bi-fractal Dimension Component 1		P Value (Prob. >Chi-sq)
Muscle Differences (Gastrocnemius Vs. Soleus Vs. Anterior Group)	All Participants	5.430e-7
	Slow-twitch Group	1.948e-9
	Fast-twitch Group	0.0545
Comparisons Bi-fractal Dimension Component 2		P Value (Prob. >Chi-sq)
Muscle Differences (Gastrocnemius Vs. Soleus Vs. Anterior Group)	All Participants	1.411e-5
	Slow-twitch Group	4.507e-6
	Fast-twitch Group	0.2042

Subject-wise Analysis

The previous between and within group analyses demonstrated variable component sensitivity. To reduce biological variability contributions of subjects between and within a particular endurance or power group, a subject-wise analysis was performed to isolate for fibre type sensitivity effects. To further specify fibre type sensitivity, we used gastrocnemius comparisons, as its mixed fibre type ratio would be skewed to that of the predominant fibre type grouping. To be stated explicitly the fast-twitch group's mixed fibre type gastrocnemius should have a relatively higher density of fast-twitch fibres than for the slow-twitch group. Thus, when comparing muscles for the fast-twitch group, its' increased FT fibre content would make discrimination between fast-twitch muscles more difficult and slow-twitch muscles less difficult were compared to the slow-twitch group. Therefore muscle comparisons to identify fibre type sensitivity were achieved through performing subject-wise, ranked-sum muscle comparison tests for each component respectively. The p-values for each muscle comparison were averaged according to predominant muscle fibre type grouping to reduce subject-specific biological variability and the important comparisons are summarized in Tab. 5.4.

There are four key observations that suggest component specific fibre type sensitivity. The first is that component 1 has the best accuracy for the most dissimilar slow-twitch group's gastrocnemius versus anterior muscle comparison. The second is that for the fast-twitch group, which have the most dissimilar gastrocnemius versus soleus muscles, component 2 has the best discrimination. This not only demonstrates that the hypothesized greatest muscle differences are most easily differentiated, but also that one component is better than the other. The third observation is that, when comparing the gastrocnemius versus soleus, which are more similar for endurance/slow-twitch group, component 1 can significantly distinguish the two muscles, whereas component 2 cannot, with a non-significant p-value. The final observation is that, when comparing the gastrocnemius versus anterior muscles, which are more similar for the power/fast-twitch group, component 1 cannot significantly distinguish the two muscles, whereas component 2 can find a difference between the muscles with marginal significance. Therefore, the slow-twitch group focused comparison showed component 1 > component 2 discriminability and the fast-twitch group focused comparison was component 2 > component 1. Based on the

knowledge that similar muscle profiles should show decreased discriminability this suggests that component 1 is influenced by fast-twitch and component 2 by slow-twitch fibres.

TABLE 5.4: Summary of activity grouping averaged single subject ranked sum test p-values for muscle bifractal dimension component 1 (comp1) and 2 (comp2). Comparisons were chosen to isolate for similar muscle comparisons on the basis of predominate twitch fibre groups.

Primary Twitch Fibre Group	Gastrocnemius Vs. Soleus		Gastrocnemius Vs. Anterior Group	
	Component 1	Component 2	Component 1	Component 2
Slow	0.0403	0.346	0.0029	0.0730
Fast	0.0824	0.0097	0.116	0.0774

5.6 Discussion

Our results show skeletal muscle of the lower leg was able to be well characterized non-invasively through two MRI techniques. The first technique used spectroscopy in the tibialis anterior and a normalization method to determine relative carnosine levels, which allowed for placement of participants into predominant fibre type groupings. Proton spectroscopy is readily available in clinical settings and does not require additional hardware as is the case for phosphorus imaging, which is predominantly used for muscle imaging. Additionally, this normalization technique requires no external reference to quantify the carnosine concentration, which makes it more suitable in a clinical setting. The practicality of this spectroscopy method to provide an estimate of fibre type makes it a feasible and attractive alternative as a preliminary fibre typing assessment that could be used clinically or in the exercise science space.

The second technique used the temporal fractal dimension of the skeletal muscle BOLD signal to determine differences between muscles at a participant and activity grouping level. This leveraged the known differences in muscle fibre type perfusion to classify muscle fibre profiles via the complexity of the blood flow signal within a given volume. Specifically, the fractal dimension differentiated soleus, gastrocnemius, and anterior muscles when looking across subjects, on a single subject basis and based on endurance/power activity groupings. Greater complexity (larger fractal dimension) corresponded to increased relative slow-twitch fibre density. To find the direct relationship of complexity value to fibre type, biopsy samples would be required to corroborate specific complexity values. Additionally, it was shown that the two components of complexity had a fibre type sensitivity. Specifically, component 1 being influenced by fast-twitch and component 2 by slow-twitch fibres. Fibre type sensitivity that is variable for each component is an important observation as this means initial predominate activity classification, created using spectroscopy verification or other methods, can now be used to inform the decision on which complexity component to be used. Choosing a particular complexity component to improve differentiation between muscles and hence fibre type would improve personalized analysis for fibre type classification assessments. This indicates that muscle BOLD FD characterization could non-invasively provide information on muscle fibre type ratios, possibly replacing the need for muscle biopsy. With further refinement of this novel metric, it could provide greater insights than biopsy as it would allow for fibre type assessment in a larger subset of muscles, and would alleviate the subsampling variance associated with biopsy since with MRI entire muscle cross sections can be examined.

The primary limitation of our research pertains to our participants. One limitation pertaining to our participants, which is currently being addressed, is the gender imbalance of our study. Female athlete recruitment is the current focus, and it is required to validate our promising technique. Additionally, due to COVID-19 safety protocols, a limited subset of the general population could be recruited, which led to some heterogeneity in our athletes. The fast-twitch group had athletes from a variety of sport disciplines whereas the slow-twitch were all long distance runners. The heterogeneous fast-twitch population may have contributed to the increased variability in the fast-twitch athlete grouping comparison, leading to lower statistical significance and less confidence in the novel technique proposed. For instance, soccer requires both power and endurance in the lower limb. In saying this, the fact that a small non-heterogeneous study still showed such encouraging results shows the promise of the technique. Another limitation of our study is based on the fact that our MRI scanner does not allow for multiband image acquisition. Without multiband, the fastest two-slice acquisition was limited to the implemented TR of 109ms, which could ideally be halved with a multiband sequence. Therefore, we could be undersampling the temporal BOLD signal which could artificially reduce variance measures that are used in the computation of the fractal dimension. Practically this is only a research-based limitation, as most clinical MRIs do not have multiband imaging and our techniques would be well suited for their use.

Our research also holds a lot of weight clinically as a non-invasive replacement for muscle biopsy, which is the gold-standard diagnostic for those with neuromuscular disorders such as muscular dystrophy and myopathy [20], [24]. Remarkably, the global prevalence of neuromuscular disease is estimated to be $0.1 - 0.3\%$, which is comparable to that of Parkinson's [21]. A non-invasive biopsy replacement would alleviate patient pain and further damage of the already deteriorating muscles, associated with biopsy [25]. It could also improve on the current non-invasive clinical alternative non-fibre specific electromyography, which showed diagnostic accuracy on the order of 70% in comparison to 90% for biopsy [25]. Therefore, the combination of the two MRI metrics of relative carnosine concentration and muscle blood-flow signal complexity shows promise to act as a non-invasive biopsy replacement. Specifically, carnosine would be used to identify predominant fibre type, which would seed the selection of the relevant complexity component to perform muscle fibre type profiling using the BOLD signal complexity.

An MR-based non-invasive muscle fibre type assessment tool would remove the associated biopsy subsampling variance contribution, allow for sampling of any muscle and reduce the associated harm to the individual undertaking the assessment. This advancement enables researchers to examine muscle fibre profiles without associated participant harm so more studies with larger participant bases can be used to inform neuromuscular disorder diagnosis. Additionally, it will promote research in elite athletics, as there will no longer be the reservation to damage their muscle during training. The ability to dynamically monitor fibre type profiles in a variety of muscle groups and over the entire body would be invaluable to the sports community to develop the optimal training programs. This work sets the foundation and can inform the development of the MR non-invasive biopsy alternative to benefit both exercise scientists and clinicians alike.

Chapter 6

Development of a MRI Compatible Erogmeter and Electromyograph

6.1 Building an MRI Compatible Ergometer

The original intent of my thesis was to image the brain during cycling exercise and assess functional activation in the brain as a function of fatigue with concurrent EEG and EMG measures, this required a cycle ergometer with dynamic weighting. The combination of the inability to use the LODE ergometer and the dysfunctional state of the MRI compatible EEG caused my research focus shift to muscle imaging. With motion artifact being one of the largest difficulties in MRI when imaging the lower leg, isometric, as opposed to isokinetic, contraction is used. It is used for the reason that the muscle will be relatively stable during rest and contraction, and only when shifting between rest and contraction states will there be gross motion artifact. Therefore this limits the amount of data that needs to be discarded throughout the scan duration. The ergometer was designed with this in mind, as a cycle ergometer would no longer be suitable for lower-leg imaging due to the gross motion of the lower leg during pedaling. Therefore an ergometer needed to be designed to allow for simple isometric and possible isokinetic contraction paradigms through ankle flexion. To remain broad in its application the ergometer would be able to placed in the scanner so the participant is either head first (for neural scans) or foot first (for lower leg imaging) so it could be used for other studies in the lab.

6.1.1 Design Plan

The description for the original designed ergometer was more extensive than the implemented design and is elaborated on below. The ergometer will use weights to provide resistance against dorsi-/planter-flexion. Weights will vary in either 0.5- or 1-pound increments and will consist of lead blocks. The weights will be attached to a rope that will loop around a hook that attaches to a pedal acting on a pendulum. Using a wooden frame that will sit on the scanner bed, foot flexion will move the weight by pulling on the rope which is situated on a pulley. The rope will be hooked on the pedal on different sides for plantar- or dorsi- flexion to provide resistance in opposite directions, respectively. A participant's forefoot will interface the front face of the pedal and press down on the pedal with the ball of the foot for plantarflexion exercise. A participants forefoot will interface the back face of the pedal and press the pedal with the top of the forefoot for dorsiflexion exercise. The pedal suspended from the top of the wooden frame will remain constant length and a prop placed under the calf to account for differing foot size. The

weighting will vary between participants in order to get relatively similar efforts. Weightings will be scaled based on initial maximal voluntary contraction (MVC) measures.

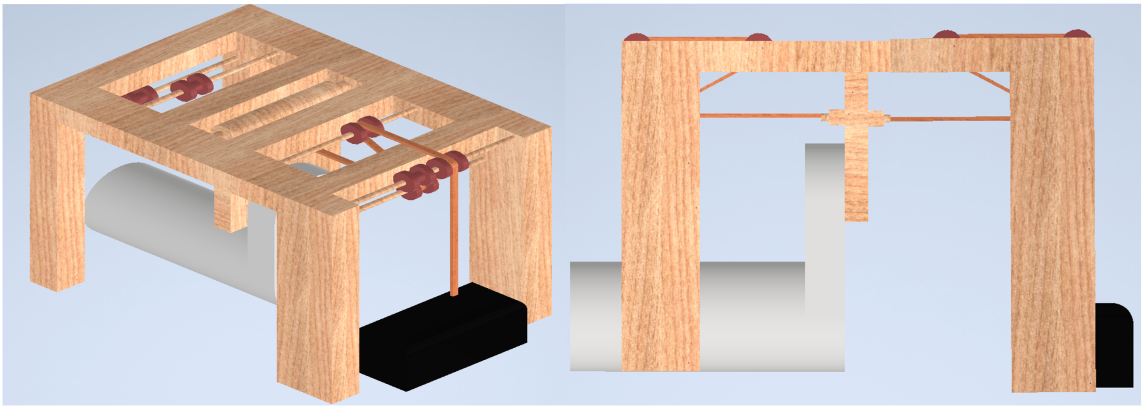

FIGURE 6.1: Original AutoCAD model of weighted ankle flexion device. Left image is the pedal in weighted dorsiflexion orientation and right image is weighted plantar flexion orientation

6.1.2 Design Considerations

General Considerations

1. The ergometer must be able to be positioned at both the foot or head of the scanner bed
   - Having the weighted pedals at the foot of the table would allow for the head coil to be used for neural imaging studies
   - Having the weighted pedals at the head of the table would allow for the leg coil to be used for muscular imaging studies
2. Small enough to place on the scanning table
3. Light enough to be able to transport from storage to the scanner room with ease
   - This could be achieved by having the ergometer in multiple parts
4. Avoid metals when possible and stick to wood and plastics
   - Ferromagnetic materials must be avoided all together
   - Non ferromagentic materials will still experience translational forces and torque within the bore, so they should be avoided
   - Metal will heat up in the magnet so any metal used should be well away from participant interfaces
5. Need to be able to perform plantar- and dorsi-flexion
   - Allows one to examine different muscles depending on the direction of ankle flexion
6. Need to have possibility to perform flexion of both ankles either both at once or one in isolation

- This is imperative to fMRI paradigms where unilateral and bilateral activation can be compared

7. Need to have weighted ankle flexion
    - This is imperative to simulate more realistic scenarios of muscle activation
    - This would allow for comparison other studies which use simple flexion or cycling ergometers
8. Need to be able to vary the weighting based on participant weight and activity level
    - This is imperative to ensure that the relative effort is comparable across participants
    - Resistance bands or sand/lead weights could be viable options to provide resistance
9. Need to quantify exertion, ideally via force based measurements
    - Force sensing resistors – simple way to compute force
    - Strain gauge – deformation of beam (i.e., aluminum)
    - Load cell – higher level version of strain gauge method
    - Optical based – can record lengthening of resistance bands
    - Ultrasound based – can record resistance band lengthening

Force Measurement Considerations

It should be noted despite consideration the forced basic metrics were not implemented and only a static weight was used. A force plate option by measuring the deformation of aluminium plates was deemed invalid. The eddy current induction in the moving metal through the field would yield inaccurate readings. An ultrasound distance measurement to determine weight displacement was also rendered infeasible. This is because the ultrasound sensor pulse rate operated in the same frequency bandwidth as the RF, causing inaccurate readings. This was not of primary concern as the weighting system could be used as an estimate of force production. This provides relative information of a force measurement, which does not specific the contribution from each muscle in the lower leg individually.

MRI Bore Restrictions

To perform ankle flexion concurrently with muscle imaging the ergometer needed to fit within the bore of the MRI as the lower-leg would be placed at the magnet iso-center. The ankle flexion system thus had to fit within the bore of the GE Discovery 750MR. The general dimensions of the bore were measured and can be seen in the sketch below, Fig. 6.2. It should be noted that the padding at the base of the bore can be removed to allow for a greater available height for the ergometer. The major restriction posed by placing the ergometer in the bore is the height restriction, as there needs to be enough clearance for the pedals, the pulley system, and the non-forefoot portion of the participant's foot, which will not be interfacing the pedal. The difficulty with designing within a circular bore is that the width at a particular height is related to the curvature of the circle. The relation for the height is width are illustrated in Fig. 6.3.

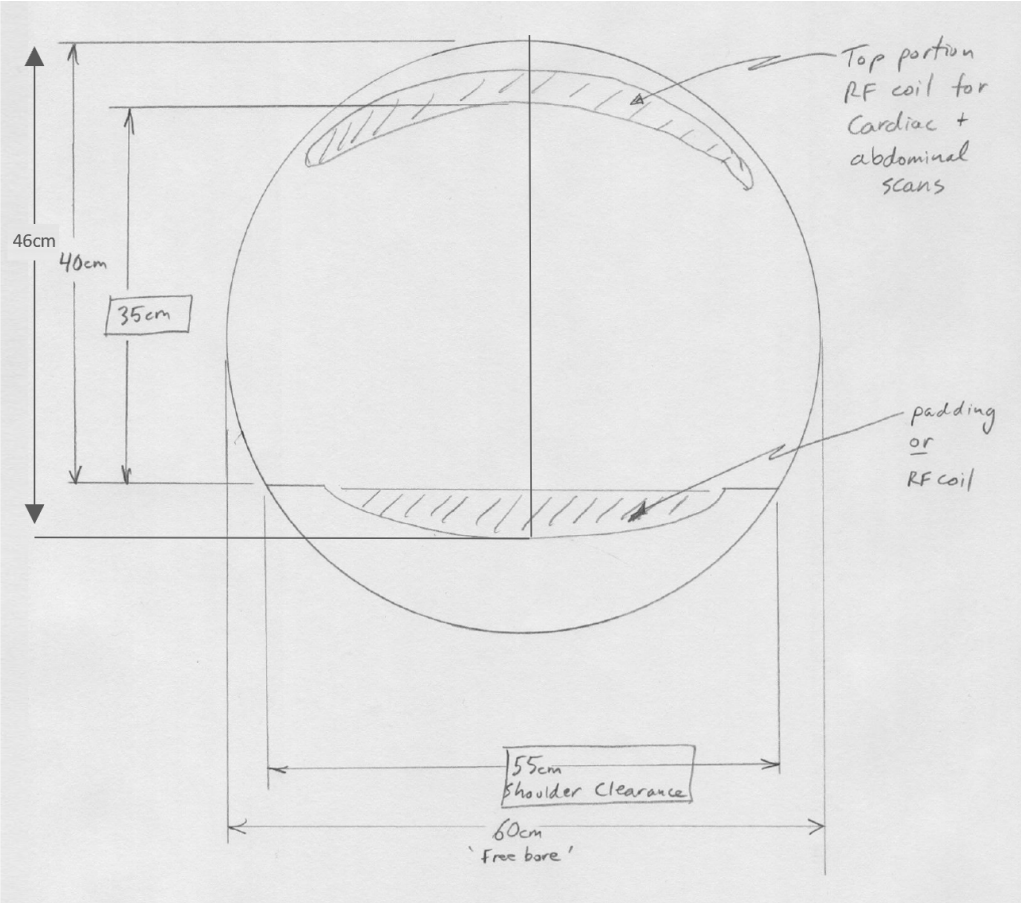

FIGURE 6.2: Sketch of primary in bore dimensions of GE Discovery 750MR

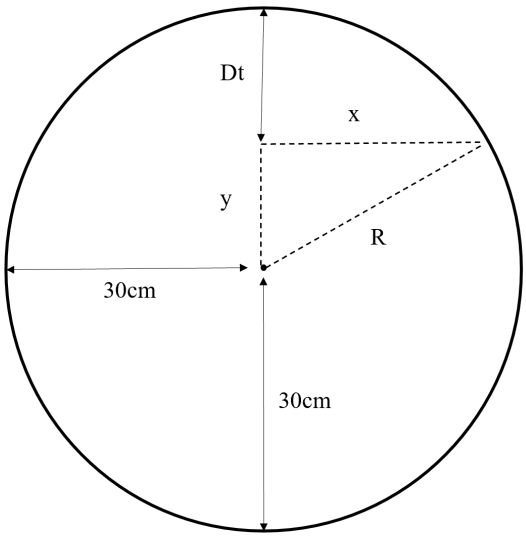

Since we know the radius of the bore is 30cm we can solve for the bore diameter at a particular height.

Distance from top = Dt = R - y
Bore diameter = Dia = 2x
Maximum allowable height = R + y

Using Pythagorean's theorem:

$$R^2 = x^2 - y^2$$

$$\text{Dia} = 2\sqrt{R^2 - y^2}$$

$$\text{Dia} = 2\sqrt{R^2 - (R - Dt)^2}$$

FIGURE 6.3: Sketch of primary in bore dimensions of GE Discovery 750MR and relation to height and width constraints

With this in mind, the major constraint on the width and height restrictions are in relation to the foot sizing. The ergometer must be designed so the pedals are large enough for the forefoot to rest on them (for plantar flexion movement), while still having a large enough gap for the leg to pass underneath so the top of the foot can press on the pedal (for doriflexion movement). The need for these sizing specification as well as the relative foot orientation for each ankle flexion movement can be seen in Fig. 6.1. Additionally, foot width influences pedal width as if you want two adjacent pedals this affects the frame width.

To accommodate the sizes differences in feet amount participants the pedals were designed in the range of size 5 women's to size 12 men's shoes. Using a standard US sizing chart and known relationships between foot height and width [121] the following constraints/conclusions were made.

- Total foot length can be gathered from a sizing chart
- Maximum foot width is 61.8% of foot length
- Based on instep height location, approximately 45% of foot is usable (i.e. can interface with the pedal)
- Based off instep height and my approximations 35-40% of foot length is "ankle thickness" (i.e. the portion of the leg which needs to pass under the pedal in dorsiflexion)

Table 6.1: Foot length and width approximations to inform pedal design specifications.

Foot Size	**Foot Length**	**Foot Width**	**Useable Foot Length**	**Ankle Thickness**
Women's 5	22 cm	14 cm	10 cm	9 cm
Men's 12	29 cm	18 cm	13 cm	12 cm

Using these constraints the pedal dimensions were approximated using the inferences from Tab. 6.1. Therefore, we can determine the minimum pedal width should be 18cm, the force sensitive part of the pedal should be approximately 13cm long, length from the top of the force sensitive part of the pedal to the scanner bed is 29cm, the gap between the bottom of the pedal and scanner bed is 12cm. In case of small women's foot can provide prop to reach the pedal. Also with these measures all feet will have ankle clearance if remove 6cm padding layer for larger feet/legs.

Frame and Pedal Sizing

Given the bore height and width restrictions and the relative pedal sizing requirements, as detailed above, the frame to hold the pedals for the ergometer was designed. The drawings detail all the frame and pedal dimensions such that they would fit on the MRI table and within the bore. This design was modeled in Inventor, Fig. 6.6, and constructed at home with a very limited tool set. 8 custom pulley's were ordered from Grainger Canada Item number WWG4FRX2 for $46. Various lumber sizing of planks, brass screws, wooden dowel's, wood glue, and aluminum bars for the axles were sourced from Home Depot to make the pedal frame. Plywood sheets, also bought from home depot, were used to make the table for the ergometer to interface. Due to the inflation of lumbar prices the Home Depot bill totaled $302.

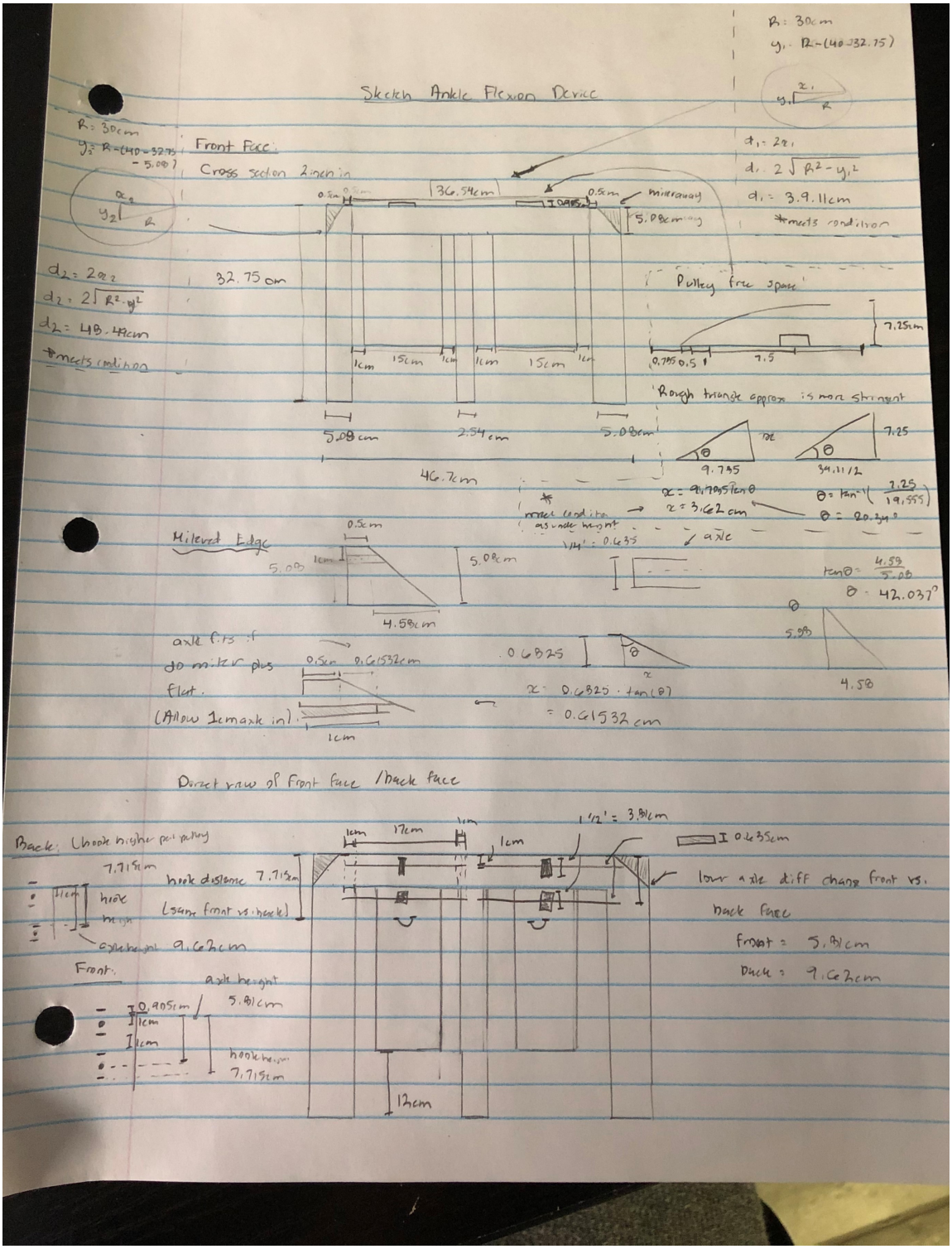

FIGURE 6.4: Sketch of ergometer pedal housing design, page 1

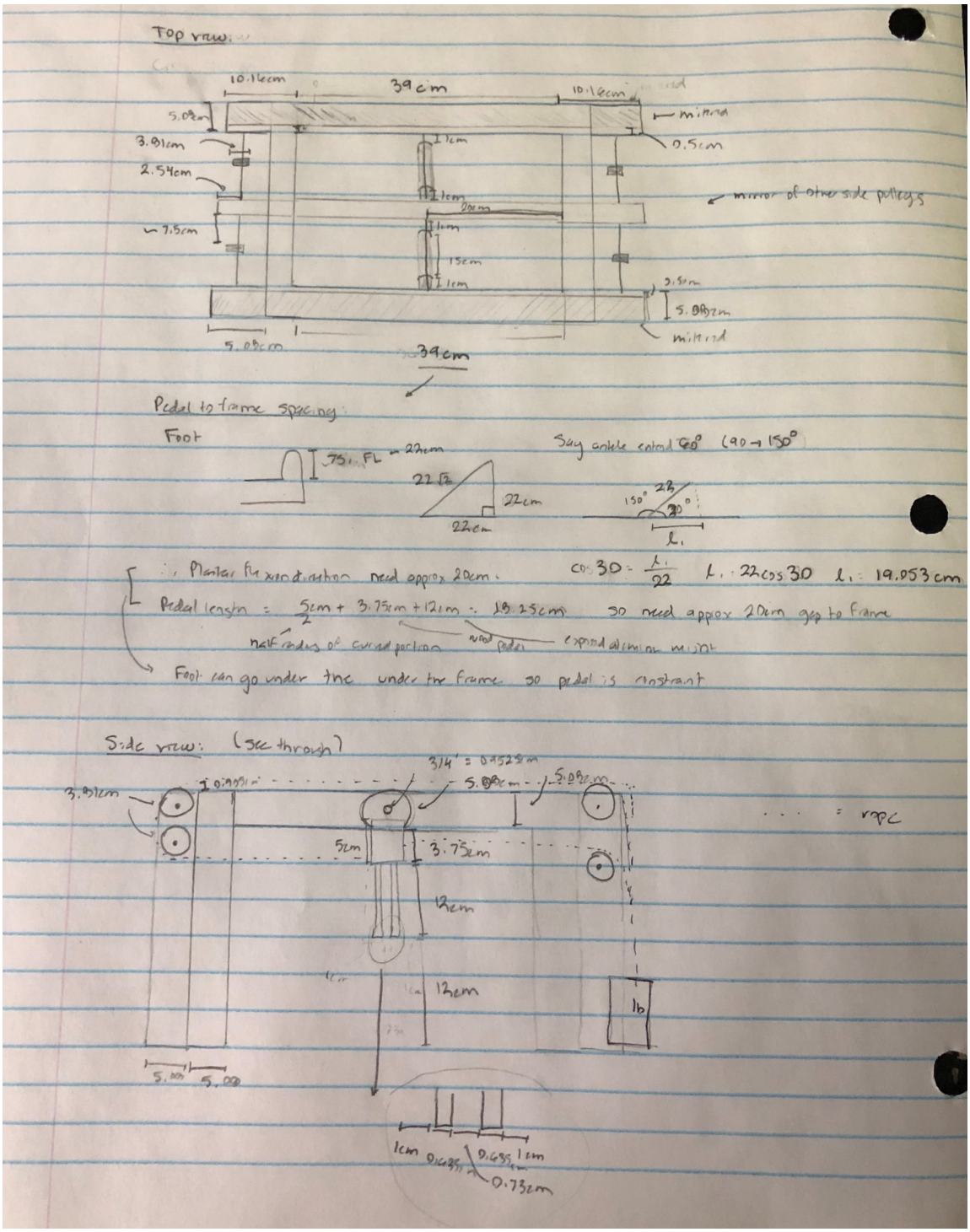

FIGURE 6.5: Sketch of ergometer pedal housing design, page 2

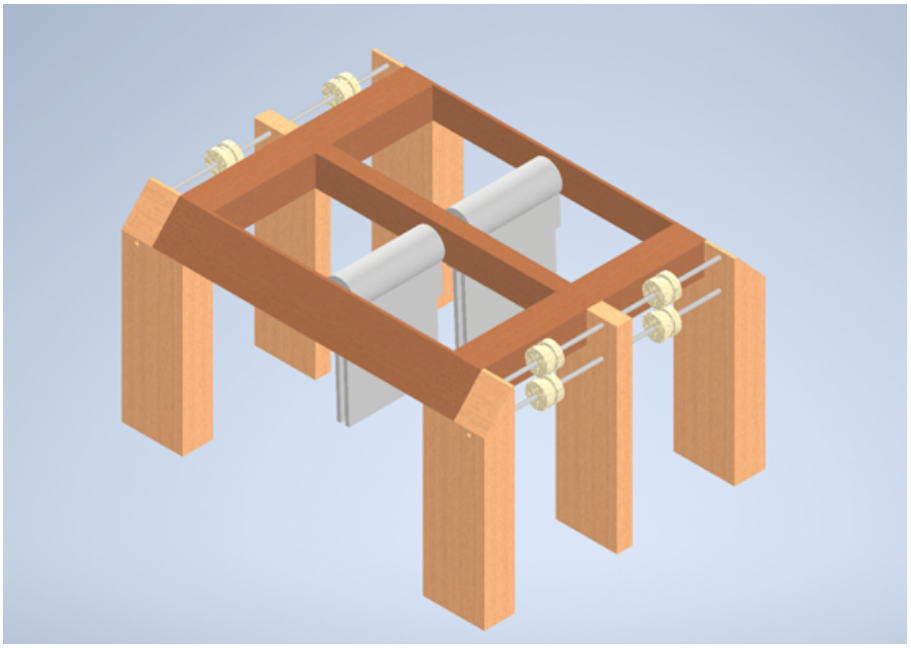

FIGURE 6.6: AutoCAD model of ergometer pedal housing design

6.1.3 Design of Interfacing Table

The pedal housing of the ergometer needed to be interfaced with the MRI table, otherwise while pushing against the pedal the housing would simply slide in the direction of the pedal push. To address this issue the pedal box was interfaced to a wooden board, where the patient would lie, by placing dowels in all the outer housing legs, which had insertion points in the wooden board. This would ensure the housing would not move translationally relative to the wooden board. This wooden board was then interfaced with the MRI scanner bed. By removing the plastic coverings on the table, as seen in Fig. 6.7, a uniform pattern of table inlets was revealed. Wood joists where made to match the inlet size and spacing and were attached to the underside of the wooden plank. Now the wooden plank would not move translationally relative to the scanner bed and thus the whole ergometer was secured.

6.1.4 Weight Boxes and Pulley's

To allow for weighted flexion a small housing was created to hold the lead weights. One box was made for each pedal respectively to provide the option of unilateral or bilateral flexion. The box was designed to fit in the same channel as the pedals (in the frame) and to be able to hold up the lead scuba weights that were available for use. The pedal box and pulley mechanism can be seen on the right hand side of Fig. 6.7. To interface the weight box and pedal dowels were used to act as hooks, one interfacing with the pedal, the other with the weight box, with fishing line connecting the dowels. Fishing line purchased was specified at 100lb line and was pre-stretched. This was done to ensure the force used to push against the pedal was not lost in stretching the rope and instead resulting in the movement of the pedal box.

FIGURE 6.7: Built ergometer pedal housing design and wooden participant bed. Left image shows wood participant bed interfacing with the MRI table (cover removed), middle image shows ergometer housing and wood bed interfacing, and right image shows the pulley mechanics in the plantar-flexion orientation

FIGURE 6.8: Pre-scan set up with participant in position for right leg plantar flexion paradigm on built ergometer pedal housing and wooden participant bed.

6.1.5 Validation of Design

Spacing/Size Testing

Prior to using the ergometer for imaging some initial tests were completed. Visual sizing tests ensured that the erogmeter fit within the bore, without (Fig. 6.7) and with a participant (Fig. 6.7). The figures show that the ergometer fit within the bore and a 6ft participant fit comfortably on the scanning bed which proved the sizing was adequate.

TABLE 6.2: Metrics computed best on resting-state fMRI scans of a phantom to assess ergometer distortion effects Abreviations SNR = signal to noise ratio, SFNR = signal to flucation noise ratio, RDC = residual decorrelation.

Trial	**Mean Ghost**	**Max Ghost**	**SNR**	**SFNR**	**Percent Fluctuation**	**Percent Drift**	**RDC**
No Ergometer	1.6371	3.82	264.15	270.71	0.0653	-0.3997	6.2045
Ergometer No Movement	1.6877	5.29	280.10	275.98	0.0668	-0.4093	5.6387
Ergometer With Movement	1.6798	4.16	288.39	268.12	0.1127	-0.1533	3.3397

Quality Assurance Testing

In addition to testing the sizing criteria some preliminary quality assurance (QA) was performed. The quality assurance was performed while the placing the ergometer in the position for neural fMRI protocols, with the pedal positioned at the foot of the table, refer to (Fig. 6.9). From referencing previous literature that indicated a cycle ergometer distorted functional readings so much that they could not discern activation patterns [122], it was determined that a simple test to see if the ergometer distorted fMRI data was used as a QA metric. To ensure the QA was as standardized the same protocol was employed that is conventionally performed at the IRC, which is modeled after the work entitled "Report on a Multicenter fMRI Quality Assurance Protocol" [123]. To test if the ergometer had a significant effect on the fMRI quality of the system, three separate fMRI runs, each consisting of 17minutes of scanning, were completed, the first without Woody (the ergometer), the second with Woody and the third with Woody while my hands were pushing the pedals (to see if the movement of lead weights in a magnetic field and the resulting eddy current effect caused any distortion). The analysis outlined in the [123] was performed in Matlab by modifying a script provided by the IRC lead Norm Konyer. This script was used as a base to then perform QA and the comparison of the QA between the three testing states. Metrics comparing signal fluctuations, signal to noise ratio and ghosting were determined through the methodology from [123] and are summarised in Tab. 6.2. Based on the suggestions in [123] no major deviations from the expected normal fMRI behaviour were observed from the tabulated metrics. Additionally difference plots between the three states of no ergometer, ergometer with and without movement were compared for the major metrics, as seen in Fig. 6.2. From looking at the differences images no major indications of distortion were seen when looking at the raw image, fluctuations or residuals other than at the boundary of the phantom. This would not be of major concern as this is the boundary of the phantom which is subject to higher levels of variation based on the need to reshim between acquisitions to change the ergometer orientation. The difference in odd and even images as seen in the bottom left of Fig. 6.2 did appear to be completely random but did not raise significant concerns.

FIGURE 6.9: QA Set-up. Left image with the HNS coil containing the 3T cylindrical phantom. Middle image showing the central slices of the phantom used for analysis. Right image showing the foot pedals positioned at the foot of the scanner bed for a fMRI scan.

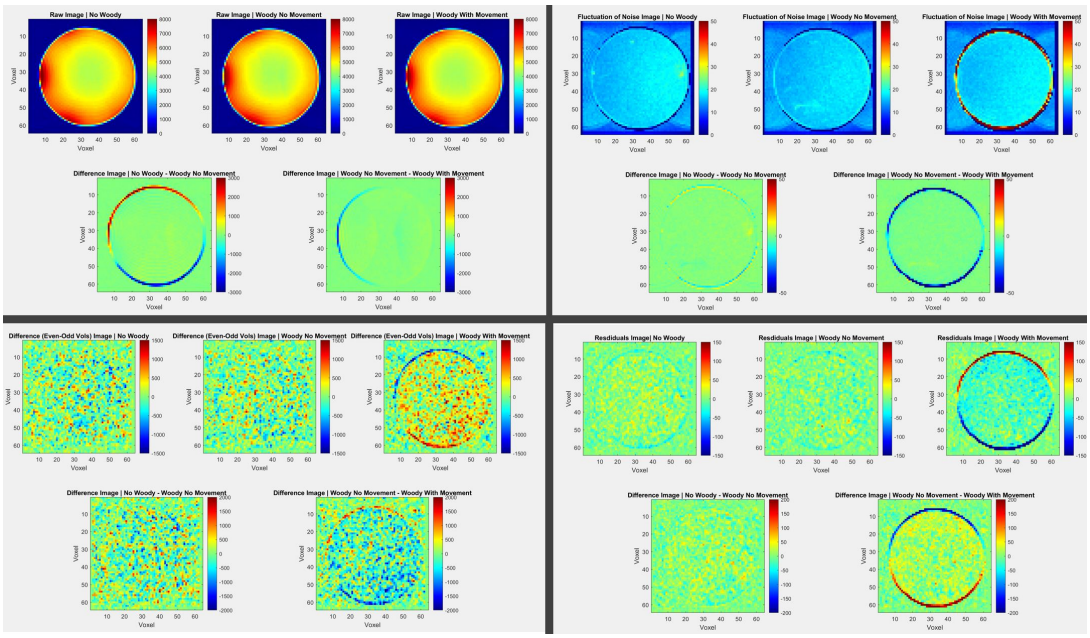

FIGURE 6.10: QA difference plots of phantom central slice assessing key metrics from [123]. Top left image shows difference images from the raw images. Bottom left shows the difference image from the average of even and odd images. Top right shows the noise fluctuation image. Bottom right shows the residuals after detrending image.

Preliminary Foot Tapping Experiment

For a final validation step a single subject simple foot tapping experiment was performed to see if regional activation could be visualized while using the ergometer. This was done due to previous literature that indicated a cycle ergometer distorted functional readings so much that they could not discern activation patterns [122]. Therefore as a proof of the ability to see activation within the brain during lower leg exercise the participant did a simple plantar flexion paradigm. The paradigm consisted of 20s blocks of alternating between rest and plantar flexion for a total of 4min. The participant was queued to change states by using an external stimulus of changing the room lighting. Isometric contraction during exercise was employed to limit participant motion. One trial was performed alternating between flexion and rest for the left leg and a separate for the right leg respectively. To visualize activation a very simple analysis framework was used. Raw fMRI images were examined in the hypothesized motor region to see if they showed increased neural activation during periods of isometric contraction, as seen in Fig. 6.11. A simple correlation analysis using a simulated hemodynamic response function in AFNI was used to identify active regions in the motor cortex and cerebellum. As can be seen from the quick analysis pipeline in Fig. 6.11, there was contralateral activation in the motor cortex and ispilateral activation in the cerebellum during the left foot plantar flexion paradigm. This simple test confirmed the ergometer did not cause significant fMRI distortions unlike [122], so it was deemed valid to proceed with use.

Usability Conclusion

It should be noted that ergometer use and its effects on muscle imaging as not as commonly assessed, which can be due to the fact that novel ergometer systems are made at specific research sites. Additionally when doing lower limb exercises the effect of motion artifact is much more significant when imaging the leg than brain, which is why muscle imaging is less rigorously studied and ergometer induced variation thus less reported. As such, a fMRI assessment of activation in the brain ensured a more standardized QA protocol that had comparable results. Although this is not directly related to muscle imaging it verified that the ergometer caused no significant distortions in neural activation patterns. This provided some validation in using the ergometer prior to completing the muscle imaging research that was to follow.

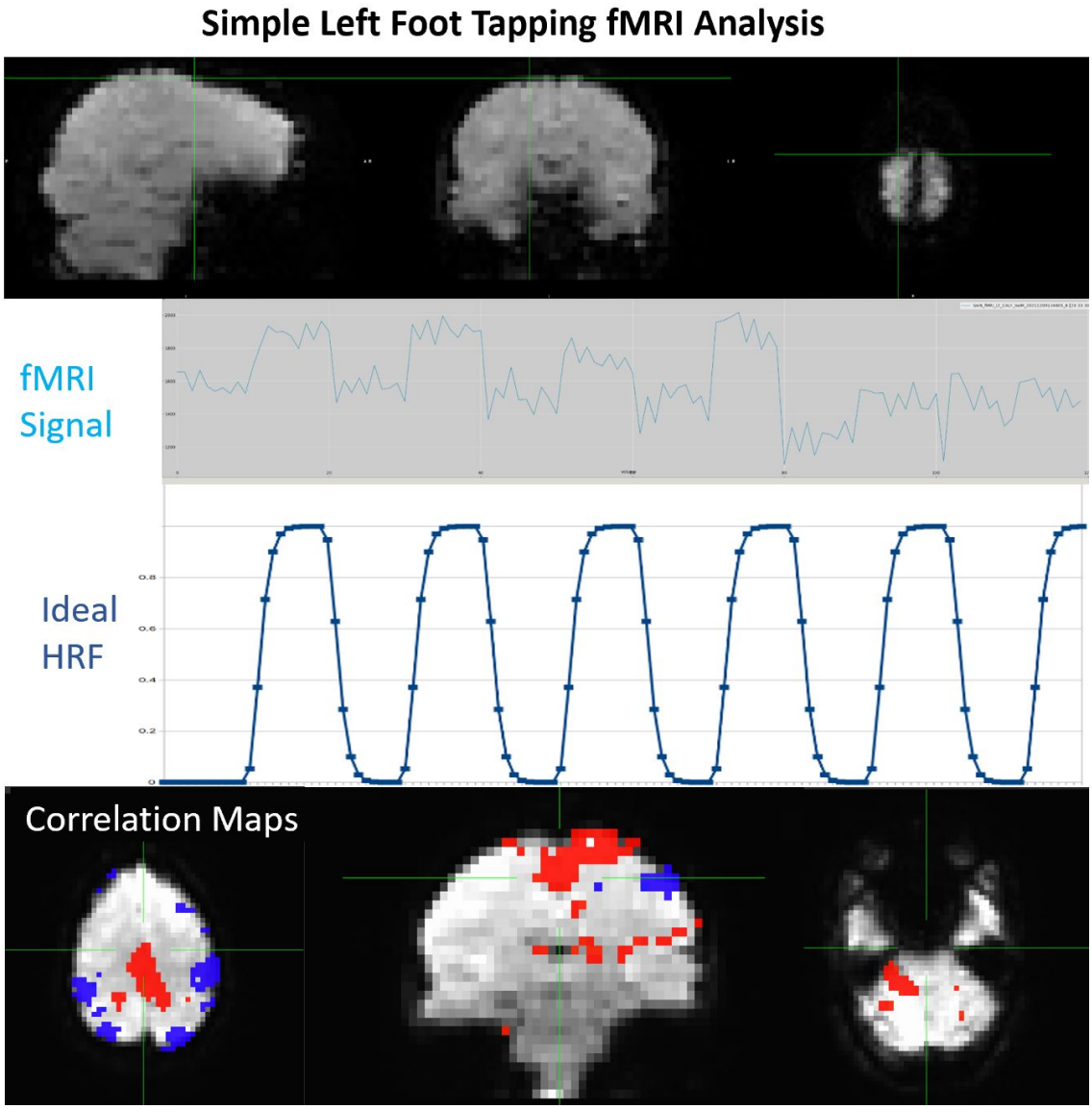

FIGURE 6.11: Simple Left foot isometric plantar flexion analysis. Showing from top to bottom unprocessed fMRI image, sample fMRI voxel signal from the motor cortex, ideal hemodynamic response function for given block design, correlation maps between hemodynamic response function and voxel-wise signal (red showing significant correlation and blue significant anticorrelation $P<0.0001$).

6.2 Building an MRI Compatible Electromygraph

EMG is conventionally used to assess functional muscle activity due to its high temporal resolution. The combination of functional MRI and surface EMG would enable an improved understanding of muscle activity due to the complementary nature of the imaging modalities. The surface EMG has a temporal resolution on the order of 0.2ms (using a sampling frequency of 5000Hz in this instance) but poor spatial resolution limited by the orientation of the set of MR compatible carbon electrodes which are spaced approximately 7cm apart. This spacing was necessary to allow for the placement of imaging slices in between electrodes, as if they are in the slice plane they can induce image distortion. The low spatial resolution of EMG is accounted for through BOLD imaging with the voxel size of 2.5x2.5x10mm. This high spatial resolution comes at the cost of temporal resolution of 110ms. Additionally, muscle activation between the two modalities is relatable as contraction will be denoted by increased electrical amplitude in the EMG recording and increased BOLD signal amplitude. Therefore the improved spatial temporal resolution of muscle activation and the relatability of the modalities demonstrated the value in using this dual modality approach. This dual modality approach although beneficial has not been extensively explored due to the difficulties with designing an EMG circuit in an MRI environment. The associated challenges were overcome and the methods to do so are described below.

6.2.1 Design Considerations

1. EMG frequency Bandwidth 20-500Hz [124]
    - Motion artifact occurs at frequencies <15Hz so need to exclude these frequencies
    - Relevant EMG components can be up to 1000Hz, depending on factors such as electrode surface area and the spacing between electrodes, but need to employ more stringent bandwidth with highly noise MR environment
2. EMG Amplitude 0.1–2mV [125]
    - With surface EMG amplitude on this order the front end gain must be between 50,000 and 2,500 so the final signal is within a 5V range and can be more easily digitized by an ADC
3. Electrode Material
    - Conventional AgCl electrodes cannot be used due to heating and eddy current affects associated with the electrodes.
    - Cardiac MR ECG electrodes, which are carbon based, can be used as an alternative.
        - These electrodes will require a specific interfacing cable with carbon leads to mitigate impedance differences that would introduce a DC offset in the signal. The leads will also need to be high impedance to reduce the current draw to the amplifiers in the RF MRI environment.
4. Sampling rate of >5000Hz
    - To have an accurate representation of a signal in time the Nyquist criteria states the necessity to sample x10 the maximum signal frequency

6.2.2 Design Plan

The preliminary EMG front end design, system design, and the rationale for stage selection is indicated below. The implemented values for the gain stage and cut-off frequencies for the associated filtering stages differed due to component availability. A block diagram of the EMG design can be seen below in Fig. 6.12.

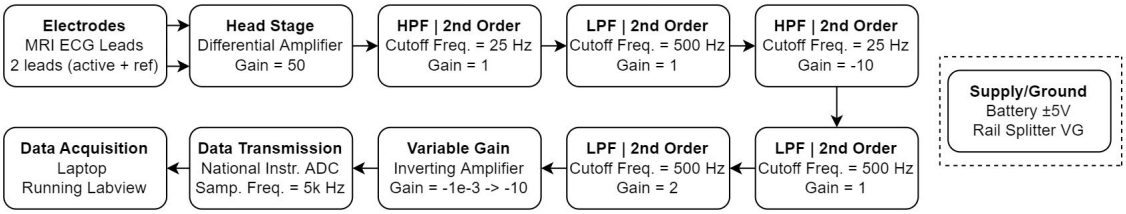

FIGURE 6.12: Block design for EMG system data acquisition set-up. Specifications are ideal and vary from implemented design due to component availability.

Stage 0 – Supply/Ground

The implemented system the Analog Discovery's ±5V supplies were used to save the need to constantly buy batteries. The virtual ground for the circuit was used to act as isolation, in the case that batteries are used provide power to the circuit this would allow for isolation. A rail splitter circuit was used to provide the virtual ground. It consists of two matched resistors and capacitors, used to smooth ripple, fed into a unity gain op-amp to provide isolation. After trial and error, it was found that relatively small capacitors were required to limit ground fluctuations.

Stage 1 – Electrodes

The electrodes that will be used are expired CONMED cardiac carbon-based electrodes, [126], from St. Joseph's Hospital. These electrodes are MRI compatible and are connected to the analog front end via a high impedance wire to reduce the relative noise contribution. This is necessary due to the high noise MR environment. The high impedance wire connects to a 9-pin serial output, which will feed into the analog front end.

Stage 2 – Head Stage

The purpose of the head stage is to use a differential amplifier (LT1920), with a large common mode rejection ratio, to receive a low noise differential input. A relatively large gain of 50 was used because the typical amplitude of surface EMG is on the order of 100uV – 1mV. Due to the high MRI noise environment two active electrodes will be used and feed into the amplifier as the differential inputs and the non-active electrode as the amplifier reference. The two active electrodes and non-active reference electrode will be placed in close proximity as the noise contribution of the MRI gradients is spatially dependent. The active electrodes will be placed on the muscle belly and the reference on the bone at the midpoint between the active electrodes to reduce gradient induced differences being amplified in the signal.

Stage 3 – High Pass Filter(HPF) One

The purpose of the HPF is to remove the DC offset introduced into the differential signal. A second order active Butterworth filter is used in a Sallen-Key implementation. Unity gain is used as the high frequency noise in the signal has yet to be removed. In the noise ridden MR environment this noise could saturate the amplifier if anything greater than unity gain is used. An active filter was chosen as a passive HPF can introduce amplitude reductions, which is undesired with the low amplitude surface EMG signal. The desired cut off frequency for the system was 20-25Hz, but based of the available components the implemented cutoff frequency may vary. This will ensure that motion artifact, which falls in the bandwidth of 0-15Hz, is sufficiently suppressed with the relatively slow roll off in the implemented second order filter.

Stage 4 – Low Pass Filter(LPF) One

The purpose of the first LPF is to remove the MRI induced high frequency noise. A second order active Butterworth filter is used in a Sallen-Key implementation. A cut-off frequency of 500Hz is employed as this is the higher frequency limitation related to rate of contraction of muscle fibres at the route of the EMG signal. In the noise ridden MR environment this noise could saturate the amplifier if anything greater than unity gain is used. The noise is caused by the spatially and rapidly changing magnetic fields induced by the gradient switching that will cause induced electrical fields at the electrode sites. Additionally, the radio frequency excitation pulses will also cause high frequency noise to be picked up on the electrodes which will have amplitudes greater than that of unamplified EMG signal.

Stage 5 – High Pass Filter(HPF) Two

The purpose of the second HPF is to remove the DC offset and motion artifact that still remains in the signal after now removing the higher amplitude MRI induced high frequency noise. A second order active Butterworth filter is used in a multi-feedback topology implementation. This topology allows for a non-unity gain, which in this case is chosen to be -10. Although this gain is moderate any amplitude increase can help the remaining function of the front-end circuit. A gain of 10 was chosen as it is theorized that the first second order lowpass filter will not adequately attenuate all of the MRI induced high frequency noise. Thus, a moderate gain is used as to not saturate the amplifier prior to further high frequency noise reduction. An active filter was chosen as a passive HPF can introduce amplitude reductions, which is undesired with the low amplitude surface EMG signal. The desired cut off frequency for the system was 20-25Hz, but based of the available components the implemented cutoff frequency may vary. This will ensure that motion artifact, which falls in the bandwidth of 10-15Hz, is sufficiently suppressed with the relatively slow roll off in the implemented second order filter.

Stage 6 – Low Pass Filter(LPF) Two

The purpose of the second LPF is to remove the MRI induced high frequency noise. This LPF filter is directly cascaded with the LPF following, which will make the filter roll of faster. A second order active Butterworth filter is used in a Sallen-Key implementation. A cut-off frequency of 500Hz is employed as this is the higher frequency limitation related to rate of contraction of muscle fibres at the route of the EMG signal. A unit gain is employed due to the concern that the higher frequency components have not been fully attenuated.

Stage 7 – Low Pass Filter(LPF) Three

The purpose of the third LPF is to participant in a cascade with the previous LPF to improve the roll of off the filter to act as a fourth order filter. This improved roll off will more effectively remove the MRI induced high frequency noise. A second order active Butterworth filter is used in a Sallen-Key implementation. A cut-off frequency of 500Hz is employed as this is the higher frequency limitation related to rate of contraction of muscle fibres at the route of the EMG signal. A conservative gain of two is employed due to the concern that the higher frequency components have not been fully attenuated and with the knowledge that larger gain stages will follow.

Stage 8 – Variable Gain

The purpose of the inverting variable gain stage is to serve to invert the waveform to its positive orientation to compensate for the second high pass filter found in stage five. The variable gain component is controlled via a switchable resistor and is used to act as a final means to increase the amplitude of the now ideally denoised EMG signal, which has been bandpass filtered in the range of approximately 20-500Hz. This final amplification is used to improve the representation of the recorded signal by expanding the range for the ADC used, serving to minimize the digitization error. A block capacitor will be used prior to the gain stage in order to remove any DC component that could have been amplified by the 1000 times gain to this point. A dip switch with varying resistor value at end connection point, to each of the 10 switches, allows for a set of finite gains to be specified. This will allow for variable gain based on muscle (which varying in contractile amplitude) and proximity of the electrodes to the excitation coil (i.e. when the electrodes are on the leg under the leg coil the artifact amplitude will be greater than when using the head coil). Finite gain settings are preferred over a potentiometer to ensure more standardized gain across trials. The maximum gain orientation was specified for bicep contraction outside the MRI, as this is a strong muscle in a low noise environment. The minimum gain was specified for tibialis anterior plantar flexion within the MRI during a functional scan with a leg coil, as this is a weak muscle in a high noise environment.

Stage 9 – Data Transmission

The data from the analog front end must be digitized prior to transmission. Originally the data was going to be converted and transmitted using the ESP32 microcontroller, which has an snslog to digital converter (ADC) with a sampling rate of 6kHz. This was done in an effort to keep the patient isolated as the microcontroller would not be connected to an outlet. After preliminary testing it was found that the 6kHz sampling of this microcontroller was limited to the transmission rate which was bottle necked when using either MATLAB, the Arduino IDE, or processing (a data acquisition environment for Arduino's). The best presented alternative was to use the National Instruments USB-6221 ADC, which has up to 10k sampling rate for a specific channel.

Stage 10 – Data Acquisition

The data from the ADC must be saved. To facilitate this, a simple Labview data acquisition script was created to allow for a single channel acquisition at 5000Hz (ten times greater than the front-end cut-off frequency to satisfy the Nyquist criteria to have adequate temporal signal

representation). The script was designed with the knowledge that it must be able to operate during a high demand acquisition with a fast sampling rate of 5000Hz for a long duration of 5min. This would mean for every 5min EMG recording session 1,500,000 samples would be saved. Two major points of consideration when designing the script to allow for this high rate of sampling while still saving the data are the file format to save the data, and the choice of continuous versus discrete sampling framework. Conventionally, for simplicity, files to record column-wise timing and signal amplitude for a single channel would be recorded in a csv format. Through experimentation it was found that saving large files as a csv was not possible due to the larger memory overhead associated with saving in this format. The memory overhead caused either non-uniform sampling at a rate less than 5000Hz or truncation of the data set at around 100,000 samples. Thus data needed to be saved as a .lvm file to allow the acquisition of data at this rapid rate. Additionally, the number of samples sitting in current memory (using continuous sampling mode in the DAC module) also had to be modified based on the original ADC tool provided with labview. The number of samples before temporary memory refresh needed to be increased to the sampling rate of 5000. This removed the memory allocation errors that were received prior to making this change. The simple graphical script that achieved this sampling can be seen below in Fig. 6.13.

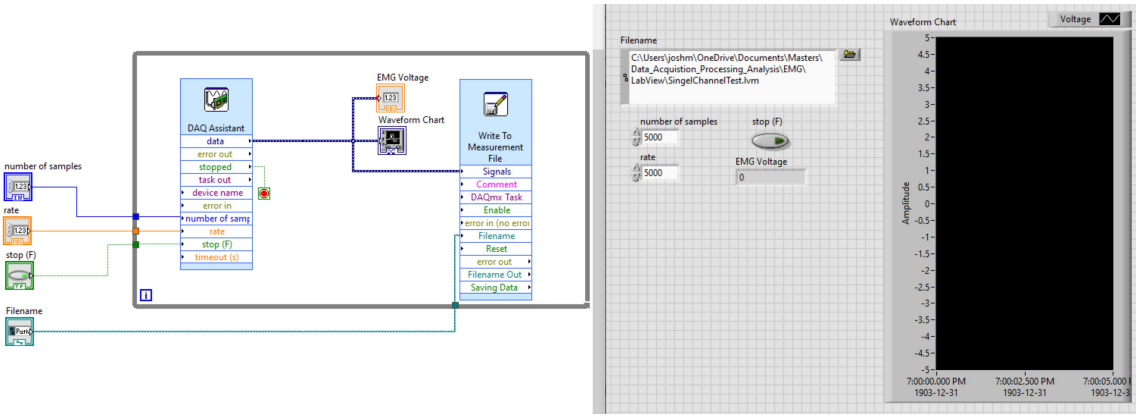

FIGURE 6.13: Single channel labview acquisition script for EMG. Sampling was done continuously, 5000 number of sample per window, at a sampling rate of 5000Hz

6.2.3 Circuit Design

To build the above analog front end the circuit components were computed and based on component availability a circuit that closely matched to the above specifications was made. Some sample calculations for the computation of the component values can be seen in Fig. 6.14. The circuit design was then modeled in a program called EasyEDA, as can be seen in Fig. 6.15. From there the designed circuit was converted to a PCB schematic and the etching design for the wire traces done manually to avoid overlap and adequate spacing to avoid capacitive coupling. The PCB was ordered and then soldered in the coil lab in the IRC. The designed and constructed PCB are shown in Fig. 6.15.

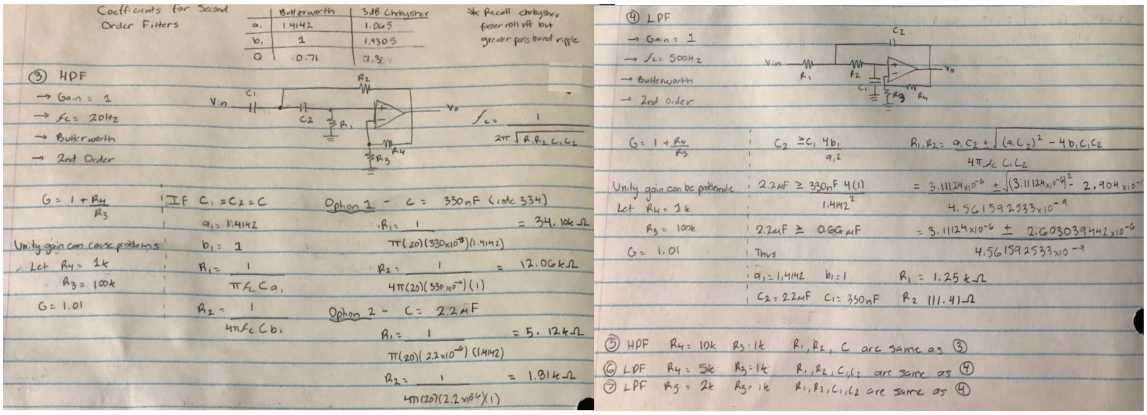

FIGURE 6.14: Sample calculations used to find the components of the high and low pass filter using a 2nd Order Sallen Key implementation .

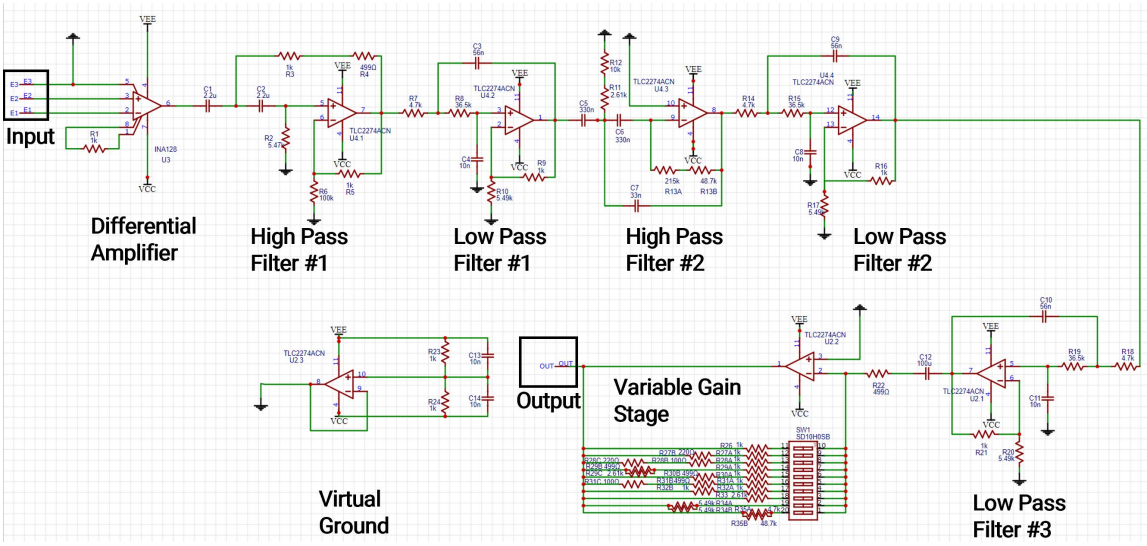

FIGURE 6.15: EMG analog front end circuit diagram with implemented component values.

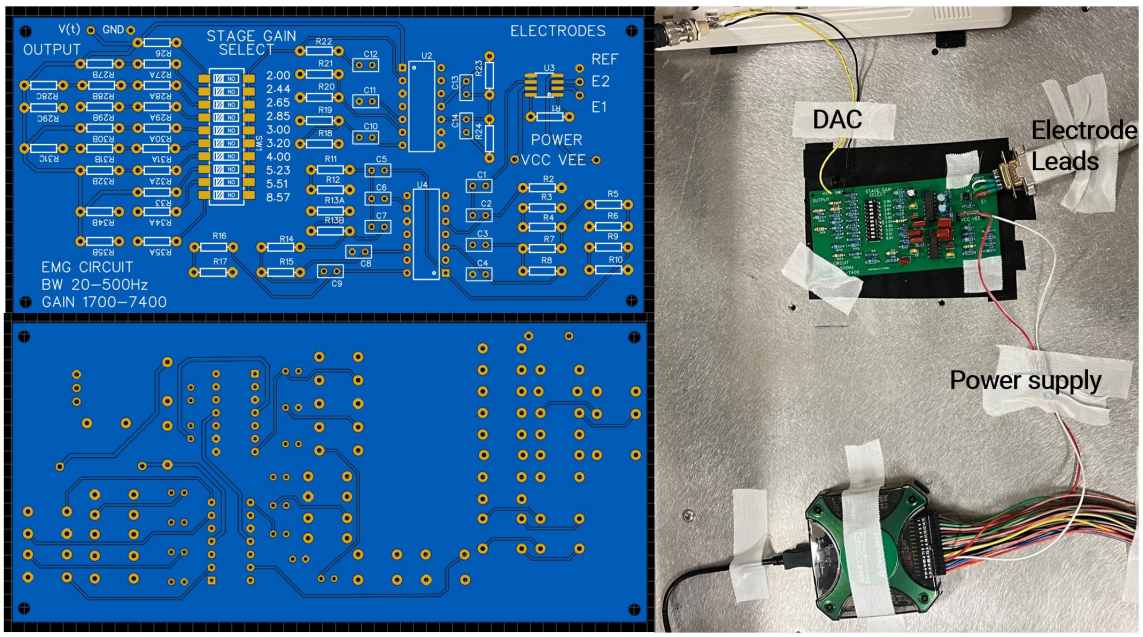

FIGURE 6.16: EMG designed and constructed PCB. Note the analog discovery power supply, the electrode leads go to high impedance MRI compatible cardiac ECG cables and the DAC leads to the National Instruments USB-6221 box.

6.2.4 Safety Testing

Temperature/SAR Testing - Phantom

To ensure the EMG system was safe, the specific absorption rate (SAR) and temperature were recorded during a variety of different sequences. If the temperature increase was too great, then the system would not have been able to be used for participant scanning. The temperature was tested under difference sequences, which would have different levels of RF, as higher levels of RF would cause more energy to be absorbed and greater relative heating. This would be worse with heavier patients as their ability to dissipate heat is impaired. The first tests were done on a phantom to ensure the system was safe. The system consisted of the EMG, with 3 carbon fibre electrodes connected to a cardiac MR high impedance cable. The electrodes have been cleared for cardiac MR studies, so little to no temperature increase during scanning was expected. The temperature under each of the electrodes was measured using optical temperature probes that were fed into the magnet room. The temperature was recorded on an old PC that was sitting outside the magnet room. For all MRI scanning, the GE Medium Flex Leg Coil was used so that the RF was more closely deposited on the electrodes. The set up is shown in the figure below (Fig. 6.17) The temperature was tested and SAR (W/kg/10s) recorded under the following scanning conditions (using the leg coil for all):

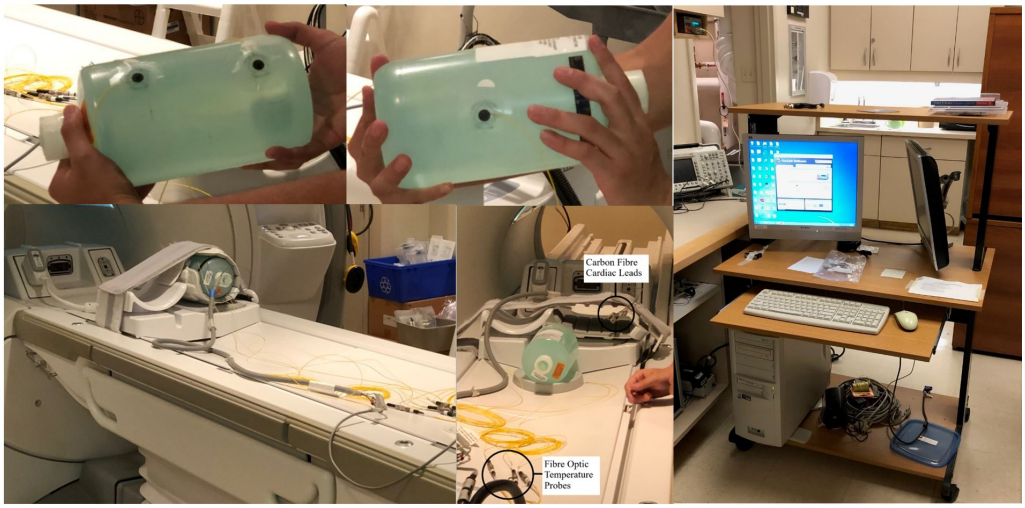

FIGURE 6.17: The 12 cm diameter by 25 cm long vendor-provided QA/QC cylindrical phantom containing dimethyl silicone fluid, gadolinium, and colorant. To study potential RF heating effects, electrodes (Conmed ClearTrace Radiotranslucent ECG Electrode) were placed on the phantom, in a similar orientation to that when used on muscle (two active electrodes along the calf muscle plane and the reference on the shin in the lengthwise midpoint between electrodes) . An optical temperature probe (ReFlex-4 RFX273A, Neoptix, Quebec, Canada) was placed under each of the electrodes, respectively.

1. Spectroscopy scan
    - There is not a lot of expected heating as k-space is not rasterized quickly and there are not a lot of RF excitations
    - Parameters: Press TR/TE 1500/30ms, NEX 8, averages 256, VOI 2x2x2 FOV 24cm

2. BOLD functional scan
    - Uses EPI so expect more heating. But only one RF pulse is played per TR=1s so heating should not be significant.
    - Parameters: TR/TE 1000/35ms, flip angle 90deg, slices 15, thickness 4mm, spacing 5mm, FOV 18cm, matrix 64x64, NEX 1
3. FEISTA scan
    - During FEISTA scan (worst case condition). The FEISTA sequence is known to have relatively high SAR. By maximizing the number of excitations and slices this can cause heating. The FEISTA sequence was run on the order of 16min, as the longest expected scan in the paradigm was to last for 8min. Double the time and high SAR sequence is an optimal sequence to test the safety for simple functional or spectroscopy scans.
    - Parameters: FEISTA TR/TE 5.1/2ms flip angle 90deg, slices 15, thickness 5mm, spacing 5mm, FOV 26cm, matrix 256x256, NEX 64, Receiver bandwidth 125kHz

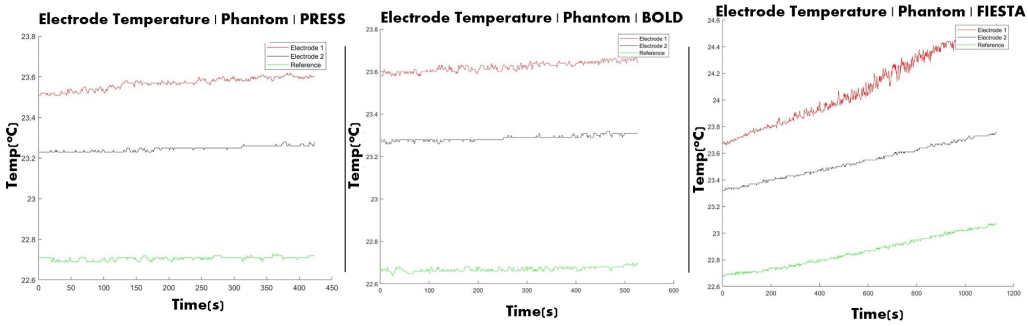

FIGURE 6.18: Electrode temperature over time for two active electrodes and reference using Spectroscopy, BOLD and FEISTA (from left to right) sequences and the GE medium Flex leg coil.

TABLE 6.3: The SAR difference from the first and maximum time point for two active electrodes and reference for the different sequences and the GE medium Flex leg coil, using a phantom.

Sequence	**Phantom Weight (lb)**	**Maximum SAR (W/kg/10s)**
PRESS	5	0.4
BOLD	5	0.3
FEISTA	5	2.4

The increase in SAR and temperature over time was of no significant safety concern **(SAR less than 4W/kg/10s and less than a 2 degree temperature change)** so testing amongst the research team followed.

Temperature/SAR Testing - Human Subject

The following test, after passing the original phantom test, was to test the system on a human subject. In this case it was tested on lab mate Alex Amador, prior to a research participant.

The exact same set-up and scanning conditions were followed from the above phantom case, with the difference that the electrodes were situated on Alex's calf. This means that the baseline temperature will change from room temperature (22°C) to body temperature (37°C). Also, the temperature change may vary as the RF absorption is dependent on the medium. As can be seen in the table and plots below, the temperature and SAR did not significantly change (to a dangerous level) over the scan time course, so it was reasonable to proceed to tests with research participants. It should be noted one of the temperature probes was not recording but data should suffice as proof. Having two active electrodes was somewhat redundant above.

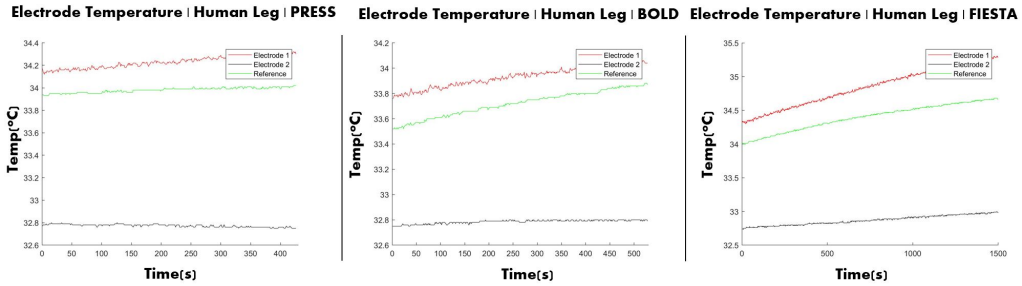

FIGURE 6.19: Electrode temperature over time for one active electrode and reference using a Spectroscopy, BOLD and FEISTA (from left to right) sequence and the GE medium Flex leg coil.

TABLE 6.4: The SAR difference from the first and maximum time point for two active electrodes and reference for the different sequences and the GE medium Flex leg coil, using a human subject.

Sequence	**Subject Weight (lb)**	**Maximum SAR (W/kg/10s)**
PRESS	170	0.2
BOLD	170	0.1
FEISTA	170	0.8

6.2.5 Circuit Testing

Out of Bore Testing

To begin the EMG analog front end was tested in the less stringent environment, which was outside of the MR environment. To test each stage respectively a frequency sweep was done to test the gain and filtering characteristics. When each stage was ensured to be performing as expected, meaning it had the desired gain in the pass band frequency bandwidth, and the input sinusoidal amplitude was attenuated by 3dB at the cut-off frequency, then the entire system was tested. The EMG front end was tested by performing simple contraction of the tibialis anterior through ankle flexion. The results are shown in Fig. 6.20), with a frequency sweep and contractions using variable gain settings. The frequency sweep shows the low amplitude below 25Hz and after 500Hz which is the bandwidth of the entire front end. Additionally, the lower gain setting was tested as it is preferred when transitioning to the MR environment where the signal from the gradient switching could saturate the amplifiers. With good performance of the front end observed more stringent tests in the MR environment followed.

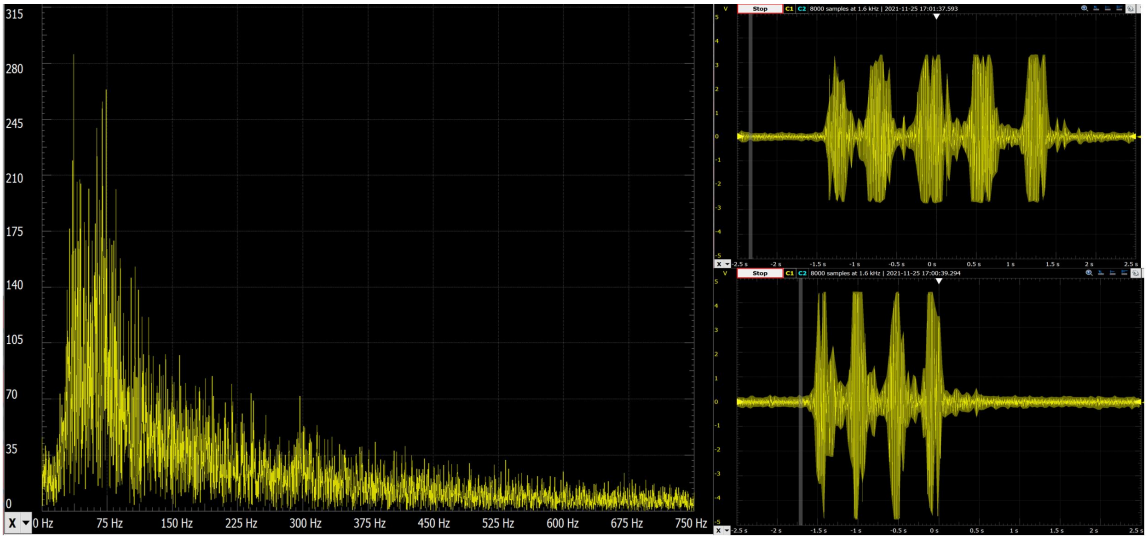

FIGURE 6.20: Frequency (left) and time domain tests (right) of EMG front end in non-MR environment. The data was collected during simple tibialis anterior contraction.

In Bore Testing - Gradient Artifact

The purpose of this test was to see if there was

1. A spatial dependence of the gradient artifact (i.e. relative leg positioning in the bore)
2. If their was a gradient artifact dependence based on the positioning of the electrode triad (i.e. the position of the electrodes relative to each other on the leg)

This was completed by using the same cylindrical phantom and electrode positioning as above, while recording the gradient artifacts using an fMRI sequence with body coil excitation. It should be noted that the entire phantom had to be coated in gel to reduce the baseline from the impedance mismatch between the phantom and electrodes. To achieve the first objective the phantom was placed at the isocenter of the magnet, followed by two position variations

1. The phantom at isocenter in the x,y,z directions
2. The phantom at isocenter then moved to the right to get closer to the bore wall
3. The phantom at isocenter then moved to the left to get closer to the bore wall

As can be seen from the figure below (Fig. 6.20) no significant differences in gradient amplitude based on spatial position were observed.

To achieve the second objective, the phantom was placed at the isocenter of the magnet and the electrode positions relative to each other on the phantom changed, as can be seen in the diagram in (Fig. 6.22). It should be noted when moving the reference there was not significant change in amplitude of the artifact. When changing the difference in distance between the electrodes the gradient artifact changed in amplitude. Therefore a standard electrode spacing between the active electrodes was employed to ensure that the artifact suppression was consistent across trials.

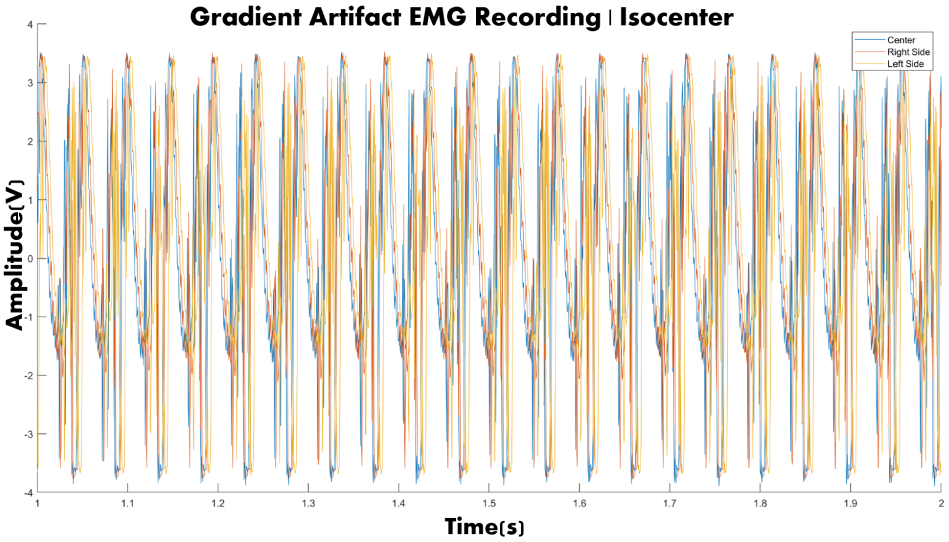

FIGURE 6.21: Plot of the gradient artifact when the phantom was position at the isocenter, and left and right of it respectively. No significant differences in gradient amplitude were observed.

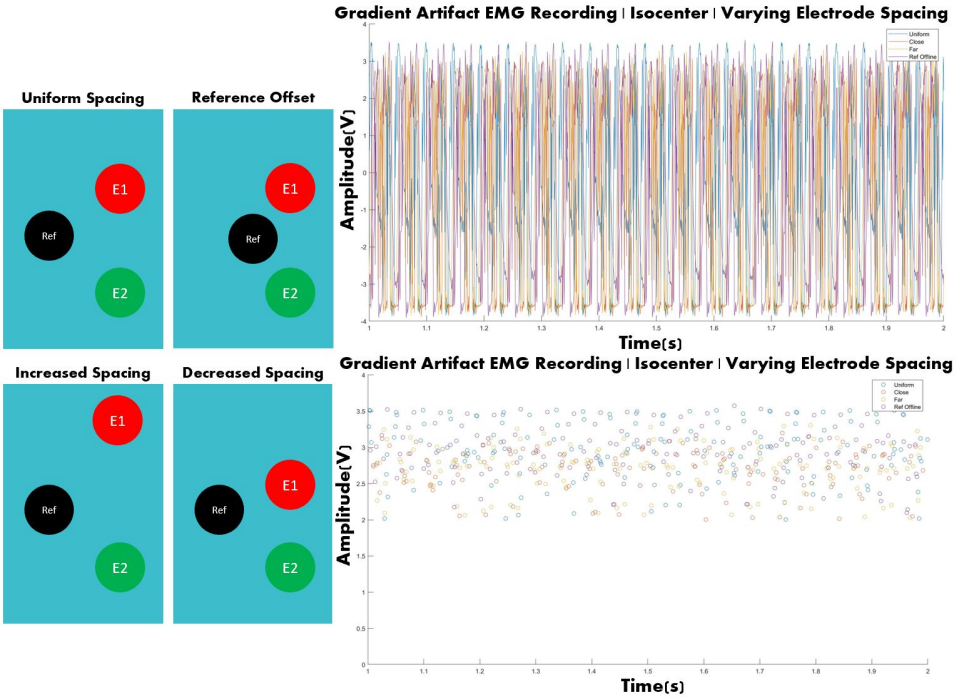

FIGURE 6.22: Plot of the gradient artifact when the phantom was position at the isocenter, electrodes were positioned in four orientation (left hand image). The entire gradient artifact and the peaks using a 2.5V, 0.05s spacing threshold shown. Increased spacing caused differences in gradient amplitude.

In Bore Testing - Muscle Contraction Trials

With the behaviour of the EMG system verified outside of the MRI environment, and the gradient artifact spatial dependence investigated, the next feasible test was assess the EMG performance during contraction in the MR environment. Due to the fact that it is a complex system, a series of tests were performed to verify that it was functioning as anticipated.

The first test was to examine the recorded EMG signal while in a less noisy orientation. This involved placing the electrodes on the bicep and scanning using a fMRI BOLD protocol while using the head coil. In this case the artifact would be less present than if the electrodes were positioned on the leg directly under the GEM medium Flex coil. Also, it should be noted that the fMRI sequence has a TR of 2s which will make the gradient artifacts appear less frequently. As can be seen in (Fig. 6.23), the EMG signal can be seen despite the heavy presence of the gradient artifact. The frequency spectrum of this signal is heavily dominated by the gradient artifact and its harmonics, but when examined more closely the EMG signal is present in the expected 20-500Hz bandwidth. To ensure the data was usable, a preliminary denoising test using EEGlab's implementation of the artifact subtraction (will be explained in detail later) was used on the bicep data. As can be seen in the figure (Fig. 6.24) the EMG signal can be isolated from the noise at the cost of reduced amplitude due to the template subtraction.

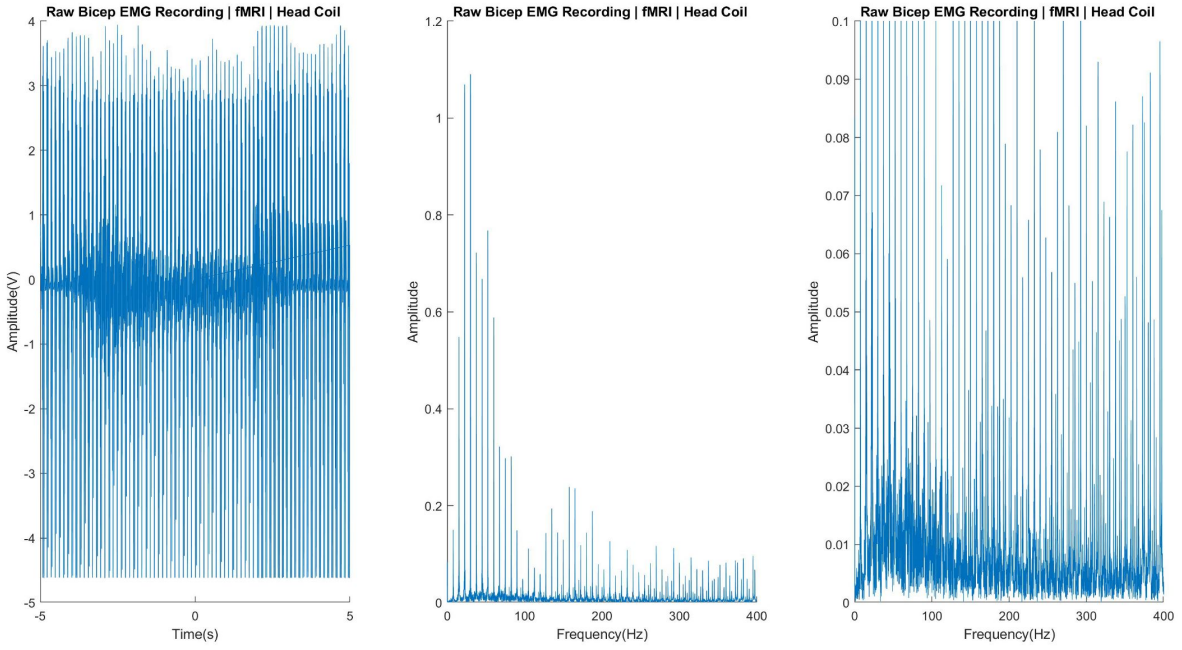

FIGURE 6.23: The time series and frequency spectrum of the EMG signal during a bicep contraction while scanning using a fMRI protocol with the head coil.

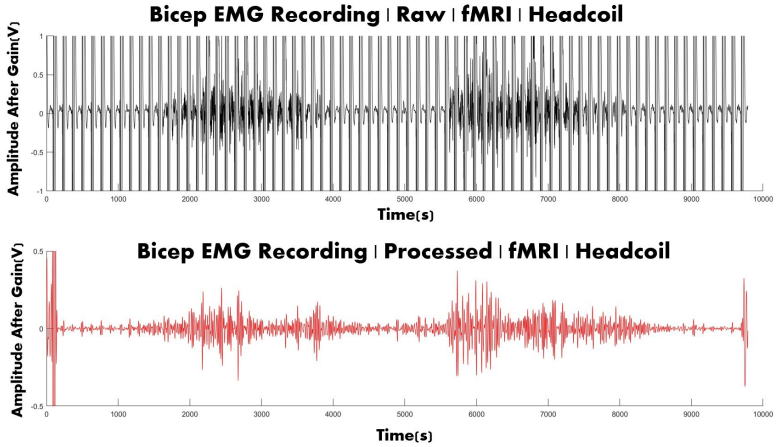

FIGURE 6.24: The time series of the EMG signal after artifact removal during a bicep contraction while scanning using a fMRI protocol with the head coil.

The next test was to examine the recorded EMG signal while in the most difficult orientation. This involved using the GEM Medium Flex Coil and scanning the lower leg using a BOLD sequence. The closer proximity of the coil during scanning and the shorter TR (one artifact occurs per TR) makes the denoising process more difficult. This more difficult implementation was the desired orientation for the study protocol. Numerous trials were performed in this orientation with little success when it came to denoising the signal. With the rapid TRs on the order of 100-250ms it is difficult to see the EMG signal within the raw data without doing any denoising. But the EMG performing well in the bicep orientation means that the system was suitable to be used in the MR environment. The two major differences that were present in this case is the proximity of the coil to the electrodes, and the reduction in the TR, which went from 2s to 0.11s. Since changing the leg coil was not a valid solution, the TR of the BOLD sequence was slowed from 0.11s t0 0.25s. This was chosen to still allow for a good temporal resolution to examine functional activation in the leg while reducing the frequency of gradient artifacts by a factor of 2.3. With this slower TR time the EMG was able to be denoised and the data was usable. The cleaned EMG signal and the baseline in the MR room during a simple ankle flexion paradigm, with electrodes positioned on the tibialis anterior, can be seen in Fig. 6.25. These positive results meant the concurrent BOLD and EMG could be recorded.

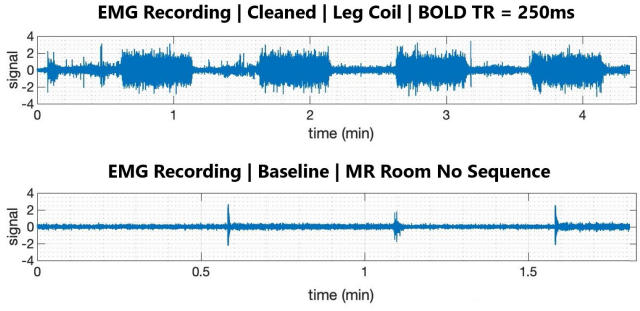

FIGURE 6.25: The time series of the EMG signal after artifact removal during ankle flexion and tibilias anterior contraction while scanning using a BOLD protocol with a TR of 250ms and the GEM Flex leg coil.

Chapter 7

Data Acquisition and Processing

7.1 Declaration

Please note all data was collected by Joshua E. McGillivray (JEM), with the assistance of Alejandro Amador (AA) and Thaejaesh Sooriyakumaran (TS). All data preprocessing was performed by JEM.

7.2 Subjects

Ten males and one female subject (n=11, age 25.7±2.2years, height 175±8.9cm, weight 73.5±11.1kg, MVC weight 15.1±3.91kg, weighted used 40.1±1.1%MVC) were recruited and consented to participation in the HREB-approved research protocol. Participant information can be seen in Tab. 7.1. Recruitment numbers and population were limited due to compliance with hospital COVID-19 safety protocols. Only subjects within the lab and hospital environment were able to be recruited for this study, as limited ethics approval was obtained. Mainly male subjects were recruited due to a limited female population availability. With this large gender imbalance the recruitment of more female participants would strengthen conclusions, as it would be more robust against biological variability. Unfortunately, of the eleven males that underwent the protocol one was excluded from analysis due do excessive motion.

The physical activity habits of all subjects was assessed in order to make preliminary endurance and power sport groupings, similar to as was employed above in Chapter 5. This was a very relative grouping, as the subjects recruited were not athletes but rather healthy individuals who performed semi-regular fitness activities. Three participants were long distance runners (endurance group), two were former soccer players (endurance/power group), four participated in either weightlifting, hockey, fencing, swimming (power group) or two in no sport (ambiguous grouping). Preliminary groupings were made on the basis of fibre profile differentiation due to habitual activity performance. [107] Therefore, endurance compared to power athletes should show a greater relative amount of slow-twitch fibres. Due to the heterogeneity of the subject sample no activity based groupings could be made, so it was more beneficial to examine the results over the entire population where a significant result would be looked upon more favourably due to the heterogeneous sample.

TABLE 7.1: Summary of participant age, weight, height and maximum voluntary contraction (MVC) characteristics. Used weight indicates the isometric plantar flexion weight during the experimental protocol.

Subject	**Sex**	**Age (years)**	**Height (cm)**	**Weight (kg)**	**MVC (kg)**	**Weight Used (% MVC)**
1	Male	25	178	65	15.4	41.56
2	Male	24	175	83	19.1	40.83
3	Male	26	180	75	14.9	40.27
4	Male	25	180	84	16.8	41.66
5	Male	27	180	77	21.0	39.52
6	Female	27	160	62	7.8	41.03
7	Male	25	178	75	19.3	40.41
8	Male	25	162	54	15	40.00
9	Male	22	186	92	11.6	38.79
10	Male	31	179	76	13.1	38.93
11	Male	26	170	65	11.6	38.79

7.3 Experimental Design

The data collection protocol was designed in order to collect information that would give a comprehensive outlook on muscle behaviour while staying within a reasonable time frame. This was done as if the scan time was too long participants would be more likely to move and less likely to volunteer for the study. Below is a list of all the scans in the muscle investigation protocol that was designed by JEM with the assistance of AA. As such, some of the scans pertain to the use of AA for use in his Master's thesis. A rationale behind the use of each scan is provided, and the specifications for the relevant scans provided in a later section.
Protocol Scans:

1. 3 Plane Localizer
    - Used to identify the leg location within the bore.
2. 3 Plane Localizer (larger field of view)
    - Used to identify the electrode positions on the leg. This provided reference to the positioning of the slices for the anatomic reference. It is also required to improve the ASSET calibration (which samples multi-channel coil sensitivity profiles to improve acquisition speeds) of the imaging volume.
3. Proton density weighted, Fat-suppressed images
    - This high resolution anatomic image provides information on tissue boundaries, vascular position, and fat deposits to allow for manual muscle segmentation/masking.
4. Hydrogen Spectroscopy
    - Provides information on muscle metabolism. As seen in Chapter 5 muscle carnosine can be used for fibre type profiling to group participants based on activity habits. This was not used in this thesis due to the lack of athletic cohort, but will be the subject of AA research.

5. Magnetization Transfer
    - Provides information on free/bound water and the movement of water in muscle. Water movement can be linked to glycolosis and muscle metabolism, this will be explored in the thesis of AA.
6. Short TR (110ms) Muscle BOLD at Rest
    - Provides information on the functional activity in muscle at rest. This is captured to examine the use of a complexity representation of the BOLD signal to perform non-invasive muscle fibre type identification as done in Chapter 5.
7. Short TR (110ms) Muscle BOLD at Rest with a SAT Band
    - Provides information on the functional activity in muscle at rest. The SAT band was placed superior to the imaging slices to see if this reduced arterial noise inflow effects, and had a significant affect on the data.
8. Diffusion Tensor Imaging at Rest
    - Provides information on the structure of the muscle fibres in the leg. This was used to provide reference to the structural integrity of muscle fibres before and after exercise. This will be explored in the research by AA.
9. B1 Field Map at Rest
    - Provides information on the spatial excitation within the imaging volume, while using the leg imaging coil. This correction map is only required for specific analysis metrics, such as peak BOLD amplitude, that are more conventionally used.
10. B0 Field Map at Rest
    - Provides information on the magnitude of the magnetic field, spatially, within the imaging volume. This correction map is required for all analysis types and is used to correct the resting-state functional scans.
11. Magnetization Transfer - Pre-Exercise
    - Used to establish the state of free/bound water and the movement of water in muscle prior to exercise. Water distribution in the muscle prior to and post exercise will be explored by AA.
12. Short TR (110ms) Muscle BOLD Block Design
    - The block design consists of 66s rest, followed by 66s of isometric weighted plantar flexion, and is repeated four times. An exercise window of 66s was chosen to allow for a 512 point sample window to enable fractal dimension analysis. Equal rest to activity was chosen to reduce fatigue and to also have this 512 point sample window for analysis. This scan provides information on the functional activity in muscle during exercise and during the fatigued rest state. This is captured to examine the use of a complexity representation of the BOLD signal to perform non-invasive muscle fibre type identification as during a fatigued rest-state where their will be increased blood-flow relative to pure rest. It was also collected to examine activation state for phase space analysis.

13. Magnetization Transfer - Post-Exercise
    - Used to establish the state of free/bound water and the movement of water in muscle after exercise. Water distribution in the muscle prior to and post exercise will be explored by AA.
14. Diffusion Tensor Imaging Post Exercise
    - Provides information on the structure of the muscle fibres in the leg. This was used to examine differences in the structural integrity of muscle fibres after exercise. This will be explored in the research by AA.
15. Short TR (110ms) Muscle BOLD Block Design with SAT band
    - The block design consists of 66s rest, followed by 66s of isometric weighted plantar flexion, and is repeated four times. The window duration was chosen to remain consistent with the previous block design. Therefore activation differences with and without the SAT band could be observed to assess its role in reducing arterial inflow effects.
16. Short TR (250ms) Muscle BOLD Block Design with a EMG
    - The block design consists of 30s rest, followed by 30s of isometric weighted plantar flexion, and is repeated five times. The window length was decreased from above, as 512 sample blocks were not required, and it still exceeded the minimum 16s block length to adequately represent the hemodynamic response. The TR was increased to enable slice artifact removal in the EMG, as detailed above. This scan provided information on the electrical and blood-flow profile of the anterior muscle in lower leg.
17. B1 Field Map Post-Exercise
    - Provides information on the spatial excitation within the imaging volume while using the leg imaging coil. Since the muscle compartment will change size after exercise another correction map is required. This correction map is only required for specific analysis metrics, such as peak BOLD amplitude, that are more conventionally used.
18. B0 Field Map Post-Exercise
    - Provides information on the magnitude of the magnetic field, spatially, within the imaging volume. Since the muscle compartment will change size after exercise another correction map is required. This correction map is required for all analysis types and is used to correct the block design functional scans.

7.4 Experimental Preparation and Set-up

7.4.1 Prior to Examination

All prospective subjects were briefed on the experiment, and the potential benefits/risks associated with participating in the non-invasive MRI/EMG based muscle assessment study. Ethics consent was obtained from all subjects prior to an examination. Subjects then underwent preliminary screening for MRI compatibility through the use of an MRI screening form provided

by the St. Joseph's MRI staff. If subjects both consented, and were MRI compatible, they underwent maximum voluntary contraction (MVC) testing to determine the weight required to have a standardized effort across participants. The MVC test was most often performed a day prior to MRI scanning, with three cases with 3hrs rest prior, to minimize the impact of the fatigue caused by a maximal effort on the functional observations. The test consisted of single leg weighted ankle plantar flexion where the participant needed to lift the box, filled with weights, 2 inches above the ground. This is the maximal distance the box with weights could be moved when the ergometer was in the MRI bore, so this set the limitation of effort. The weight the participant had to push was incrementally increased until they could no longer raise the box to the two inch ground clearance. During MVC trials subjects were visually monitored to ensure no additional muscle recruitment causing artificially high MVC trials were recorded. From the available lead weights, which are MRI safe, the closest combination to 40% MVC was chosen for the exercise paradigm. This relative low level of weight was chosen to not induce high levels of fatigue through the experimental protocol, as their was multiple bouts of exercise totaling 11min and 20s of isometric contraction, with an equal duration of rest. Prior to the MRI examination participants were instructed to not consume alcohol [127], caffeine [128], or perform strenuous exercise for 24 hours before scanning due to their known effects on the vascular system and BOLD signal.

7.4.2 Examination Day

On the day of the exam, subjects were also required to rest for 30min while lying supine to allow for blood flow normalization in the legs, which impacts muscular imaging. [111] During the initial portion of this rest period the subject's right leg was prepared for the non-invasive assessment using MRI and EMG. To improve impedance matching between the skin and MRI compatible EMG electrodes the skin underwent the following preparation, as can be seen in Fig. 7.1. The shin of the right leg was cleaned with an alcohol wipe to remove any oils sitting on the skin. Then an abrasive gel was used to remove any dead skin cells on the surface, which are the highest impedance layer of the skin. The subject was then informed to perform plantar- and dorsi-flexion to palpate the insertion point of the tibialis anterior. Below the bony protrusion of the tibia at the insertion point of the muscle, with sufficient spacing so none of the electrode pad touched the bone, the top electrode was placed on the tibialis anterior muscle belly. The second active electrode was placed 7cm, center to center, from the top electrode within the tibialis anterior muscle belly. This 7cm allow for sufficient space for the imaging slices to be placed in between the electrodes, and it was maintained constant due to the affects of gradient artifact spacing previously discussed. The reference electrode was then placed 3.5cm inferior to the top electrode, and medial such that it was on the tibial shaft. This ensured the reference was equally spaced between the active electrodes and was on bone, which would remain as a constant reference regardless of ankle flexion state. A 7cm spacing was chosen to allow for a sufficient distance between electrodes for the imaging slices to be placed within. The electrodes will cause signal distortions in the surrounding regions and thus need to be avoided. The shielded box that contained all EMG components was placed outside the 5 Gauss line to limit RF that could contaminate the EMG recordings. The box was also placed offline from the bore as it was observed that this reduced some of the RF exposure to the circuit. Additionally, this reduced the RF that the recording laptop was exposed to. This was important as if too high levels of stray RF was received at the laptop USB input the power supply or DAC would lose connection to the laptop.

FIGURE 7.1: EMG preparation materials and set-up. Alcohol wipes, abrasive gel, carbon based MRI compatible MRI electrodes and electrode positioning on a sample participant.

During the first 15min of the rest period, prior to the electrode set-up, the MRI scanner bed was prepared. The ergometer was placed on the scanner bed by first removing the table covering to allow for the ergometer base to interface with the scanner bed. The box of the ergometer was placed on the ergometer table base. The GEM Flex coil TR switch box was placed in the empty space behind the left leg foot pedal (since the left leg remained at rest the whole time), and the flex coil connector fed under the ergometer table. Padding was placed in the notches where the feet were placed to ensure the mid-foot of the participant lay within the middle of the pedal. Sand bags were placed on either side of the flex coil to limit lower leg motion both translationally and rotationally. A Velcro scrap ran across the scanner bed over the participant's lower leg within the coil, which when strapped down prevented vertical lifting of the leg during exercise. Additionally padding was placed under the hamstrings to ensure they would not remain in constant flexion to keep the foot well positioned to interface the pedal. Additional padding was placed under the lower back and head to ensure patient comfort, which would mitigate any unnecessary motion. This set-up can be seen in Fig. 7.2.

After the scanner bed and electrode set-up, approximately 20min into the rest period, the participant was transferred to the MRI scanner bed through the use of an MRI compatible wheelchair. The participant was not allow to weight bear on their right (imaging) leg at any time during the transfer. The participant was then given a MRI compatible mask, ear plugs, over ear protection, and a panic ball to communicate distress during scanning. The EMG electrode leads were taped down to the electrodes to ensure contact was maintained. The high impedance cardiac lead cable was unwound and taped to the floor to ensure no loops formed in the cable, as loops within a time varying magnetic field would induce a current in the cables. The EMG baseline amplitude was observed to assess the quality of lead connections. The leg coil was then closed and the participant's leg was braced. The participant was then asked if anything was uncomfortable prior to land marking the coil position and putting them in the

MRI scanner. The power to the EMG circuit was then killed by disconnecting the laptop, to only be connected during the EMG acquisition. The MRI scanning session then began once a total time of 30min of rest was achieved. The scan time totaled approximately 1hr including shimming and scan execution.

FIGURE 7.2: A sample of pictures showing relevant images of a sample participant MRI set-up. The MRI compatible wheelchair, EMG box position, lower leg bracing, and subject positioning on the scanning table are shown.

7.5 Data Acquisition

The specific parameters pertaining to the scans above that are used in this thesis can be found below. Note for all functional scans and the B0 and B1 field maps the slice location, and where applicable the SAT band location, was copied to ensure region consistency.

1. Proton density weighted, Fat-suppressed images
    - Voxel Size = 0.625x0.625x4mm
    - Number of slices = 15 (1mm spacing)
    - TE/TR/flip angle = 30/3000ms/111deg
2. Short TR (110ms) Muscle BOLD at Rest
    - Voxel Size = 2.5x2.5x10mm
    - Number of slices = 2 (no spacing)
    - TE/TR/flip angle = 35/110ms/70deg, 2434 volumes
3. Short TR (110ms) Muscle BOLD at Rest with a SAT Band
    - Voxel Size = 2.5x2.5x10mm

- Number of slices = 2 (no spacing)
- TE/TR/flip angle = 35/110ms/70deg, 2434 volumes
- 50mm thick SAT band flush with superior slice

4. B1 Field Map at Rest
   - Voxel Size = 2.5x2.5x10mm, Number of slices = 2 (no spacing)
     Default GE Parameters
   - TE/flip angle = 6.2ms/15deg
   - # TEs per scan = 1, BLS Pulse Type = Adiabatic 2ms
5. B0 Field Map at Rest
   - Voxel Size = 1.25x1.25x10mm, Number of slices = 2 (no spacing)
     Default GE Parameters
   - TR/flip angle = 100ms/20deg
   - # TEs per scan = 1, B0 Field Mapping Range = 200Hz
6. Short TR (110ms) Muscle BOLD Block Design
   - Voxel Size = 2.5x2.5x10mm
   - Number of slices = 2 (no spacing)
   - TE/TR/flip angle = 35/110ms/70deg, 4800 volumes
7. Short TR (110ms) Muscle BOLD Block Design with SAT band
   - Voxel Size = 2.5x2.5x10mm
   - Number of slices = 2 (no spacing)
   - TE/TR/flip angle = 35/110ms/70deg, 4800 volumes
   - 50mm thick SAT band flush with superior slice
8. Short TR (250ms) Muscle BOLD Block Design with a EMG
   - Voxel Size = 2.5x2.5x10mm
   - Number of slices = 2 (no spacing)
   - TE/TR/flip angle = 35/250ms/70deg, 2400 volumes
   - The EMG signal was sampled at a rate of 5000Hz with a system gain of 2448
9. B1 Field Map Post-Exercise
   - Voxel Size = 2.5x2.5x10mm, Number of slices = 2 (no spacing)
     Default GE Parameters
   - TE/flip angle = 6.2ms/15deg
   - # TEs per scan = 1, BLS Pulse Type = Adiabatic 2ms

10. B0 Field Map Post-Exercise
    - Voxel Size = 1.25x1.25x10mm, Number of slices = 2 (no spacing)
      Default GE Parameters
    - TR/flip angle = 100ms/20deg
    - # TEs per scan = 1, B0 Field Mapping Range = 200Hz

7.6 Data Preprocessing

7.6.1 Functional Images

The focus of this thesis was on functional muscle imaging using BOLD and EMG. As such, after collecting the data using the parameters above it needed to be preprocessed prior to analysis. The preprocessing of the functional data was scripted in Bash, and can be found in the appendix, and used the tools from FSL[117] and AFNI[129]. The preprocessing was mainly automated, but required some work on a participant-wise basis.

The first step of the process was converting the dicom images exported from the scanner to nifti files, so they could be recognized by the tools such as FSL and AFNI. This was achieved by using the dcm2niix() function where the specific path of the dicom images must be specified and a nifti file created by concatenating the images in both the spatial and temporal dimension. The specific series path where the data were contained remained relatively constant between participants but needed to be modified if any errors occurred during a scan, which would offset the series numbering for the remaining scans. After all scans were converted to nifti files and followed a standard naming convention then underwent motion and field map correction. All resting-state functional scans were motion corrected by spatially aligning all time points in the resting-state scan without and with the SAT band to the first time point of the first resting-state scan. The resting-state scans were then corrected for static field variations from using the magnitude of the main magnetic field, spatially, within the imaging volume, by using the B0 map collected after rest. The block design functional scans were also motion corrected by spatially aligning all time points to the first time point of the first resting-state scan. This would allow for one common mask of muscle regions for the resting-state and block design functional scans to be made, allowing for a relevant comparison between scans. The block scans were then corrected for static field variations from using the magnitude of the main magnetic field, spatially, within the imaging volume, by using the B0 map collected after exercise, to take into account the changing size of muscle compartments post exercise. Both the motion and field map correction were achieved by using the flirt tool in FSL[117].

Other common corrections, such as B1 field map correction, were not employed as the absolute BOLD intensity was not required in any of the newly developed analysis metrics. Additionally, no spatial or temporal filtering was applied to the data. Spatial filtering was not used as metrics were derived on a voxel-wise basis, so the spatial blurring could lead to not statistically independent voxel wise observations. Non-independent observations are more of a concern when developing new metrics, thus to ensure the results were not being confounded by the filtering it was not employed. Additionally, temporal filtering was avoided, as once again its influence on the newly derived metrics could confound or obscure results. Specifically, in the functional

studies the relative variance of the data is observed, to quantify the fractal dimension, so temporal filtering would inherently decrease variance which was undesired. Also it was verified that temporal filtering was not required to see activation, as high levels of HRF correlation, during the block design scans, in hypothesized active region of the tibialis anterior (during plantar flexion) were observed with no filtering. It is considered best practice to perform the minimal amount of preprocessing required to not unduly influence the results to show significance which is not innately there.

The final step of the preprocessing pipeline involved manual muscle segmentation. This was achieved by using FSL. Turning FSL into editor mode and specifying the display space to be in the BOLD scan resolution, the anatomic reference was used to manually trace out the muscle masks by drawing the regions of interest voxel by voxel. When drawing these masks the first consideration was to avoid the tissue boundaries between muscles, which would not be reflective of muscle activity. It should be noted that due to the use of the foot pedals, and the height of the coil, the lower leg lay on a slight declined angle. This meant that the tissue boundary between muscles found in the anatomic reference slices (4mm thick) changed position through the length of the functional slice (10mm thick). Therefore a conservative mask boundary was required to make sure the functional voxels did not lie on a tissue boundary in any of the anatomic reference slices. Second, the major blood vessels, including a minimum of one voxel in each direction in the surrounding areas, were avoided due to the pulsatility artifact propagating to the surrounding regions. Third, the minor blood vessels were inspected for a pulsatility artifact through using the resting-state fMRI timeseries as reference, and only avoided if the artifact was visible. Masks were made for the gastrocnemius [slow-twitch/fast-twitch dense], soleus [slow-twitch dense] and anterior muscles (tibialis anterior, peroneus and extensor longus groups) [fast-twitch dense] for their differing twitch fibre profiles. These muscles are also heavily involved in ankle plantar flexion so are relevant to exploration in all aspects of the study. It should be noted that the tibialis posterior was not included in the anterior compartment because although it is a fast-twitch predominate muscle, it is surrounded by the three major arterial venous pairs of the pernoa, anterior and posterior tibial. Therefore the BOLD data from this muscle would contain heavy amounts of pulsatility artifact, which would affect both the resting-state and block design studies. Fig. 7.2 shows some of the sample data for one participant that is used to perform motion and field map correction, as well as manual muscle segmentation / mask creation. Any specific preprocessing steps relevant to the analysis techniques that were developed is covered in their respective sections.

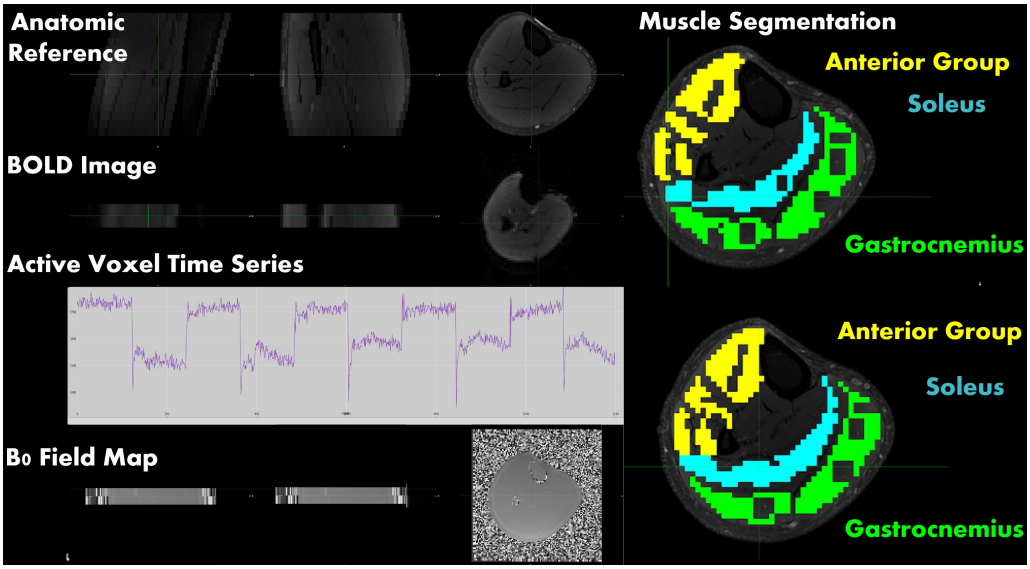

FIGURE 7.3: This shows the sample data from one Block design trial for a single participant. It shows the anatomic, functional and field map images, as well as the segmented muscles for this specific participant.

7.6.2 Electromyography

In addition to the filtering that is performed by the analog front end, as described in the development section above, the EMG data needed to be cleaned to be suitable for analysis. The EMG data were collected by labview and saved as an LVM file at a sample rate of 5000Hz. This data was imported to MATLAB to be cleaned through the use of an in-house script. To import the data the open source script downloaded off the Mathworks website lvm_import.m is used. To perform the denoising portion the EEGLab [130] was used. EEGLab requires an EEG structure, generally output by the commercially used MRI compatible EEG systems, to determine when the slice triggers during the MRI acquisition occur. From a series of experiments using the TTL pulse output by the MRI scanner, during EPI acquisitions, it was determined that the slice triggering remained stable over time, as can be seen in Fig. 7.4. Therefore with the used TR=250ms and a 2 slice acquisition an artifact would be expected every 125ms. Therefore, the triggers did not need to be recorded for every EMG trial, but rather a trigger timing structure file could be created using the same format required by EEG lab, while knowing the first slice trigger would appear at the start time of the EMG recording. This was achieved using the function eventTable.m originally written by AA and modified for use by JEM.

With the slice timing file created, the EMG data then underwent denoising by first using the EEGLab function FASTR. FASTR will create an artifact template and perform subtraction of the slice artifacts induced by the MRI gradient traversal. The algorithm consists of four main steps, slice timing trigger alignment, local slice artifact template subtraction, PCA residual removal and adaptive noise cancelling (ANC). A comprehensive explanation of these four steps can be found in section 3.3.3 in the following reference [104]. The main parameters that can be modulated for the FASTR algorithm are the low-pass filter cutoff, the degree of upsampling, the averaging window size to create the artifact template, and the ANC process, where the ANC will suppress noise that is above the low pass filter cutoff specified. The upsampling

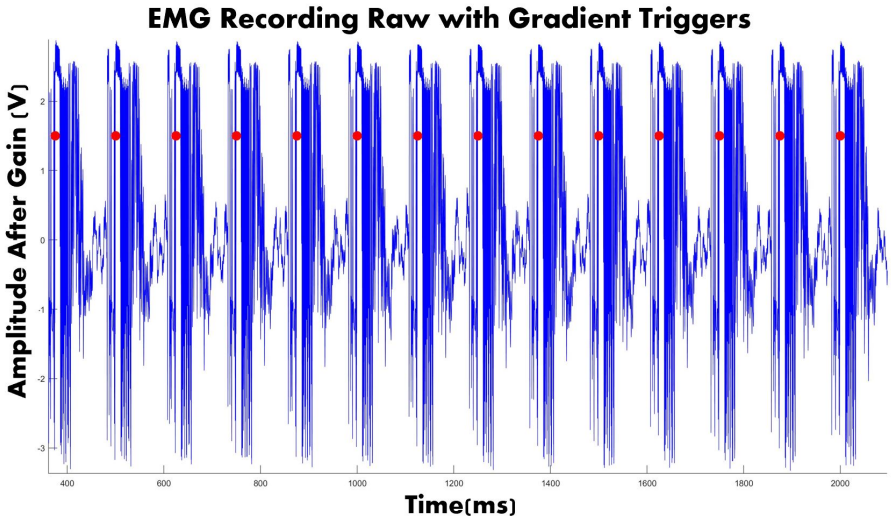

FIGURE 7.4: This shows sample EMG data during the resting state of one participant. The repetitive and stable nature of the gradient triggers allowed for the creation of a slice timing file to facilitate a simple denoising procedure

recommended by EEG is to use a factor to get to 20kHz, in order to sufficiently represent the high frequency gradient artifact. A factor of 10 was used to get a sampling rate of 50kHz to exceed this requirement. A window of 4 artifacts per window was used instead of the standard 30 artifacts per window. This was chosen as FASTR is primarily used for EEG where they specify the window length should be decreased if there is a lot of participant motion causing spikes in the data. The EMG bandwidth is 20-500Hz compared to an EEG bandwidth of roughly 0.1-70Hz, so the rapid onset of the EMG spikes means a smaller window is preferred for artifact template creation. Additionally if the window length is too long the rest and active states, which are vastly different in amplitude, will overlap which can confound the artifact template that is created. To test the optimal window length the SNR of the EMG recordings was assessed by iterating through varying window sizes. SNR was computed by rectifying the EMG signal, then computing the ratio of the signal summed squared magnitude to the noise summed squared magnitude, while reporting in decibels. The benefit of this window length of 4 artifacts per window can be seen clearly in Fig. 7.5. The other factor that could be modified was the use of the ANC. Through employing the same SNR testing framework it was determined that when the participant had a noisy baseline signal ANC was able to improve the SNR, as is seen in Fig. 7.6. It should be noted the ANC cuttoff threshold was changed from 70Hz to 500Hz to increase the suitably for use with EMG. But after examining the frequency spectrum of the EMG data with and without ANC, it was seen that the ANC caused suppression of the frequency components in the bandwidth of 0-70Hz, even though not specified to, and it has a more aggressive 500Hz cuttoff. Therefore the ANC was not used to clean the data. Additional filtering to improve data quality was performed after FASTR as the high frequency components should initially remain in the data to create a more accurate artifact template prior to its removal. The filtering included a 60Hz notch filter (from any noise introduced from the electronics brought into the room), HPF cuttoff at 20Hz and LPF cuttoff at 500Hz. All EMG trials were inspected visually to determine the success of the denoising procedure.

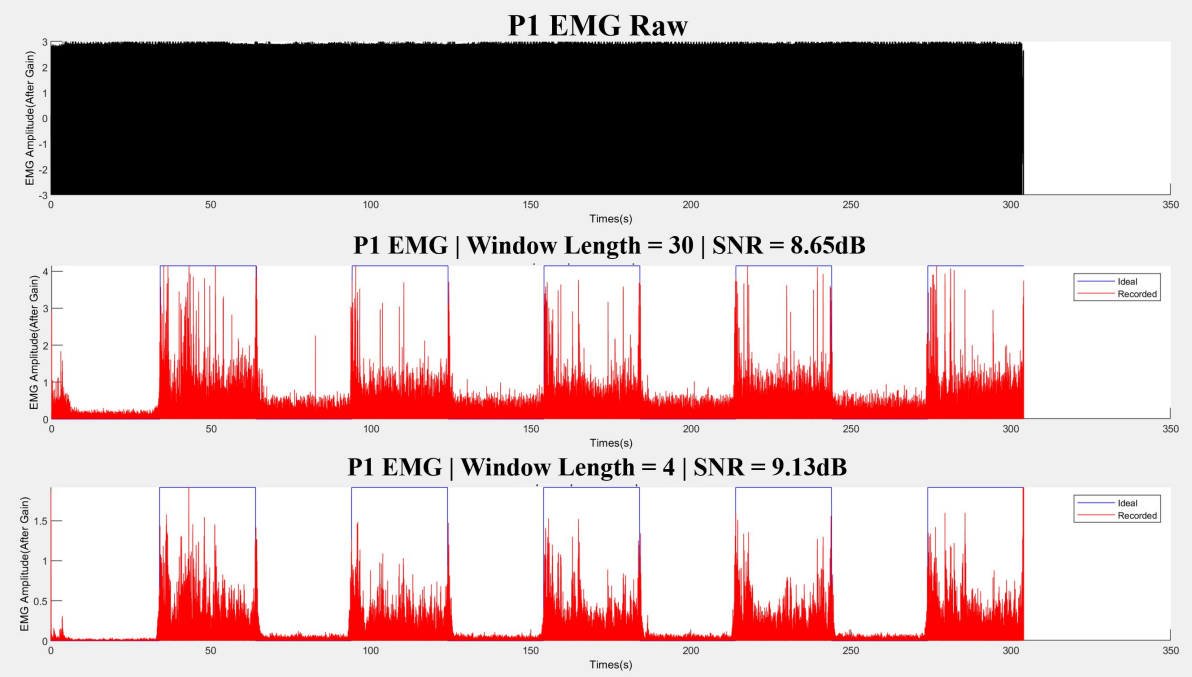

FIGURE 7.5: This shows sample EMG data that is cleaned using FASTR of different window lengths follwed by additional filtering with a 60Hz notch filter, HPF cuttoff at 20Hz and LPF cuttoff at 500Hz.

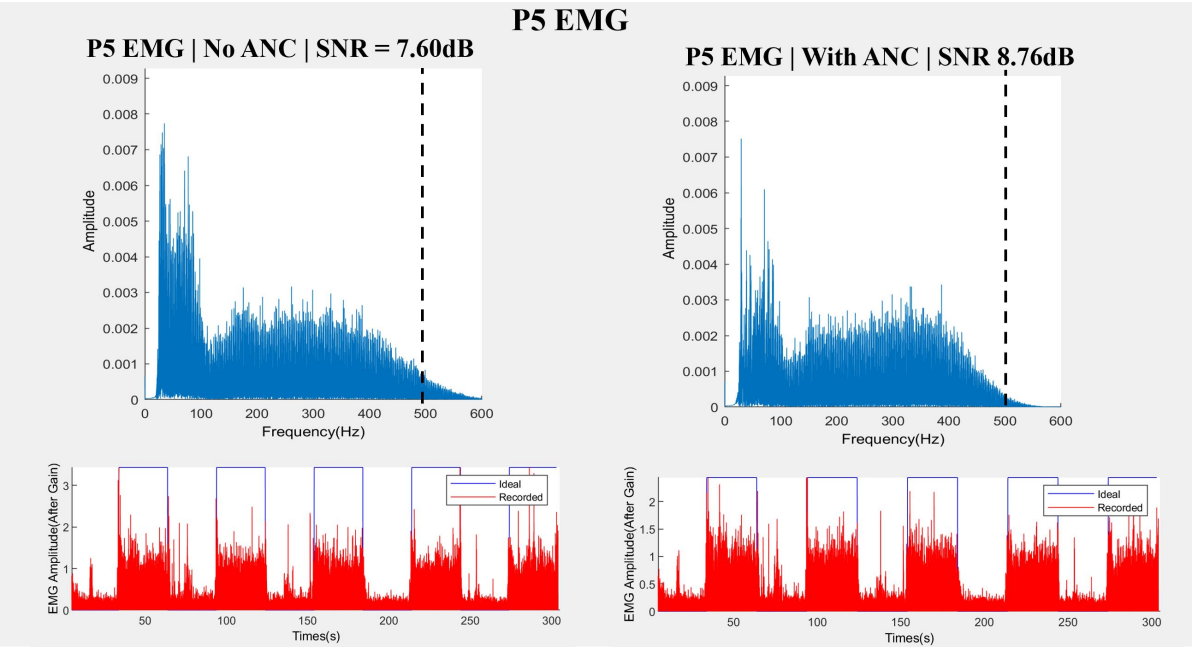

FIGURE 7.6: This shows sample EMG data that is cleaned using FASTR with and without ANC followed by additional filtering with a 60Hz notch filter, HPF cuttoff at 20Hz and LPF cuttoff at 500Hz.

Chapter 8

Determining Relative Skeletal Muscle Fibre Composition

8.1 Introduction

The rationale behind the exploration into determining skeletal fibre muscle composition is well explored in Chapter 5. However this investigation into the use of a bi-fractal dimension description of the muscle BOLD signal, to perform muscle fibre type profiling, takes a different approach. Firstly, this cohort of participants is a subset of non-athletes who will be hypothesized to present less differentiated muscles due to reduced muscle tone. This will make fibre type classification more difficult than in the athletes as used in the pilot in Chapter 5. Additionally, the encouraging results from this pilot lead to the extended exploration of this technique using a fatigued rest paradigm. Originally, the muscle fibres were differentiated using 4 512point windows while a participant was purely at rest. An exploration at rest was chosen as the relative perfusion differences between slow-twitch and fast-twitch muscle fibres were the driving factor with the differences in the muscle BOLD signal, and exercise would cause a non-uniform increase in blood flow across the muscle which could confound the results. However it was hypothesized that if the fractal dimension of the muscle was assessed using the 4 resting-state blocks of 512 point length within an exercise paradigm the differentiation between muscle groupings would be easier. This was made on the basis that post-exercise blood volume increases in the muscle would increase the amplitude of the BOLD signal, meaning it would be less likely to be contaminated by noise. The windows of rest between exercise stints would not be as impacted by regional increases in blood-flow that are dependent on the particular exercise performed. Therefore this chapter investigates a non-athlete subject group, with the same methodology employed in Chapter 5, either during a pure rest or fatigued resting state. This will provide insight on whether the method is robust across a less ideal population and whether a pure rest or fatigued rest is the optimal paradigm.

8.2 Methods

8.2.1 Data Acquisition and Preprocessing

The paradigm design, rationale, parameters for MRI data acquisition, and fundamental preprocessing steps are outlined in Chapter 7. The data which was used in this particular analysis was the motion and field map correction functional data from the BOLD resting-state scan and from the BOLD plantar flexion block design.

8.2.2 Data Analysis

The frame work to use a bi-fractal representation to determine muscle fibre type is covered in detail in Chapter 5, so only a brief overview of the data analysis will be covered. The BOLD resting-state data where the leg was purely at rest, underwent truncation to 2048 volumes, which made it suitable for fractal dimension analysis, accounts for the required relaxation due to violating the Ernst condition and reduces motion artifact. The BOLD voxel time series was then normalized to the first time point to account for variations in the excitation and sensitivity profiles of the coil channels. The BOLD time series was then segmented into 4 512 time point segments, where the bi-fractal dimension was computed for each window using the scaled windowed variance approach, with linear detrending. The bi-fractal dimension was computed by estimating the slope by fitting two lines, components 1 and 2, to the non-saturated portion of the log-log plot for a given voxel and segment, then averaging across segments. The same process was applied with the BOLD plantar flexion block design data, with the additional step of segmenting the time series into the relevant window of the fatigued resting-state, between the stints of exercise. All 66s windows which correspond to 600 time points were truncated to 512 point windows, of suitable length for fractal dimension analysis, by discarding the first and last 44 time points for each rest and active block respectively. This was done as when transitioning between active and rest states for multiple reasons such as the gross motion causing spikes in the BOLD time course, to allow the muscle compartments (which change orientation between states) sufficient time to normalize, and to allow for the participant to reach a stable ankle flexion position. Then the 4 512 resting-state segments from the plantar flexion block design were used in the bi-fractal analysis. The same steps as indicated above were performed. The voxel BOLD series was normalized by the first time point (which is valid as the block design paradigm begins with rest), followed by computing the bifractal dimension for each window using the scaled windowed variance approach, with linear detrending, and averaging across all windows. The next step was to identify the voxels that were within a specific muscle by using the manually created masks for reference. The three masks covering the gastrocnemius, soleus and anterior group (tibialis anterior, peroneus and extensor longus groups), were created for the muscle's varying twitch fibre type profiles. This was performed for each participant and muscle respectively and the voxel timeseries was stored for later analysis.

Due to the non-athletic cohort of subjects, they could not be grouped into predominate fibre type groupings, as was examined previously in Chapter 5, which limits comparisons to solely between muscle differences. To begin all bi-FD distributions for a given participant, component, and muscle were tested for normality. All bi-FD voxel distributions were negatively skewed, even post log transform correction. Therefore Wilcoxon rank sum tests were used to examine within participant muscle differences. The soleus and gastrocnemius were compared to assess slow-twitch differentiability and the gastrocnemius and anterior group for fast-twitch differentiability. Individuals were tested for differences in the fractal dimension between muscles with tests for each component respectively, and for the pure rest and fatigue rest states. Since the intent was to compare between muscles, within a given participant, the multiple pair-wise comparisons for a given participant needed to be accounted for to not artificially report significance. With performing two tests for each muscle and with two resting-states per participant, bonferroni correction for multiple comparison requires the $P<0.05$ threshold to be corrected to $p<0.0125$. Additionally, for each resting-state acquisition respectively, a Kruskal-Wallis test was used to test between muscle differences, for each bi-fractal dimension component, while using all subjects

to account for biological variability factors. With the intent to compare between the three muscle groups, every voxel belonging to a particular muscle (including all participants) is used for the statistical comparison between muscles. Therefore to correct for the reported p-values with these comparisons, the muscle with the largest number of voxels needed to be used to scale the significance threshold. When concatenating all participant data the number of voxels per muscle group was: gastrocnemius 5081 voxels, soleus 4438 voxels and anterior group 3107 voxels. Therefore for the Kruskall-Wallis muscle comparison tests the $p<0.05$ threshold was corrected to $p<9.84e\text{-}6$. This was followed by multiple comparison testing to investigate specific muscle differences, which took into account this correction factor. Finally, to examine the differences between paradigms of pure rest compared to fatigue rest a Kruskal-Wallis test was used for each muscle and component.

8.3 Results

To assess the ability of the bi-fractal dimension of the muscle BOLD signal to determine fibre type differences, the participant biological variability effect was first removed by performing participant specific muscle comparisons. Tab. 8.1 provides a summary of the p-values for the ranked sum muscle comparison tests for each participant for each component and resting-state separately. When examining the pure resting-state data it can be seen when comparing the gastrocnemius (mixed fibre type) and soleus (slow twitch fibre type) that 6/11 participants show significant differences between muscles, surviving multiple comparisons, for component 1 and 7/11 for component 2. When comparing the gastrocnemius (mixed fibre type) and anterior group (fast twitch fibre type) 8/11 participants show multiple comparison corrected significant differences for both component 1 and component 2. When examining the differences between muscles during the fatigued resting-state the number of participants that showed significant differences, surviving multiple comparisons, for the gastrocnemius vs. soleus was 6/11 for component 1 and 6/11 for component 2. For the gastrocnemius vs. anterior group the number of participants surviving multiple comparison correction was 9/11 for component 1 and 5/11 for component 2. Therefore when examining the differences on a individual participant level the fatigue rest-state did not significantly affect the gastrocnemius vs. soleus comparison, but performed worse for the anterior group vs. gastrocnemius comparison.

Subsequent to the individual participant analysis, the group analysis for each respective component was undertaken to account for biological variability factors. Since Kruskal-Wallis test can only test one-way comparisons 4 separate tests were run, one per component and resting-state, and are summarized in the Tab. 8.2. For both components and both states of rest, significant differences were found when comparing the soleus, gastrocnemius and anterior group. Notably, the differences between muscles were more significant during the fatigued resting-state for both components. When performing multiple comparisons, regardless of resting-state or component, the soleus fractal dimension was significantly greater than both the gastrocnemius and anterior group, but the gastrocnemius and anterior group did not significantly differ in their fractal dimension. The results are summarized in Fig. 8.1, where notably the difference between the soleus and the fast-twitch predominate muscles increases during the fatigued resting-state. This observation explains the increased significance seen in the Kruskal-Wallis tests.

Finally, the investigation into the differences in the fractal dimension of the BOLD signal during pure and fatigued rest showed significant results. When comparing between the pure

TABLE 8.1: P-value Summary, p<0.0125 multiple comparison significance threshold, for the ranked sum muscle comparison tests for each participant, component and resting-state separately.

	Pure Resting State Ranked Sum PValues				Fatigued Resting State Ranked Sum P Values			
	Soleus Vs. Gastrocnemius		Gastrocenmius Vs. Anterior Group		Soleus Vs. Gastrocnemius		Gastrocenmius Vs. Anterior Group	
Subject	*Comp1*	*Comp2*	*Comp1*	*Comp2*	*Comp1*	*Comp2*	*Comp1*	*Comp2*
1	1.25e-11	1.26e-13	2.72e-08	1.51e-15	8.07e-15	1.32e-07	1.48e-19	3.23e-12
2	7.74e-06	0.000408	2.15e-08	9.06e-07	0.171	0.0590	0.255	0.779
3	0.686	0.907	0.583	0.0557	0.515	0.377	0.00651	0.244
4	0.916	0.0363	1.66e-06	0.378	0.00568	0.722	6.41e-06	0.273
5	1.60e-10	3.85e-05	5.41e-12	1.15e-07	0.0628	6.23e-11	0.000592	3.09e-12
6	0.0357	9.03e-05	0.0299	1.56e-05	4.02e-11	0.0180	7.93e-40	0.00628
7	0.825	1.18e-16	0.0246	3.24e-16	0.188	2.85e-14	0.553	0.351
8	7.94e-05	1.11e-08	0.0110	0.000406	1.32e-06	2.21e-17	1.69e-07	5.58e-19
9	1.69e-21	3.43e-08	1.12e-09	0.0251	1.24e-37	1.12e-27	1.58e-33	7.38e-34
10	0.124	0.146	5.45e-09	5.27e-15	7.04e-14	0.000215	2.36e-11	0.551
11	0.00313	0.0640	0.000451	0.00150	0.0166	0.678	0.000434	0.121
Mean	**0.236**	**0.059**	**0.105**	**0.0419**	**0.0874**	**0.0742**	**0.1686**	**0.212**

and fatigued resting-state the fractal dimension decreased during the fatigued state for the gastrocnemius, soleus, and anterior group, all with a significant of p<1e-7. The box plot results from the Kurskal-Wallis test are summarized in Fig. 8.2, which show the decreased fractal dimension during fatigued rest. In addition, the distribution of the fractal dimension measures appears larger during fatigued rest.

TABLE 8.2: Summary of the p-values, corrected significance threshold p<9.84e-6, for Kruskal-Wallis tests for differences between muscles when using all participants.

Comparisons Bi-fractal Dimension Component 1		Pvalue (Prob. >Chi-sq)
Muscle Differences (Soleus vs. Gastrocnemius vs. Anterior Group)	*Pure Resting-State*	3.31e-36
	Fatigued Resting-State	9.98e-48
Comparisons Bi-fractal Dimension Component 2		**Pvalue (Prob. >Chi-sq)**
Muscle Differences (Soleus vs. Gastrocnemius vs. Anterior Group)	*Pure Resting-State*	4.68e-37
	Fatigued Resting-State	2.26e-43

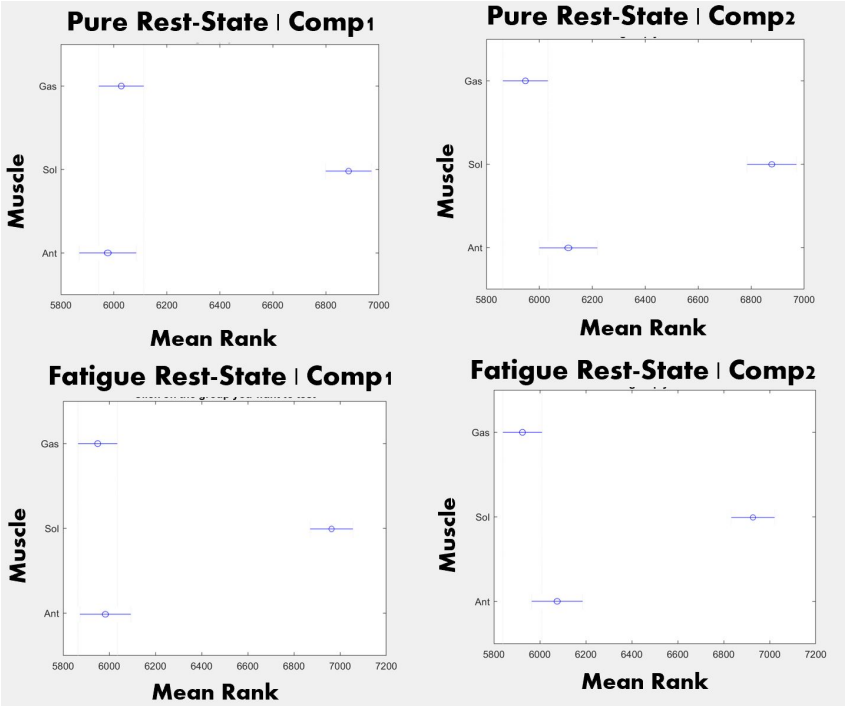

FIGURE 8.1: Multiple comparison tests of differences between muscles using a ranked sum comparison, which does not assume a normal distribution. Comparisons are performed for each component and resting-state separately, with the soleus showing strong significant differences between the fast-twitch muscles.

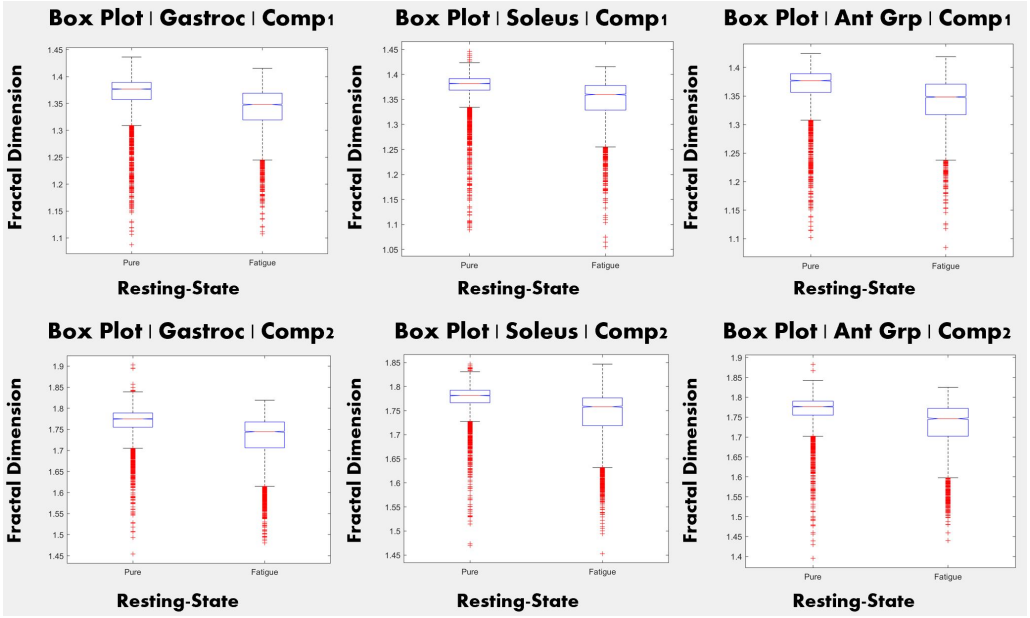

FIGURE 8.2: This shows the box plots from the Kruskal-Wallis comparisons between the resting-state acquisitions. Decreases in the fractal dimension, were significant, and are seen when comparing pure to fatigued rest.

8.4 Discussion

The discussion of the significance of the results of using the BOLD bifractal dimension to differentiate between muscle fibres, and its clinical significance, is well covered in the discussion in Chapter 5. Therefore the focus of this discussion will be comparing the results seen in Chapter 5, and the effect of using a fatigued resting-state. When compared to the pilot study results both participant groups showed significant differences when comparing muscles when including all participants. While saying this, in the pilot study with the athlete cohort larger differences were seen between the mixed fibre type gastrocnemius and fast-twitch anterior group. In addition the fractal dimension of muscle groupings followed the order of soleus > gastrocnemius > anterior group, which suggests that a larger fractal dimension corresponds to greater slow-twitch fibre density. When examining the pure-rest fractal dimension relation with the non-athletes the order of muscle fractal dimension for component 1 was soleus > gastrocnemius > anterior group, and component 2 soleus > anterior group >gastrocnemius. Although for component 2 this is contrary to the trend seen in more athletic group, no significant differences were seen between the gastrocnemius and anterior group in the non-athlete cohort, so the relative magnitude in the fractal dimension between these muscles cannot be reliably assessed. Encouragingly, in both cohorts of subjects the fractal dimension of the soleus was greater than other two more fast-twitch predominant muscles, suggesting a larger fractal dimension corresponds to a greater density of slow-twitch fibres. The current results with the non-athletic cohort indicate that the fibre type profiles of non-athletes is less differentiated than athletic individuals, but this would have to be corroborated with biopsy results. The less well developed muscles in the lower-leg in this cohort, although non-ideal is more reflective of the clinical population. Therefore if this novel bi-fractal dimension tool were to be translated to clinical implementation it must be refined to allow for the differences between the anterior muscles and gastrocnemius to be more readily identified on a global population basis.

The next point of discussion is the effect of using a fatigued resting-state as opposed to a pure resting-state in differentiating muscle fibre type profiles. To begin, when examining the differences on a individual participant level the fatigued rest-state did not significantly affect the gastrocnemius vs. soleus comparison, but performed worse for the anterior group vs. gastrocnemius comparison. This was in-contrast to when examining results over the entire subject population where the differences between muscles was more pronounced during the fatigued resting-state. This was seen by the larger significant differences found in Tab. 8.2 and the larger separation between the soleus and other muscle groupings seen in the multiple comparisons in Fig. 8.1. This could be caused by the larger variation in the fractal dimension measures, as seen in the boxplot graphs when comparing the two different states of rest (Fig. 8.2). The larger variation in the group fractal dimension measures within each muscle, could attribute to the worse gastrocnemius and anterior muscle classification seen on an individual participant basis. Therefore on an individual subject basis the fatigue rest-state is comparable to pure rest and when looking at trends over the subject population it performs better. The worse classification performance could be due to participant biological variability, which would have to be confirmed by muscle biopsy. Therefore the marginally worse classification accuracy could be more reflective of the ground truth, as when looking at trends over groups the fatigue resting-state does perform better. This statement should be taken with caution, as without biopsy as a validation of participant specific muscle fibre type ratios a definitive conclusion cannot be made. Regardless, in future work where biopsy is required to validate the bi-fractal muscle

BOLD metric to perform muscle fibre typing, both the pure and fatigued-resting state should be examined as neither shows superiority while currently using hypothesized muscle fibre type ratio estimation based off of normative data.

The final point of discussion is the decrease in the fractal dimension measure when comparing the pure to fatigued rest state. This showed across all muscles and components. This indicates that as a function of fatigue the relative complexity of the BOLD signal decreases. Since the BOLD signal is related to metabolism and perfusion this implies that as a function of fatigue perfusion complexity decreases. To state this differently this indicates that as a function of fatigue muscle perfusion and metabolism becomes more regular or structured. Therefore this result suggests that as a function of fatigue muscle perfusion becomes less random and more structured in order to meet the increasing demands of the muscle. This results shows parallels to decreases in neural BOLD complexity during task has been described through decreased randomness in neural activity when compared to rest [131]. Therefore, a decrease in BOLD signal complexity, or blood flow complexity may be a metric of fatigue. To the author's knowledge this is the first investigation that has shown the decrease in mBOLD complexity as a function of fatigue. With further investigation this could be used to understand the relative difference in perfusion as a function of fatigue, which could be imperative in assessing diseased muscle dysfunction in disease, as muscle dysfunction is associated with rapid fatigue onset.

Chapter 9

Determining Muscle Activation State

9.1 Introduction

The focal point of this thesis to provide a more comprehensive understanding of muscle through novel measures and a more complex representation of the inherently complex functional and structural composition of muscle. As such, this section uses a phase space representation of muscle activation to more accurately characterize muscle behaviour. The phase space describes a signal's state/state-transitions over time. The phase space provides novel insight instead of the conventional temporal BOLD analysis techniques, such as correlation with an ideal response function, its time to peak, hyperemic peak value, peak area, and peak width. [46], [50], [51]. The phase space representation of the BOLD signal has shown promise in classifying neural activation patterns, as seen through my abstract presented at ESMRMB 2021 entitled Functional Magnetic Resonance Imaging Analysis Revisited: A Model Free Approach [89]. This work showed that during a simple finger tapping block design paradigm that phase space separability metric agrees with hemodynamic response function correlation activation patterns, yet is model free. Specifically, a phase space where the active and resting states could be readily separated was a more functionally active region. Additionally, the work showed how the phase space separability was sensitive to hand-dominance, and thus could show activation as a gradient due to brain state organization and not, subject specific amplitude. This work laid the foundation for the use of the phase space to assess muscle activation, through using a phase space separability metric. Additionally, it was hypothesized that a phase space analysis would provide insight into the activation of muscle and whether or not it was a binary classification of active during contraction and inactive during rest. As was discussed in Chapter 3, the phase space has not been used commonly in BOLD imaging, with the primary focus of examining neural process non-linearity. Therefore to the author's knowledge this phase space approach to quantifying BOLD muscular activity is unprecedented.

9.2 Methods

9.2.1 Data Acquisition and Preprocessing

The paradigm design, rationale, parameters for MRI data acquisition, and fundamental preprocessing steps are outlined in Chapter 7. The data which were used in this particular analysis was the motion and field map correction functional data from the BOLD plantar flexion block design

without the SAT band. This was chosen as this was the longest exercise paradigm without a SAT band, thus it would be more likely to show fatigue provides insight into differing muscle activation characteristics. The non saturation band acquisition was also chosen, as a SAT band for muscle BOLD acquisitions is not conventionally used, so any conclusions on muscle activation did not want to be confounded by the use of a SAT band.

9.2.2 Data Analysis

To assess muscle activation using the novel outlook of the phase space, the analysis was performed by writing a set of scripts in MATLAB. The first step involved segmenting the voxel time-series to reduce the influence of motion artifact. To facilitate comparison with the previous analysis techniques the window lengths were chosen to remain consistent. All 66s windows which correspond to 600 time points were truncated to 512 point windows, of suitable length for fractal dimension analysis, by discarding the first and last 44 time points for each rest and active block respectively. Once again this was done to reduce gross motion BOLD spikes, to allow for muscle compartment size and participant ankle position normalization. The next step was to identify the voxels that were within a specific muscle by using the manually created masks for reference. The three masks were consistent from the previous investigations covering the gastrocnemius, soleus and anterior group. The phase space for all relevant voxels that fell within muscle masks was created by using the time-series and its temporal derivative. This method was preferred over plotting the time-series against a latent term. This is because the latent term requires a metric of determination, such as principal component analysis. Therefore the latent term may vary across voxels, whereas the derivative computation would remain constant which is preferable for the voxel-wise analysis employed. With the outlook to use phase space metrics to quantify muscle activation, an activation reference was required. Thus, for all participants, and all voxels within muscle masks, the correlation between the voxel time series and the ideal activation function was computed. This ideal activation was a boxcar function, with block lengths of 512 points, where the resting-state was given an amplitude of zero and active state an amplitude of one. The correlation with the ideal hemodynamic response function (HRF) served as the activation reference, or ground truth, prior to finding activation using novel phase space approaches. The first means in which activation was assessed in the phase space is by assessing the phase space separability. Phase space separability into active versus rest states was assessed with a linear discriminant classifier. For a given voxel phase space, a linear boundary between the time points in the four rest blocks and time points during the four plantar flexion (active) blocks was generated using the MATLAB function MdlLinear(). Then the separability of the phase space into rest and active states was determined by assessing the classification accuracy of this linear boundary. Voxels that had a high degree of separability between the active and rest states would have high classification accuracy. Voxels that were agonists (well correlated with the activation function with a positive correlation coefficient) and antagonists (well correlated with the activation function with a negative correlation), would both appear to have a high phase space separability. As such, the absolute correlation of the HRF activation was compared to the phase space separability to see if both metrics came to the same conclusion on the regions of activation in the muscle. Fig. 9.1, shows a comparison of the absolute HRF correlation and the phase space separability classification accuracy for a participant, where the mappings look remarkably similar. This observation was assessed by finding the correlation between the absolute HRF correlation value and phase space separability classification accuracy at every voxel for each participant and muscle respectively, as summarized

in Tab. 9.1.

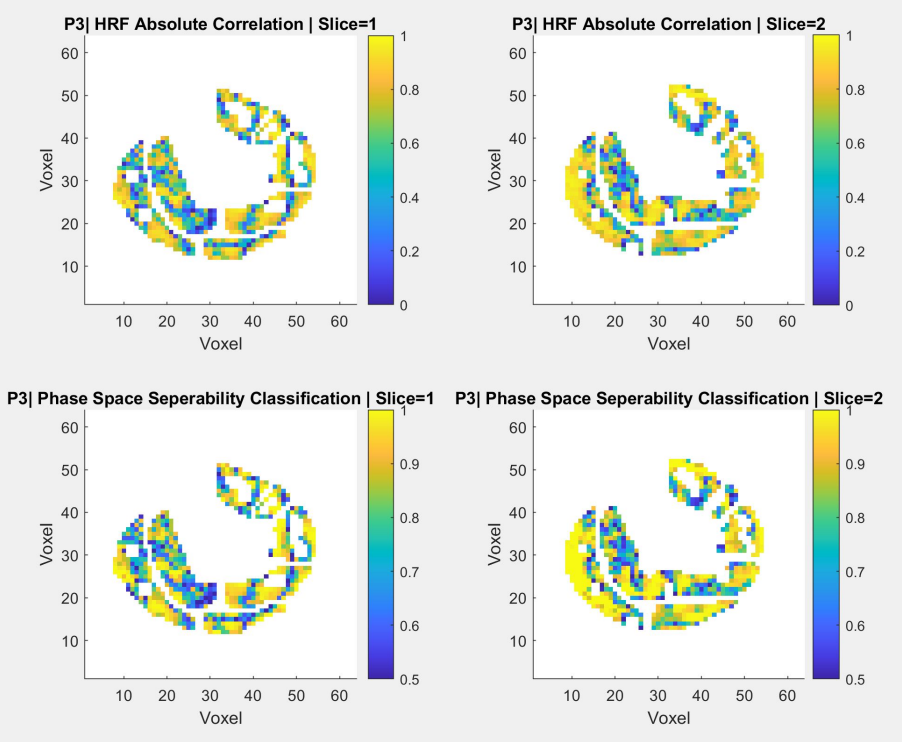

FIGURE 9.1: This shows a subject's activation maps using (top) an absolute ideal HRF correlation with a boxcar model versus the model independent (bottom) phase space separability metric. The absolute correlation ranges from 0 to 1 and phase space separability from 0.5 to 1 where 1 is perfectly separated resting and active states. Both maps show the involvement of agonist and antagonist regions, with a great similarity.

Next, the phase space was plotted at voxels that had a high correlation with ideal hemodynamic response function and a high phase space separability, to determine if the phase space could provide novel insight into the activation state of muscle. Fig. 9.2, shows two example voxels with high activation. The conclusions that were made from the initial plots seeded the further analysis and will be explained in further detail in the results section. But in short, the initial plots showed that both agonist and antagonist active muscle regions had multiple states, and provided insight into muscle fatigue.

Subsequently, to test if the anecdotal evidence of muscle showing multiple states during exercise held over all participants and regions, a clustering analysis was done. The first step of this analysis was to find the optimal number of clusters that a given voxel phase space possessed. This was achieved using k-means classification and the silhouette metric to determine decision validity. Since the block design consisted of 8 blocks, 4 during rest and 4 during plantar flexion, the maximum number of states/clusters the phase space would show is 8. Therefore, for a given voxel time-series, a k-means approximation was generated for a range from 2 to 8 clusters. The silhouette coefficient was then found for all data points, for a particular cluster number variation, to assess the degree of separation between clusters. Silhouette coefficients range from [-1 1] where being near 1 indicates the sample is far away from the neighboring clusters, 0

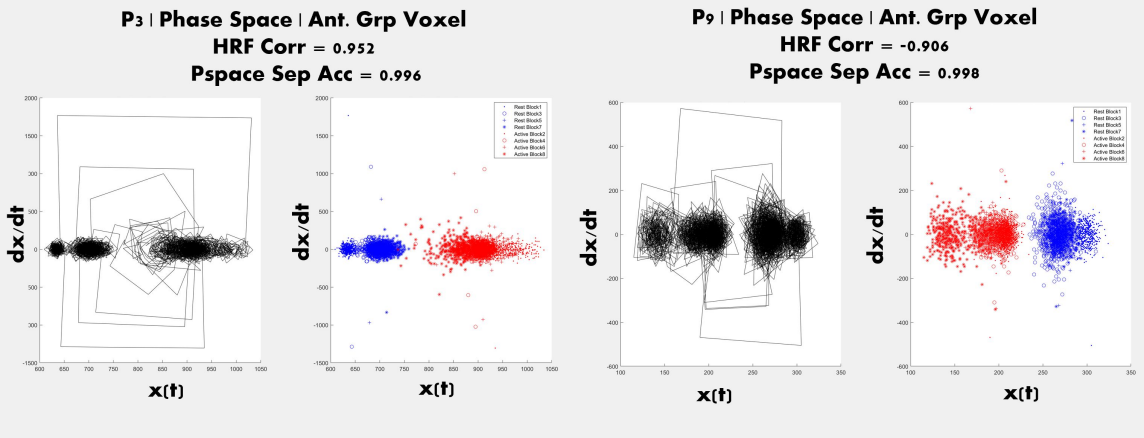

FIGURE 9.2: This shows the phase space of two voxels that were confirmed to be highly active during exercise (i.e. had high correlation with the ideal HRF and also high phase space separability). This was used in order to visualize the number of clusters and the distribution of the clusters over time. Both voxels show multiple state clusters, and a fatigued rest state more closely approaching the active state, during the simple plantar-flexion paradigm

indicates the sample is close to the decision boundary between two neighboring clusters, and -1 the sample might have been assigned to the wrong cluster. The silhouette coefficients were averaged for all time points to assess the degree of separation using a given number of clusters. An example of a multi cluster phase space can be seen in the bottom image in Fig. 9.3, which is indicated by a large positive silhouette score. The number of clusters in a voxel phase space was then chosen by selecting the number of clusters that lead to the largest average silhouette coefficient, but if the optimal number of clusters was 2 and silhouette coefficient was less than 0.75 this suggested low state separation, and the region was assigned to one cluster. The rationale behind this threshold can be seen in an example silhouette plot (Fig. 9.3), where what appears to be a single cluster would be classified as have two clusters if this threshold was not employed. The optimal number of phase space clusters was determined on a voxel-wise basis for all participants and muscles respectively. To see if the number of clusters was related to muscle activation, the correlation between the relative activation of the muscle, via the HRF correlation, and the number of phase space clusters was computed for all participants and muscles separately.

The final point in this analysis was to assess the other observation when plotting the different rest and active blocks, where the resting-state approached the active state due to fatigue (Fig. 9.2). The analysis was performed for each participant, and all their voxels within the three muscle groupings, separately. For voxels that were determined to be active, having an absolute correlation of greater than 0.75, and were multi-state, had more than two states, three phase space centroids were computed. The centroids were of the mean of all active blocks, of the first resting-state block, and the final resting-state block. The distance from the initial resting-state to the active cluster and from the final rest-state block to the active cluster was computed. The percent of voxels within a muscle that had the final resting-state closer to the active cluster, was computed. If the participant's muscle had more than 10 voxels that were active and multi-state, providing a reliable behaviour estimate, they were included in the average across muscles.

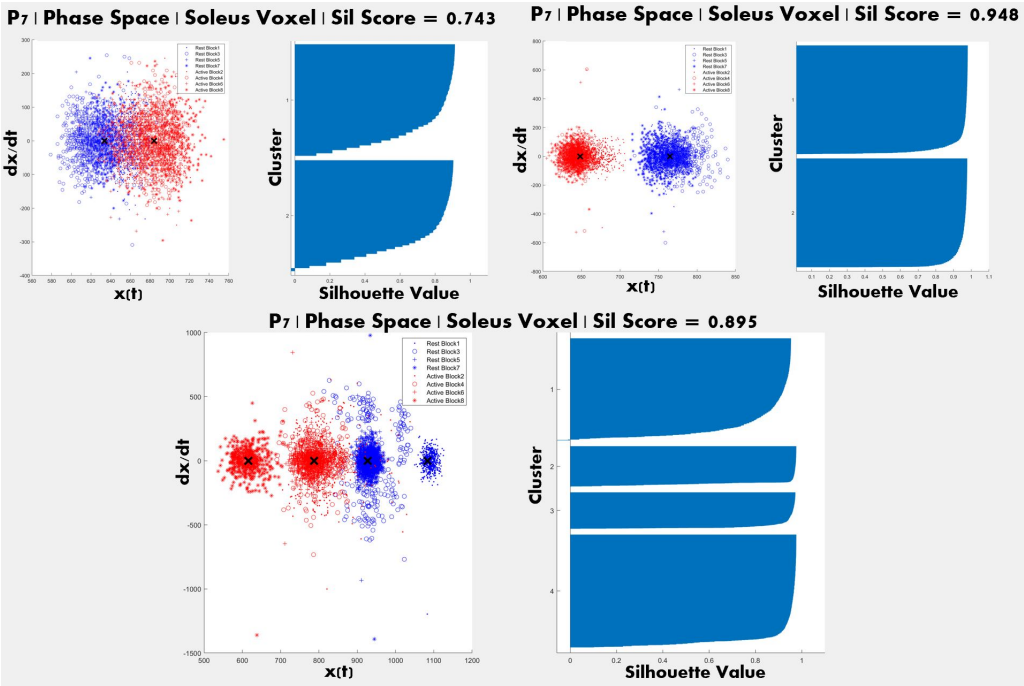

FIGURE 9.3: This shows the phase space which have multiple states and their corresponding silhouette plots to decide the optimal cluster number. Top left: a case where due to low separation between the resting and active state the phase space is assigned to one cluster. Top right: a clear two cluster system indicated by a high silhouette score. Bottom: A four cluster system with two rest and active states, the high silhouette score indicates the significance in the four cluster observation.

9.3 Results

To assess if the phase space separability could be used as a model free approach to quantify muscular activation, the absolute correlation of the HRF activation was compared to the phase space separability to see if both metrics came to the same conclusion on the active regions in the muscle. The results in Tab. 9.1 show the clear similarity between the metrics, where the correlation between metrics in their decision of activation ranged from 92.44% to 98.51%. The very high correlation between the two metrics means that the phase space separability can reliably quantify muscular activation, while presenting the advantage of not requiring correlation with an ideal HRF, which is dependant on the chosen HRF model.

The next point of discussion are the results gained from the voxel visualization, a sample of which is seen in Fig. 9.2, which shows two example voxels with high activation. The key features to note is firstly that based on the correlation sign, which indicates if the muscle within the voxel is a agonist or antagonist, the relative position of the active cluster compared to the origin (left vs. right) changes. Therefore although the absolute correlation is previously compared to the separability, the correlation sign could be recovered by finding the relative cluster position in comparison to the origin. Additionally, the voxel phase spaces' show multiple clusters, where the resting blocks are shown in blue and active blocks in red, in the colour phase space plots. These plots show more than 2 clusters (i.e. one for active and one for rest), which illustrates

TABLE 9.1: Summary of correlation between the absolute HRF correlation value and phase space separability classification accuracy for each participant and muscle respectively.

	Correlation between muscle activation metrics of the absolute correlation with the ideal HRF and the phase space separability		
Subject	*Gastrocnemius*	*Soleus*	*Anterior Group*
1	96.89%	92.75%	97.74%
2	96.76%	97.15%	98.51%
3	96.59%	97.26%	97.47%
4	97.16%	96.34%	96.99%
5	97.63%	97.02%	97.07%
6	96.06%	95.90%	96.24%
7	92.44%	96.93%	96.13%
8	97.59%	97.67%	95.40%
9	96.11%	97.21%	95.58%
10	96.54%	94.13%	96.58%
11	94.27%	94.87%	96.82%

that an active muscle region is not solely active or inactive. In addition to this, when examining the resting-state blue clusters, on a block by block basis, the initial resting-state block, where no exercise is performed, appears the furthest away from the active block clusters in red. The other three resting blocks appearing closer to the active state then the initial resting block suggests that as the muscle fatigues it more closely approaches the active state. This result was profound, and it was verified visually in other participant muscles before performing a multi-state activation and resting-state fatigue analysis.

The results of the multi-state activation assessment showed that voxels within the muscle showed multiple states, with a regional dependency. This can be seen through a sample participant's absolute correlation map and the map showing the number of states within a given voxel phase space (Fig. 9.4,). When assessing if the number of states within a particular voxel was correlated to the degree of activation no significant correlation was found. Additionally, when comparing if their was a correlation between relative voxel activation and if the voxel had single, dual, or multi-state (all number of clusters from 3-8 stated as one term) their was also no significant correlation.

The final point of investigation was if the final resting-state more closely approached the active state than the initial resting-state, where no prior exercise had been performed. The percentage of voxels where the final state was closer to the active state than the initial state is summarized in Tab. 9.2. While there is some variability amongst participants, when looking at the means averaged across participants for each muscle a trend is present. The resting-state at the end of the block design is closer to the active state then the initial rest in the multi-state voxels 50.11% of the time in the gastrocnemius, 61.89% of the time in the soleus and 74.66% of the time in the anterior group. This indicates that as the muscle fatigues it more closely approaches the active state.

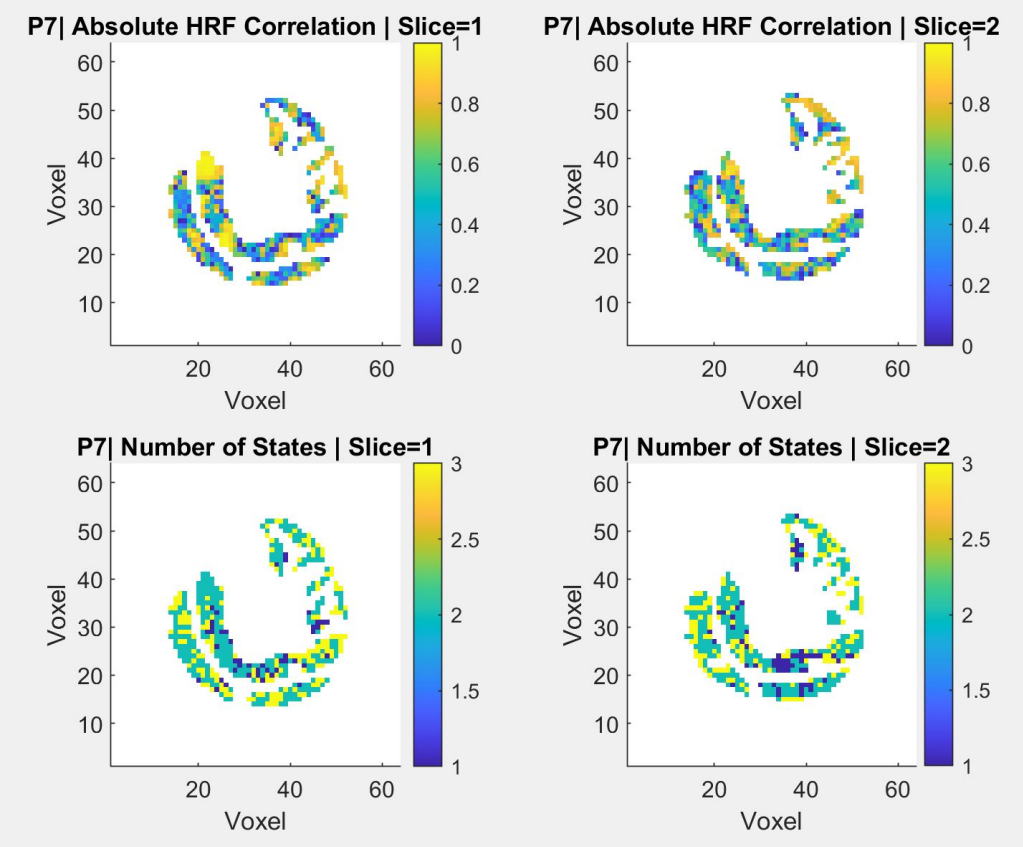

FIGURE 9.4: This shows a subject's voxel-wise activation maps using (top) an absolute ideal HRF correlation with a boxcar model versus the optimal number of states determined by performing kmeans clustering (bottom). The optimal number of states is chosen by silhouette analysis and must remain between 1-8 due to the 8 block exercise paradigm. This shows the muscle activation and how it relates to the number of blood-flow states.

9.4 Discussion

The phase space representation of the BOLD which has not been readily explored proved to be insightful when examining muscle behaviour. Similar to the findings in [89], there was a high degree of similarity between the activation mappings via the absolute correlation of the HRF when compared to the phase space separability. The similarity between the metrics was strong, where the correlation between metrics in their decision of activation ranged from 92.44% to 98.51%. This suggests that although these metrics are closely related they are not identical, therefore the phase space separability may provide novel activation insight compared to the conventional HRF correlation metric. Although the novel insights from the phase space separability as an activation metric was not explored, this result still will have a profound affect. Firstly, the phase space separability could be used as a model free approach to quantify muscular activation. The HRF model used will affect the correlation with the BOLD time-course, so a solution that does not assume a specific model is advantageous. Additionally, muscle activation which can be quantified by the amplitude of the BOLD signal, is highly dependant on the B0 and B1 field homogeneity which will affect amplitude measures. This phase space separability

TABLE 9.2: Summary of the percentage of voxels where final was closer than initial resting-state to active phase space clusters for each participant and muscle respectively.N/A indicates participant did not have 10 multi-state highly active (correlation >0.75) voxels.

	Percentage of voxels where final was closer than initial resting-state to active phase space clusters		
Subject	*Gastrocnemius*	*Soleus*	*Anterior Group*
1	52.94%	55.00%	68.75%
2	56.75%	58.33%	N/A
3	71.67%	57.69%	80.00%
4	50.00%	N/A	N/A
5	59.02%	42.86%	83.87%
6	23.53%	69.23%	54.54%
7	42.86%	80.00%	86.11%
8	16.67%	80.00%	N/A
9	52.00%	88.89%	85.71%
10	N/A	N/A	N/A
11	75.76%	25.00%	63.64%
Mean	**50.11%**	**61.89%**	**74.66%**

metric does not rely on amplitude and is a relative measure, which could be more robust in the case of field inhomogeneities within the imaging volume.

The next major point of discussion is the result from performing a multi-state activation and resting-state fatigue analysis. The novel finding is that the muscle BOLD phase space presents more than two clusters in some regions. This suggests that muscle activation cannot simply be binned into an active or inactive state. This means that our understanding of muscle activation needs to be completely reevaluated. The multi-state activation indicates one of three possibilities, one is that throughout the state of exercise muscle does not return to its initial resting-state as we fatigue. The second possibility is that throughout the state of exercise muscle does not reach the same active state as we fatigue. The third option is a combination of the previous two, where both the resting and active state changes position as a function of fatigue. This third option, based off the initial visualization of the muscle phase space plots, appears to be the most common, but this still needs to be validated with rigorous investigation.

Building on this new found multi-state activation of muscle BOLD, more interesting findings were observed when examining if the fatigued resting-state more closely approached the active state then when at pure rest. When examining active multi-state voxels, and averaging across participants, this was true for 50.11% of the time in the gastrocnemius, 61.89% of the time in the soleus and 74.66% of the time in the anterior group. This indicates the final fatigued resting-state of muscle is closer to the active state then when at pure rest. This suggests that as the muscle fatigues it more closely approaches the active state. Although the high levels of fatigue are not expected in the anterior group during plantar-flexion, it can be hypothesized that fatigue is caused by the slight dorsi-flex position of the foot while it is resting against the pedal. This finding although impactful, needs to be further validated due to the heterogeneity of the results across subjects. This heterogeneity could be in part due to the fact that not all

subjects experienced high enough levels of fatigue for this pattern to be present. The block design was not initially designed to elicit high levels of muscle fatigue as it consisted of equal rest to plantar-flexion blocks performed at 40% MVC. Therefore a block design with shortened rest blocks, and increased weight for the plantar-flexion, could be used to increase fatigue and validate this finding of fatigued muscle approaching its active state. To conclude, the phase space analysis of muscle BOLD activation provided a novel non-model dependent approach to quantify muscle activation, identified that muscle activation is not a binary process, and that when compared to muscle purely at rest, fatigued muscle at rest appears more similar to its contracted state.

Chapter 10

Determining SAT Band Effects on Muscle BOLD

10.1 Introduction

In this thesis the main outlook is to improve our description and understanding of muscle through the use of novel metrics. As such, this section explores the novel use of a saturation band placed superior to the muscle BOLD imaging slices, as in Fig. 10.1. This was done in an effort to reduce the affect of the pulsatility artifact that can be caused due to arterial in-flow. The pulsatile nature of the arterial BOLD signal can propagate to surrounding voxels, causing periodic spiking in the data which could obscure muscle activation. The amplitude of the arterial BOLD signal can be larger than that found in the muscle tissue as it is highly oxygenated, and has relatively less deoxy-hemoglobin, which induces spin dephasing and signal loses. Therefore as specified in the data acquisition section, to saturate arterial spins a 50mm SAT band was placed flush with the top imaging slice to reduce the arterial signal contributions. The decreased arterial signal intensity due to the SAT Band can be seen visually in the peroneal, anterior and posterior tibial arteries in Fig. 10.1. By comparing activation patterns during an identical exercise paradigm the relative affect of the SAT band on muscle activation classification could be assessed. To the author's best knowledge the use of a SAT band to reduce arterial in-flow effects in muscle BOLD imaging during exercise has never been explored. With the potential of this technique to reduce noise contributions, muscle activation could be more accurately quantified, which promotes a more comprehensive understanding of muscle BOLD.

10.2 Methods

10.2.1 Data Acquisition and Preprocessing

The paradigm design, rationale, parameters for MRI data acquisition, and fundamental preprocessing steps are outlined in Chapter 7. The data which was used in this particular analysis was the motion and field map correction functional data from the BOLD plantar flexion block design both with and without the SAT band.

10.2.2 Data Analysis

To assess if there were differences in muscle activation with and without the SAT band a simple analysis was performed using the script SATBandAnalysisActivation.m. The first step

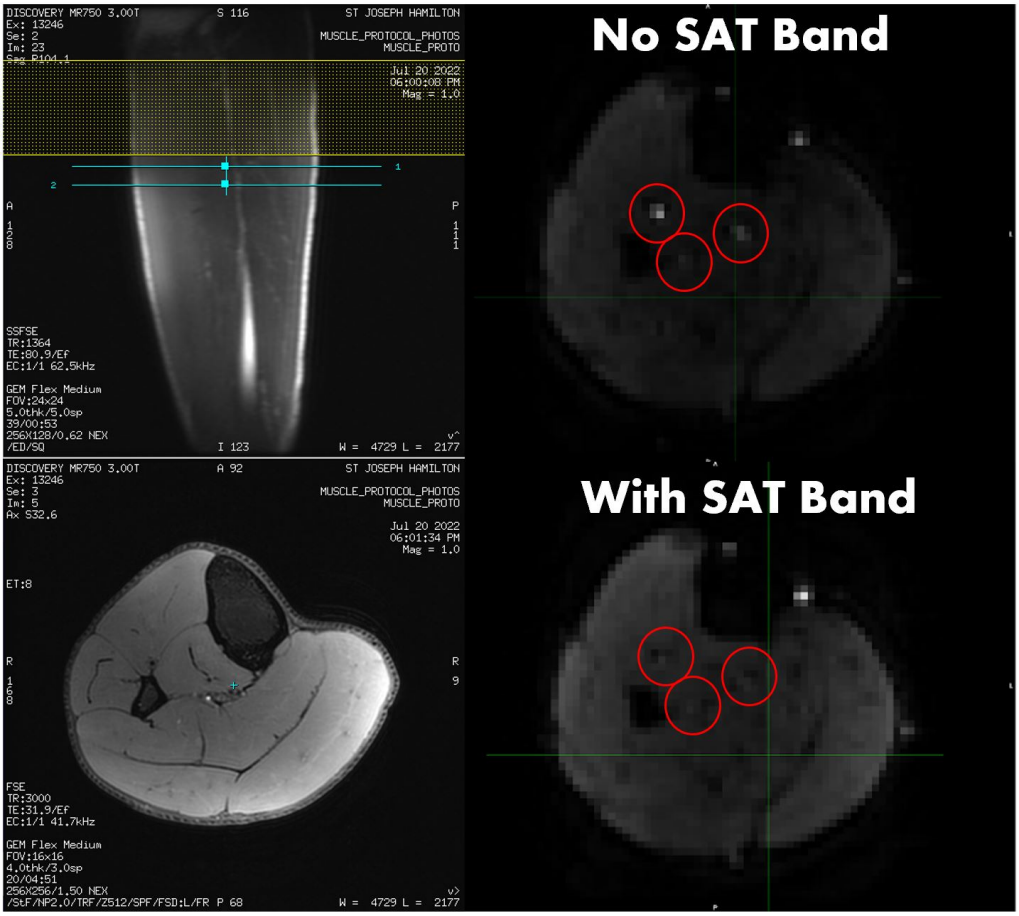

FIGURE 10.1: This shows sample placement of the SAT band superior to the imaging region. It also shows the reduced intensity in the peroneal, anterior and posterior tibial arteries due to the SAT band.

involved segmenting the voxel time-series to reduce the influence of motion artifact. To facilitate comparison with the previous analysis techniques the window lengths were chosen to remain consistent. All 66s windows which correspond to 600 time points were truncated to 512 point windows, of suitable length for fractal dimension analysis, by discarding the first and last 44 time points for each rest and active block respectively. The next step was to identify the voxels that were within a specific muscle by using the manually created masks for reference. The three masks were consistent from the previous investigations covering the gastrocnemius, soleus and anterior group (tibialis anterior, peroneus and extensor longus groups). This was performed for each participant and muscle respectively and the voxel timeseries was stored for later analysis.

The relative activation for each voxel was computed by assessing the correlation between the voxel time series and the ideal activation function. This ideal activation was a boxcar function where the resting-state was given an amplitude of zero and active state an amplitude of one. The correlation with the ideal hemodynamic response function (HRF) for the given paradigm was computed at all voxel locations for each muscle, participant and SAT band variation. The correlation was quantified using a correlation coefficient ranging from -1 to 1, where -1 indicates perfect anticorrelation (the region was active during the rest period), 0 indicates no correlation

(the activation is not related to ankle flexion) and 1 indicates perfect correlation (the region is active during the active period). To assess activation preliminarily, the voxel-wise absolute correlation for each SAT band was plotted. The absolute correlation was used as it describes how active a voxel is, as the muscle agonist and antagonist pair would show positive and negative correlation respectively, even though they are both essential for contraction. A sample participant's correlation comparison can be seen in Fig. 10.2.

After verification of activation in relevant muscle regions, the activation differences due to the SAT band placement was assessed through using multiple one-sided t-tests. The first set of t-tests was performed by comparing each muscle group for each participant respectively. For each voxel in a muscle grouping the correlation with the SAT band is subtracted from the correlation without the SAT band. A subtraction of correlations is required to perform a valid voxel wise comparison between metrics that is not influenced by the overall correlation average over the entire muscle. If a single sided t-test comparing these subtracted correlations has a non-zero mean then this implies that the activation maps differ either in magnitude or sign of correlation. To isolate solely for the magnitude of correlation difference between the differing SAT band conditions the absolute correlation was subtracted voxel-wise as described above, and a single sided t-test was used for each muscle and participant respectively.

Since differences were found between activation maps after using the SAT band, two comparisons were used to assess if the SAT band reduced noise to improve active/in-active classification accuracy. The first comparison compared the ability of the SAT band to improve classification accuracy at very active, correlation magnitudes of $>75\%$, or inactive, correlation magnitudes of $<25\%$, states. This was completed by identifying all voxels in the No SAT band data that had correlation of <0.25 or >0.75 and comparing to the SAT band correlation. The number of voxels where the with SAT band outperformed the no SAT band was tallied based on muscle and participant. Outperforming was defined as improving classification accuracy, which was when the SAT band acquisition had increased correlation for the active voxels and decreased correlation for the inactive voxels, relative to the standard no SAT band acquisition. The second comparison compared the ability of the SAT band to improve classification accuracy at the borderline active state, where arterial noise would have the greatest effect. This was completed by identifying all voxels in the standard No SAT band data that had correlation of >0.4 and <0.5 or >0.5 and <0.6 and comparing to the SAT band correlation. Once again the the number of voxels where the with SAT band outperformed the no SAT band was tallied based on muscle and participant. Similarly in the >0.45 and <0.5 window, decrease in accuracy indicates a more definite inactive decision, and in the window from >0.5 and <0.55 an increase in accuracy indicates a more definitive active decision. The percentage of voxels where the SAT band acquisition outperformed the no SAT band was tallied for each of the three muscle regions for all participants individually. Then this percentage was averaged across participants for each muscle to provide insight into how the SAT band affected activation classification in each muscle.

10.3 Results

The first notable result can be seen when examining a sample participant's correlation comparison can be seen in Fig. 10.2. Visually activation (high correlation values with the ideal activation function) can be seen in the tibialis anterior, exstensor hallicus longus, and in the medial gastrocnemius and soleus, which are all involved in plantar flexion as either an agonist or

antagonist. Comparatively, with the SAT band acquisition greater regions of activation can be seen, this corresponds well to the significant differences seen for participant 7 (row 7, columns 4-6) in Tab. 10.1.

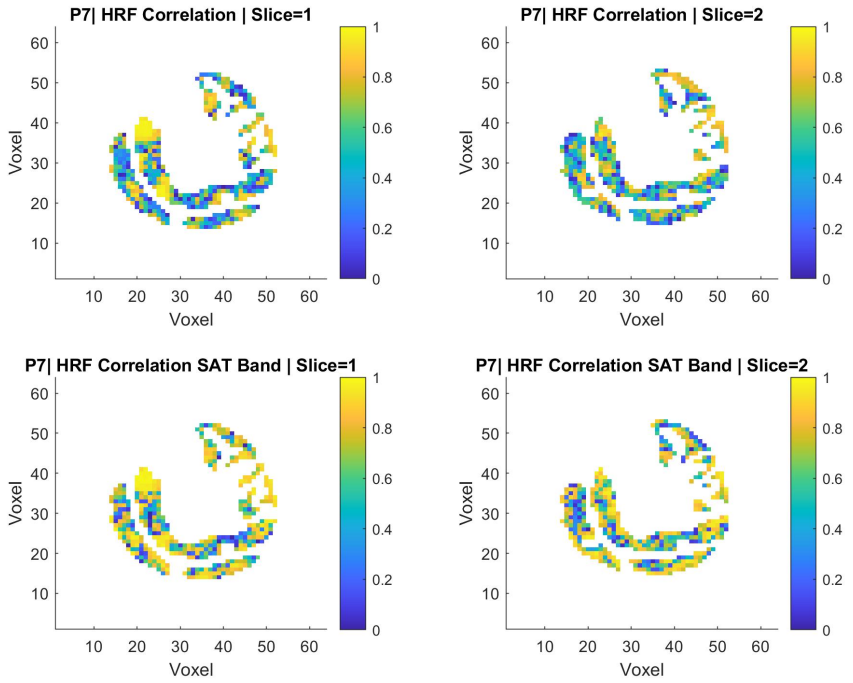

FIGURE 10.2: This shows the activation maps of one participant with (top) and without (bottom) the SAT band. Activation is assessed using the absolute correlation with a binary boxcar hemodynamic response function for the given block design with 4 periods of rest and 4 periods of plantar-flexion exercise. Absolute correlation is used to show both agonist and antagonist regions involved in plantar-flexion. Notably the activation map using the SAT band acquisition differs.

As specified above, the visual investigation of the activation differences was corroborated through the use of muscle specific t-tests for differences in correlation induced by the SAT band. The results of these single sided t-tests for the difference in activation and absolute activation are summarized in Tab. 10.1. For each participant 6 comparisons are performed (3 muscles and two correlation conditions), therefore to account for these multiple comparisons using bonferonni correction the significance threshold should be adjusted from $P<0.05$ to $P<0.00833$. Each participants data is statistically independent in this instance so no correction needs to be made for performing comparisons for all subjects. When examining the difference in the activation due to the SAT band, all participants show significant differences in at least one muscle, and 7/11 showing significant differences in two or more muscles. Furthermore, when examining the difference in the magnitude of activation due to the SAT band, 9/11 participants show significant differences in at least one muscle, and 4/11 showing significant differences in two or more muscles. This suggests that the primary differentiating factor between the activation differences is due to the magnitude of activation not the sign.

TABLE 10.1: Summary of the p-values, corrected significance threshold P<0.00833, for the single sided t-tests performed for each muscle and each participant respectively. The two metrics of comparison were the voxel-wise correlation and absolute correlation differences for the with and without SAT band acquisitions.

Subject	**P Value HRF Correlation Differences With and Without SAT Band**			**P Value HRF Correlation Differences With and Without SAT Band**		
	Gastrocnemius	*Soleus*	*Anterior Group*	*Gastrocnemius*	*Soleus*	*Anterior Group*
1	0.2246	0.0016	0.0544	0.5202	0.0012	0.0088
2	0.0389	1.338e-5	0.0090	0.8444	0.3715	0.3632
3	2.632e-5	0.0337	7.372e-5	8.9279e-5	0.1868	0.2955
4	7.0439e-8	0.3539	4.998e-20	6.2080e-9	0.5506	0.0254
5	2.697e-22	1.031e-8	1.555e-12	3.4769e-32	0.0387	8.204e-5
6	9.671e-6	5.990e-9	0.050	0.5757	0.3562	0.0105
7	3.919e-7	0.1892	2.798e-4	4.8308e-15	3.276e-7	9.8145e-5
8	0.7787	6.539e-7	4.944e-10	0.0789	0.0418	5.9818e-6
9	8.4868e-8	2.652e-12	0.8794	0.2511	0.1359	5.7358e-4
10	3.488e-11	0.0301	3.530e-10	4.2142e-28	1.3030e-50	3.5669e-33
11	3.285e-6	0.3443	0.8738	1.471e-16	4.115e-22	0.0671

TABLE 10.2: Summary of the average number of voxels within a muscle group, averaged across participants, where the SAT band improved classification. The classification at relatively confident and boundary decisions was assessed.

Correlation Window	**Percentage of Activation Classification Improvement With vs. Without SAT Band**		
	Gastrocnemius	*Soleus*	*Anterior Group*
High Confidence Correlations (<0.25) OR (>0.75))	31.58%	34.75%	36.89%
Boundary Condition Correlations (>0.45 AND <0.5) OR (>0.5 AND <0.55))	67.36%	67.23%	71.92%

The comparisons testing the relative active/in-active classification power with and without the SAT band yielded interesting results, which are summarized in Tab. 10.2. The first area of interest is if the SAT band increased the classification accuracy at relatively simple decision points, where the standard non-SAT correlations were extremely high or low. The SAT band did not improve the activation classification accuracy at these extreme values. On the other hand, when the SAT band was used to look at activation around the boundary correlations, where the voxel could be active or inactive, the activation classification was improved. The SAT band decreased the correlation for voxels in the range of 0.45-0.5 correlations, which are borderline inactive, and increased the correlation for voxels in the range of 0.5-0.55, which are borderline active. When averaging for all participants the percentage of voxels where the accuracy increased using the SAT band was gastrocnemius = 67.4%, soleus = 67.2%, anterior group = 71.92%. The percent improvement for individual participant's reached as high as 94.2% meaning that the SAT band can have profound improvement for some individuals.

10.4 Discussion

There has been very little exploration of the effects of saturation bands in the use of muscle BOLD imaging, with only one abstract to date [132]. The work examined resting-state muscle BOLD signal after intense exercise, with the major conclusion that the BOLD signal recovery characteristics, described through the heights of recovery curves, do not appear to be affected by SAT bands. This work although insightful does not provide insight into how the SAT band affects muscle BOLD during exercise, which was explored in this work. The results show that when using a SAT band there is a significant difference in the activation profiles of muscle when using a correlation based analysis. This was presented with some heterogeneity across participants and when comparing muscles. This variance could be due to differing muscle tone and recruitment between participants. None the less, all participants showed significant differences in their activation, which was primarily caused by varying amplitude of activation. Although this result is interesting it does not provide any information on whether these activation differences are related to reduction of arterial in-flow affects. This was directly addressed by assessing classification accuracy improvements when using a SAT band at areas that are heavily influenced by noise, borderline active states. Through referring to Tab. 10.2, it can be clearly seen that classification accuracy was improved by the SAT band when assessing if a voxel was borderline active or inactive. In contrast, when looking at voxels that were extremely active or inactive the SAT band did not increase the confidence in the decision of this state. This suggests that the SAT band is aiding in suppressing arterial in-flow noise, due to the improved classification in the nosiest state (correlation of 0.5) where a decision is hard to make. In addition, the SAT band can be linked to noise reduction as it does not artificially improve classification confidence overall, as this effect is not seen at high states of activity/inactivity. The significant difference in activation profiles, in combination the evidence of improved activation classification in the presence of uncertainty, indicates that a SAT band placed superior to BOLD imaging slices could improve data reliability. This result is important to drive the exploration of muscle activation profiles with more certainty. It also has clinical utility as [132] demonstrated that BOLD signal recovery during rest is not hindered by SAT bands and this work indicates that the SAT band improves muscle BOLD activation classification, so the SAT band could be used for both resting-state and active muscle BOLD imaging. The placement of a SAT band flush to the superior imaging slice would not be a difficult modification to existing clinical protocols and is relatively simple to standardize, so its adoption would be beneficial to clinicians.

Chapter 11

Concurrent Muscle BOLD and EMG

11.1 Introduction

In this thesis the main outlook is to improve our description and understanding of muscle through the use of novel metrics. As such, this section explores the novel use of muscle BOLD and EMG of the lower leg to investigate activation coherence and fatigue. BOLD and EMG studies are conventionally limited to the exploration of EMG with neural BOLD activation profiles. This is due to the fact that producing a MRI compatible EMG system is difficult, and that muscular imaging during activity paradigms is a challenge due to gross motion of the imaging volume. For those that undertake the task of constructing an MRI compatible EMG, with in house denoising techniques, it is more feasible to investigate neural activation as the head will move less than the contracting limb during simple exercise paradigms. Feasibility of collecting concurrent muscle BOLD and EMG of the lower leg was demonstrated in [104]. This to the author's knowledge is the only work that investigates muscle BOLD and EMG, and was focused more on feasibility, with a small exploration into the relation of muscle contractile strength and BOLD time to return to rest. Thus, the current work allows for novel insight into muscle behaviour, as its functional output is derived from the surface EMG, which measures the activation of muscle on the motor unit level, which can be linked to its demand with functional MRI, that will describe the metabolic/perfusion differences in the muscle at a millimeter resolution. Investigation into the relative muscle activation and the coherence of muscle perfusion and metabolic demand, is one exploration that will be covered. Additionally, fatigue which is conventionally derived through EMG has not been related to differences in perfusion/metabolic demand due to the lack of concurrent measure of muscle activation and perfusion. To address this lack of knowledge novel metrics of fatigue from the muscle BOLD signal were derived and validated by corroborating EMG fatigue measures.

11.2 Methods

11.2.1 Data Acquisition and Preprocessing

The paradigm design, rationale, parameters for MRI data acquisition, and fundamental preprocessing steps are outlined in Chapter 7. The MRI data used in this particular analysis were the motion and field map correction functional data from the BOLD plantar flexion block design both with concurrent EMG. The EMG data is the data that were cleaned as also outlined in Chapter 7.

11.2.2 Data Analysis

To assess if the interrelation between muscle BOLD, which conveys information on muscle blood oxygenation, flow and volume, to muscle EMG, which conveys information on muscle fibre contraction rate and amplitude, a simple analysis was performed.

The first step of analysis involved aligning the BOLD and EMG acquisitions. For the MRI acquisition 5min 5s of data were collected with only the final 5min saved. This was done to allow for normalization of BOLD signal intensity due to the reduced flip angle not satisfying the Ernst angle condition. The EMG acquisition which started at the start of the BOLD acquisition would have a 5s offset from the BOLD data. But due to complications with the MRI (the new GE update caused these errors) the initial number of images discarded by the scanner ranged between 3-5s (i.e. the total scan time ranged between 5min 3s - 5min 5s). Therefore to align the time series the final 5min of the EMG data were aligned with the saved 5min of MRI data.

With the time series aligned the EMG and BOLD data was then segmented to account for the motion artifacts that would contaminate the muscle BOLD signal. Motion artifacts will cause spikes in the muscle BOLD signal, which impacts measures of activation. Therefore, the first and last 2.5s (10 time points) were truncated for each rest and active block respectively. The block length of 25s was of sufficient length to observe a BOLD response, as block lengths of as little as 10s have been shown to be optimal in assessing BOLD activation. [133] This truncation is also important for the EMG data as the gradient artifact removal is hindered at the initial and final time points in the 5min acquisition due to the inability to do sufficient window averaging. Additionally, it was observed that when a participant was transitioning from a plantar-flexed to resting state they would not simply let their foot relax, but rather dorsi-flex then relax. Dorsi-flexion also will engage the anterior muscle compartment, which causes a large amplitude spike in the EMG during the rest period. This is not of primary concern for the BOLD data due to longer time course of the hemodynamic system in the leg, on the order of seconds as opposed to the EMG's milliseconds, to respond to increase blood flow in response to this action. Therefore in the EMG the initial dorsi-flexion spike could contaminate resting baseline measures by inaccurately increasing its amplitude. Therefore this 2.5s window time not only aids with the slice artifact removal but allows the participant some time to reach stable ankle flexion or rest position.

With the BOLD and cleaned EMG truncated to a suitable length the block design now consisted of 25s rest followed by 25s of plantar-flexion, which was repeated 5 times. To verify whether there was sufficient muscle activation captured from the the muscle BOLD, the voxel-wise time-series correlation with the ideal activation function was computed. This ideal activation was a boxcar function with 25s blocks, where the resting-state was given an amplitude of zero and active state an amplitude of one. The activation in the anterior compartment was visualized, as it should be involved in plantar-flexion in a limited capacity as it is primarily a dorsi-flexor. The spatial activation in the anterior compartment and the EMG muscle activation was visualized for each participant prior to performing analysis, as can be seen in Fig. 11.1. Attention should be placed on the agonist and antagonist voxels which can be determined by examining the EMG amplitude and BOLD amplitude relations. Agonist voxels will have increases in the BOLD signal that correlates with the EMG or the ideal activation function (appearing as yellow in the top correlation mapping). Whereas the antagonist voxels, will have increases

in the BOLD signal that is anticorrelated with the EMG or the ideal activation function (appearing as blue in the top correlation mapping). This means that the agonist and antagonist voxels represent muscle fibres that contract or relax respectively, to cause plantar-flexion.

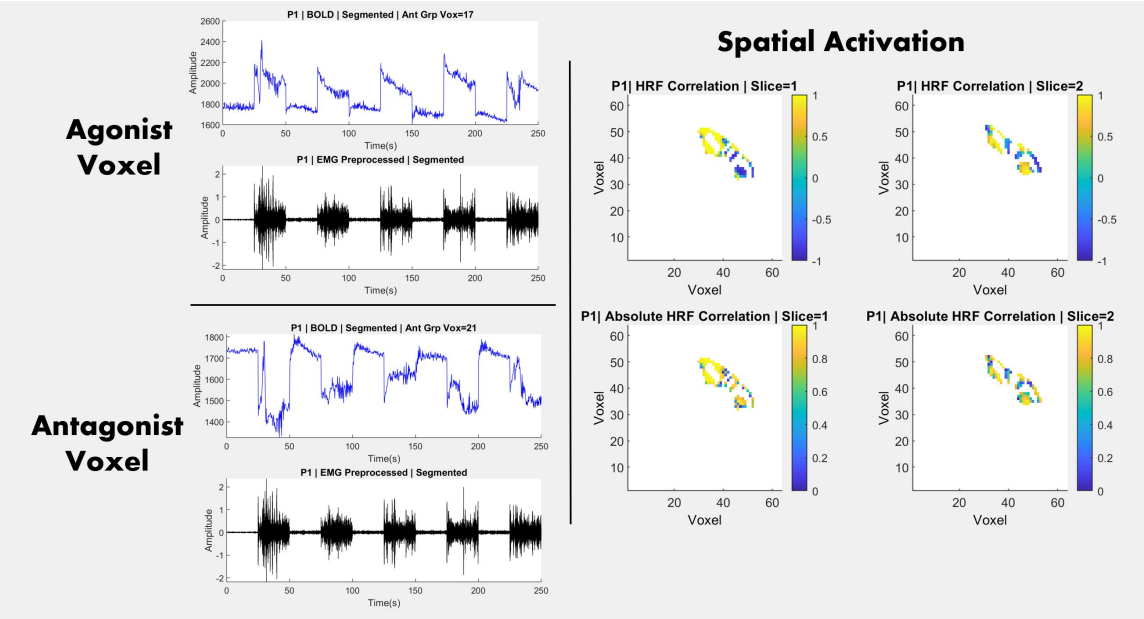

FIGURE 11.1: Comparison of muscle activation using EMG and BOLD measures. Left: The EMG recording is compared to an agonist (top) and antagonist(bottom) voxel BOLD signal time course to demonstrate how the electrical and metabolic profiles are related during muscle activation. Right: activation maps, in the anterior lower leg, of one participant performing plantar-flexion. Activation is assessed using the correlation with a binary boxcar hemodynamic response function. The relative activation maps (top) show the strongly active agonist (yellow) and antagonist regions (blue), whereas the absolute activation maps (bottom) show both strongly active agonist/antagonist regions in yellow.

With verification of muscle activation both metabolically and functionally, the relationship of this activation was explored. To quantify how active the anterior muscles were with the EMG acquisition the metric of signal to noise ratio (SNR) was used. SNR was computed by rectifying the EMG signal, then computing the ratio of the signal summed squared magnitude to the noise summed squared magnitude, while reporting in decibels. Noise was considered as the rest periods. The SNR provides insight into the increase in amplitude of the EMG during activity in comparison to rest. To quantify how active the anterior muscles were with the BOLD acquisition the metric of the magnitude of correlation, with the ideal activation function, was used. The absolute correlation was found for all voxels within the anterior compartment and then averaged to yield one correlation value for the entire compartment. The absolute correlation shows the relative activation of both agonist and antagonist voxels, which are both involved in muscle activation. These metrics were generated for each participant individually. The correlation between the EMG SNR and BOLD absolute correlation for the anterior compartment was assessed using all participants.

The next area of examination was into the fatigue state of the muscle, which is conventionally investigated using EMG. The two metrics of fatigue that are conventionally used with EMG,

the centroid frequency and root mean squared (RMS), were computed for each window for all participant acquisitions. Participants were then identified to be experiencing muscle fatigue by fitting a linear approximate to both metrics over time. If the participant had a decreasing centroid frequency, negative slope, and increasing RMS, positive slope, they were experiencing muscle fatigue during the trial. Fig. 11.2. shows a fatigued participant's sample EMG centroid and RMS over time. With a trial of only 5min, equal rest to recovery periods, and only 40% MVC, high levels of muscle fatigue were not expected. However since the plantar-flexion exercise stint occurred post two other exercise blocks, some fatigue could be present. After examining the previous EMG SNR values, participants 8, and 10 were discarded from the fatigue analysis as they had an SNR of 1.15dB and 1.82dB respectively, which is on the order of 100,000 times less than the average participant EMG SNR of 6.43dB. Fatigue was observed in 7/9 of the participants with viable EMG data, which were included for further analysis.

These known EMG metrics of fatigue over time were then compared to newly created hypothesized metrics of fatigue from the muscle BOLD signal. Four metrics were derived and investigated, with the knowledge that the BOLD signal conveys information on muscle metabolism and perfusion. The first metric was the area under the curve (AUC) of the BOLD signal. This metric provides insight into the blood volume in a region as a function of time. It was derived by finding the area under the curve during each rest and active window respectively. The second metric was change in BOLD AUC over time. This provides insight into the change in muscle metabolism/perfusion when transitioning between rest and active states. The metric was derived by finding the difference in the BOLD AUC of the current block from the previous block. The third metric was the BOLD centroid frequency. This metric would provide insight into the primary rate of vascular perfusion, which can be related to changing vascular patency over time. It was computed by finding the spectral centroid in all windows. The final metric was the change in the BOLD centroid frequency. This metric would provide insight into the change in rate of vascular perfusion between rest and active states.The metric was derived by finding the difference in the BOLD centroid of the current block from the previous block.

To ensure that only the spatial regions in the muscles that were related to activation were assessed all three metrics were evaluated for only active agonist and antagonist voxels. Agonist voxels were identified as having correlations of >75% and antagonists as having correlations of <-75% with the ideal activation function. The four metrics were then averaged for all agonist and antagonist voxels respectively. Therefore for all 7 participants who experienced fatigue they each had the following fatigue metrics, with one value per rest/active window, EMG centroid, EMG RMS, BOLD AUC for agonist voxels, BOLD AUC for antagonist voxels, BOLD AUC change for agonist voxels, BOLD AUC change for antagonist voxels, BOLD centroid for agonist voxels, BOLD centroid for antagonist voxels, BOLD centroid change for agonist voxels, BOLD centroid change for antagonist voxels. The correlation between each EMG fatigue metric and BOLD metrics was assessed by comparing the metric values across time, using all participants.

11.3 Results

Prior to investigating the results into the relation between the relative muscle activation between the BOLD and EMG acquisition and the hypothesized novel metrics of fatigue using the BOLD signal, the validity of the time series segmentation needs to be explored. By removing the initial and final 2.5s of the EMG signal, which as discussed would be profoundly affected by the

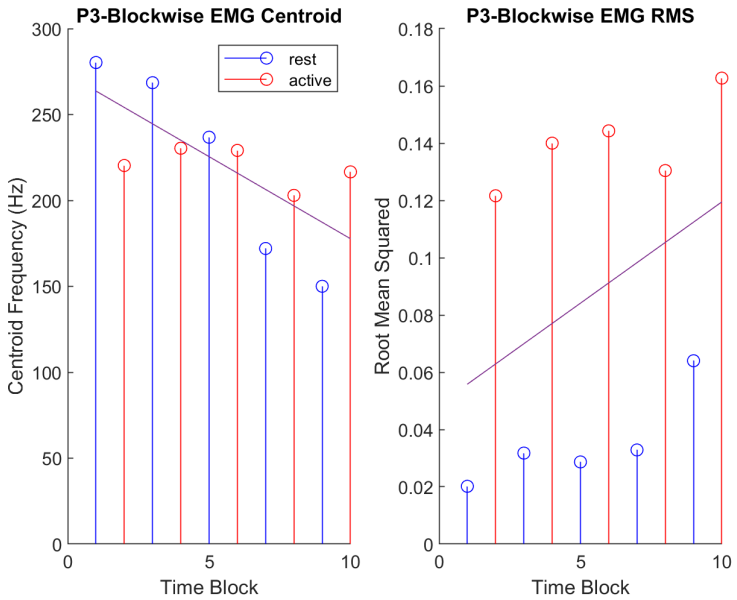

FIGURE 11.2: This shows a participant who is experiencing muscle fatigue. This is characterized by a decrease in the EMG centroid frequency and increase in the root mean squared over time. This conclusion was made by assessing the sign of the fitted slope (shown in purple) and if the participant was fatiguing they were included in the fatigue analysis.

dorsi-flexion compensation when transitioning from activity to rest, the SNR increased. This can clearly be seen with the two participants, P1 and P5, referenced in the initial preprocessing steps outlined in Chapter 7, who had the following SNR improvements; P1 9.13 -> 13.55dB and P5 7.60 -> 10.88dB.

TABLE 11.1: Summary of the EMG SNR, which conveys difference between activation during activity, and the average correlation of all anterior muscle voxels with the ideal activation function. These metrics indicate relative muscle activation during exercise.

Subject	**EMG SNR**	**BOLD Absolute Correlation Coefficient**
1	13.55dB	0.7099
2	4.70dB	0.4965
3	9.57dB	0.7061
4	9.98dB	0.4671
5	10.88dB	0.6162
6	4.12dB	0.4523
7	7.75dB	0.7427
8	1.15dB	0.5691
9	2.68dB	0.5478
10	1.83dB	0.3503
11	4.51dB	0.6369

The next point of discussion is the relation between the electrical and metabolic activation in the anterior compartment. This was quantified by the metrics of EMG SNR and the BOLD average voxel absolute correlation with the ideal activation function, and is summarized in Tab. 11.1. Notably, the correlation between the two metrics was 56.12%, which indicates a marginal positive correlation. This indicates a larger difference in the electrical activation of muscle between rest and active states, will result in an increase in how coherently the muscle fibres are perfused.

The final point of discussion is the exploration of the correlation between the known EMG fatigue metrics to the hypothesized BOLD fatigue metrics, to uniquely describe muscle fatigue using the BOLD signal. The correlation between each BOLD fatigue metric and EMG fatigue metric is summarized in Tab. 11.2. The first set of correlations that displayed interesting findings were the correlations of the novel BOLD change in AUC fatigue metric. The correlation of the EMG RMS and BOLD change AUC for the agonist = 0.6457 and antagonist = -0.6499. These strong correlations indicate as the RMS increases with fatigue the change in amplitude between rest/active increases for the agonist, whereas the trend is opposite for the antagonist. This suggests that BOLD AUC, which is a metric of perfusion/metabolism, increases relative to rest as a function of fatigue to agonist regions and decreases to antagonist muscles. This is in line with the shunting of blood to metabolically active regions (agonists) instead of less active regions (antagonists) as a function of need with exercise. Additionally, the correlation between the EMG Centroid BOLD and change AUC for the agonist = -0.3484 and antagonist = 0.2235. Although these are relatively weak correlations, the opposite correlation sign when comparing to EMG Centroid and RMS measures is encouraging as we know that as the RMS value increases with fatigue the centroid frequency decreases. In addition the agonist and antagonist voxels once again differ in their correlation sign which indicates that as one increases, its rate of perfusion/metabolism, the other decreases. The AUC correlation did not yield any significance, which indicates that the absolute value of muscle perfusion/metabolism does not inform fatigue, but rather the relative change in perfusion. Additionally, the BOLD centroid metric did not show any correlation with the EMG fatigue measures, suggesting the rate of BOLD signal change does not seem to be influenced by fatigue. The change in the BOLD centroid showed a weak correlation with the EMG RMS for the antagonist = 0.3278 and a smaller correlation with the agonist = 0.1936. This suggests the change in the rate of perfusion/metabolism in antagonists will increase with fatigue, but remain relatively constant in agonists. This statement cannot be made with much confidence, and higher fatigue states should be captured before validating or invalidating this conclusion on perfusion/metabolism rates.

11.4 Discussion

There has been very little exploration of the effects of concurrent muscle BOLD and EMG of the lower leg, with only one thesis to date [104]. The work firstly demonstrated that a MRI compatible EMG and a denoising framework can be developed from scratch. This current work extended upon this by quantifying the relationship between of muscle activation via EMG and relative muscle perfusion/metabolism via the BOLD signal. The positive correlation between the level of muscle activation difference between rest and contraction and the amount of perfusion over the entire muscle, suggests that muscle output is directly related to the degree of muscle perfusion. This relationship although seemingly intuitive, has not been corroborated using concurrent measures, but rather via EMG and muscle BOLD in isolation. This finding thus sets

TABLE 11.2: Summary of the correlation between the EMG fatigue metrics of the centroid frequency and root mean squared (RMS) with the newly developed BOLD fatigue metrics. Notably the change in BOLD AUC shows correlation with the EMG fatigue metrics.

	Correlation Coefficients Between Muscle EMG and BOLD Fatigue Metrics		
		EMG Fatigue Metric	
Contraction Type	*BOLD Fatigue Metric*	EMG Centroid	EMG RMS
Active Agonist Voxels (Correlation >0.75)	BOLD AUC	0.0750	0.2441
	BOLD AUC Change	-0.3484	0.6457
	BOLD Centroid	0.1050	-0.0500
	BOLD Centroid Change	-0.0354	0.1936
Active Antagonist Voxels (Correlation <-0.75)	BOLD AUC	0.2160	-0.0261
	BOLD AUC Change	0.2235	-0.6499
	BOLD Centroid	-0.1259	0.1360
	BOLD Centroid Change	-0.0153	0.3278

the foundation for the use of either the EMG or BOLD modality in isolation with the ability to infer what is happening both metabolically and functionally, at the level of the motor unit. The additional insight provided by this work is into a novel metric of muscle fatigue. Although this paradigm was not explicitly designed for muscle fatigue, 7 of the eligible participants showed muscle fatigue. Since EMG and muscle BOLD have rarely been paired, metrics to describe muscle fatigue using BOLD are difficult to derive. The use of EMG fatigue metrics during the concurrent measurement of the BOLD signal allowed for direct knowledge that the muscle was fatiguing, so the fatiguing muscle BOLD signal could be examined for measures of such. The results showed that the EMG RMS was strongly correlated (R=0.65) with change in the BOLD area under the curve change. Additionally, the agonist and antagonist regions showed opposite trends, where the agonist regions increased and antagonist regions decreased in the change in the BOLD AUC as fatigue increased. This suggests that with increases in fatigue agonist muscle will increase its relative level of perfusion over time, and that antagonists will decrease in perfusion overtime. This is inline with the relation shunting of blood based on metabolic need. Not only this, but it provides the additional insight that there is not only a difference in how the blood is shifted to active or inactive regions, but how over time the relative perfusion discrepancy between these regions changes. Additionally the use of the change in BOLD AUC overtime with an exercise paradigm can be used as a novel measure of muscle fatigue during BOLD imaging. A metric to measure muscle fatigue using MRI, which has excellent spatial resolution, provides the ability to identify how muscle regionally fatigues as a function of time. This could be imperative in assessing muscle function in disease, as muscle dysfunction is associated with rapid fatigue onset. Additionally, the ability to non-invasively use measures of muscle BOLD to examine fatigue could be used to assess how muscle fatigue varies throughout rehabilitation paradigms. To conclude, the concurrent recording of muscle BOLD and EMG is not only feasible, can be used to examine the functional and metabolic profiles of muscle, and arguably most importantly has provided insight into novel a BOLD fatigue metric that should be further explored and translated to clinical use.

Chapter 12

Discussion

12.1 Integration of Results

The results and discussion from the pilot study, (Chapter 5) and additional investigations into muscle function (Chapters 8-11), while relevant in isolation can be integrated to generate a broader outlook on muscle behaviour. The first major point of discussion is Chapter 10, and the use of the superior SAT band to null the arterial spins. This data was collected with the intent to investigate noise reduction and its ability to reduce arterial noise. The results showed that there was improved discrimination between the active or inactive state of a voxel when using a SAT band. Significantly, this improvement in classification was seen at the decision boundary, but not in voxels that were already highly active or inactive. This suggests that SAT band does not arbitrarily increase activation classification, but only improves it in regions where noise profoundly affects the decision. These results suggest that a SAT band to reduce arterial noise should be employed in all muscle imaging studies. To limit the scope of this thesis, and to ensure that the SAT band was not confounding the results, all other investigations were performed on BOLD acquisitions with no SAT band. But the profound results in this Chapter 10 indicate that all of the analysis in this work should be repeated with the SAT band acquisition data.

Additionally, regional activation mapping is a point of intersection between these analysis techniques. The voxel-wise correlation of the BOLD time series with the ideal hemodynamic response function (HRF), which has an amplitude of 0 at rest and 1 during contraction, served as an activation reference for all studies. The use of the phase space separability, with larger separability between active and rest states as an indicator of muscle activation, proved to be a model free approach that closely resembled the conventional ideal HRF correlation. This is suggested by the results in Tab. 9.1, which show the high correlations between conventional and phase space activation mapping's for all participant and muscles. While the phase space served as a novel activation determination metric, that was not dependent on the form of the ideal HRF chosen, the SAT band activation mapping showed larger differences to what is seen with this common activation reference of the ideal HRF with no SAT band. As can be seen in Tab. 10.1, when using the same activation reference as in the phase space separability analysis, activation profiles differed when using the SAT band. The noise suppression properties of the SAT band and the high correlation between phase space separability and ideal HRF correlation suggest that a combination of the two techniques would be the optimal technique to generate activation maps in muscle. Using a SAT band and the phase space degree in separation between

the active and resting-state, would provide a model independent solution that is robust to the noise associated with arterial inflow effects.

Finally, fatigue is another intersection of the analysis techniques that should be discussed, with fatigue effects being observed in the bi-fractal dimension, phase space, and concurrent BOLD/EMG analysis. To begin, the bi-fractal dimension analysis in Chapter 8, showed a decrease in the fractal dimension measure across all muscles and components when comparing the pure to fatigued rest state. This indicates that as a function of fatigue the relative complexity of the BOLD signal decreases. Since the BOLD signal is related to metabolism and perfusion, this implies that as a function of fatigue muscle perfusion and metabolism becomes more regular or structured. The phase space analysis (Chapter 9) also presented insight into muscle fatigue when examining the state of the initial pure rest and fatigued rest to the active state. When examining active multi-state voxels and averaging across participants and muscles the fatigued rest state was closer to the active state 62.15% of the time. This suggests that as the muscle fatigues it more closely approaches the active state. The concurrent BOLD/EMG investigation (Chapter 11) also provided insight into muscle fatigue observations through the BOLD signal. Using the EMG metric of fatigue, increasing root mean squared as a function of exercise duration, a strong correlation with change in the BOLD area under the curve change was observed in agonist (R=0.65) and antagonist (R=-0.65) regions. This suggests that with increases in fatigue agonist muscle will increases its relative level of perfusion over time and that it will decrease in antagonists overtime. These results taken in combination suggest that as a function of fatigue, muscle perfusion/metabolism will become more regular, show relative increases, and more closely resemble contracted muscle while at rest.

12.2 Limitations

I would be remiss not to discuss some of the limitations of the current work. The first major limitation of this work was the experimental population. In a study on understanding muscle through the development of novel metrics an ideal population would be athletes, either endurance or power, as they have good muscle tone and a low body fat percentage. These athletes would have well defined muscle boundaries, increased perfusion which is especially important due to the use of BOLD imaging throughout, and less epidural fat which attenuates the surface EMG signal as an additional impedance layer. Unfortunately, due to more stringent recruitment procedures and limited MRI access as a non-essential worker, due to the COVID-19 pandemic the subject sample was done out of convenience consisting of other graduate students. Additionally, this limited experimental population lead to a gender imbalance within the study. This reduces the generalizability of the result, and a crucial next step would be to gender balance the study. By recruiting more women the work would be more robust against biological variability. This would also have the added benefit of increasing the subject sample size which would provide more statistical power to the results if they held at the existing level.

A second major limitation pertains to the image acquisition. Functional images were acquired at a rapid rate with a TR=110ms, which was the fastest that the scanner would allow. Without multi-band functionality, which allows for increased acquisition speeds due to simultaneous slice excitation given sufficient spacing between slices, only two slices were acquired at this rate. This meant to get a sufficient coverage of the leg to get an accurate representation of the leg, and to increase signal levels, a 1cm slice thickness was used instead of the conventional thickness on

the order of 3-4mm. The loss of spatial resolution in the slice direction is not ideal, but when muscle fibre lengths can be on the order of 5-7.5cm long in the lower leg this is not of primary concern. [134] The more significant limitation of our study is based on sampling rate of the sequence being inadequate. Therefore, we could be under sampling the temporal BOLD signal, which could artificially reduce variance measures that are used in the computation of the fractal dimension. Practically, this is a research-based limitation as most clinical MRI's do not have multiband imaging and our techniques would be well suited for their use.

A third limitation of this study pertains to the tools available for muscle MRI analysis. Currently there is no openly accessible tool to allow for MRI analysis of the lower limb. Specifically, there is no atlas for muscle belly's in the leg, unlike the numerous brain atlases developed and available on software packages such as FSL [117] and AFNI [129]. This meant that in order to segment the muscles in the lower leg such as the soleus, gastrocnemius, and tibialis anterior, manual masks needed to be created using an anatomic reference. The anatomic reference allows for segmentation into major muscle compartments and to avoid large visibly apparent blood vessels, but tissue boundaries and smaller blood vessels are not always visible. Thus, manual muscle mask definition is subject to human error. Additionally, it is a time consuming process which means that the muscle analysis is not well scalable to large datasets without investing sufficient time into segmenting the muscle bellies. In saying this, this is still the current standard in the literature. The creation of a muscle atlas for segmentation of the lower limb into the major muscle groups would allow this work to be scalable to mass datasets and for clinical use. Another software based limitation is associated with the lack of development of noise correction techniques for muscle imaging. For instance software such as FSL has tools to perform eddy current correction for distortion due to EPI sequence acquisition, but this tool is optimized for use on the brain and could not be used on the muscle. The effects of eddy currents were mitigated by performing field map correction and time course normalization where applicable but the data could still serve to benefit from eddy current correction amongst other denoising techniques.

12.3 Future Work

The work detailed in the thesis above, in regards to understanding muscle behaviour through the non-invasive methods of EMG and MRI, although extensive is not all encompassing and can be expanded upon. The first major point of action in the future would be to address the limitations discussed above. To reduce the gender bias of the existing study, female participants need to be recruited. Additionally, athletes from a power and endurance background should be recruited too, as the ideal test ground for this exploratory muscle study. This is because they would have more well differentiated muscle groupings, promoting ease of comparison, and less peripheral fat, leading to improved EMG data. In terms of addressing the imaging speed limitation, this would be addressed through discussions with GE to enable the multi-band functionality to be used on the GEM lower leg flex coil, as it currently is only enabled on multi-channel headcoils (as was verified by speaking with GE reps and performing my own trials). To address the limitation in regards to the software analysis tools, or lack thereof, a preliminary muscle atlas could be developed. Through collecting high resolution anatomical images, using the parameters employed in this work, one leg could be acquired in approximately 5min. Due to the relative symmetry of the leg, both the left and right leg of the participant could be captured, and one leg simply transposed in order to create two sample points for one participant. With the averaging

of the leg and through scanning enough participants this would allow an atlas to be generated. Therefore a single detailed segmentation of the new atlas could be completed and all new studies spatially transformed into the common space to perform the muscle segmentation. Additionally, a collaboration could be done with the researchers, such as Mark Jenkins of the FSL team, to modify their existing eddy current architecture to also encompass muscle imaging.

After addressing the limitations of the work there are many feasible extensions of the work, as this is a foundational study on exploring muscle through a novel complex representation. One such extension is to further examine the non-invasive muscle fibre type differentiation with the muscle bi-fractal dimension. The temporal bi-fractal dimension representation showed excellent differentiation power in an athlete group (Chapter 5) and in a non-athlete group in this work. It would be of interest to examine the bi-fractal dimension using a power spectrum representation similar to that employed in [63]. This could either serve as a confirmative measure or provide novel insights with information found in the frequency instead of the time domain. By using a frequency representation of the data it is also possible to try to segment the data into fractional Gaussian noise versus Brownian motion, which is an advantage over the time domain metric. Thus there is merit in performing a frequency based fractal dimension approach in future work. Arguably more importantly it is necessary to perform biopsy as a confirmatory measure to the non-invasive fractal dimension metric. Histological samples of muscle fibres in the tibialis anterior, gastrocnemius, and soleus would allow for more accurate assessment of muscle fibre types, as opposed to the use of muscle fibre type norms, which are good estimates [37] of the relative fibre type composition but are not participant specific. Additional ethics would be required to perform biopsy sampling of the lower leg as this means the experiment is transitioning a from non-invasive to invasive approach of assessing muscle fibre type profiles. In saying this, in the leg muscle biopsy is conventionally performed in the quadriceps [44], so either the imaging study would need to transition to imaging the quadriceps, or a skilled biopsy professional would be needed to sample the muscles of lower leg. Preferably the biopsy of the lower leg would be used due to the varying spectrum of the twitch profiles in the lower leg (in order of fast twitch predominance: tibialis anterior > gastrocnemius > soleus).

One such extension is related to refining the exercise paradigm to accentuate fatigue affects. The existing paradigm used a block design with rest and active periods of approximately 60s with contractions at the level of 40% MVC. This was chosen to allow for the ideal window length for the fractal dimension analysis and equal duration of rest and exercise blocks. In the future increasing the weight to 70-80% MVC would be of interest to introduce fatigue. This would provide novel insight into the fatigue state of muscle, with the hopes of providing insight into the multi state muscle representation, and novel BOLD fatigue metric outlined above. The preliminary evidence of the resting-state approaching the active state of the muscle as a function of fatigue could be more readily confirmed with higher fatiguing exercise.

Another avenue of future work is through modifying the EMG acquisition. Currently the EMG was acquired by placing electrodes over the tibialis anterior during plantar flexion. This specific exercise not only activates the anterior muscle compartment but also the lateral gastrocnemius so electrodes placed at this site could be of interest to examine muscles that generate more force. This measurement could be done by changing the placement of the electrodes using the current set-up or through using a multi-channel EMG system. Additionally, although the framework for denoising the EMG, through modifying the EEG based FASTR technique, was

validated and yielded good results it could be further improved. The existing denoising technique through FASTR does not take into account the dependence of gradient artifact amplitude based on electrode position, that was shown through preliminary tests of the EMG suitability. More extensive tests could be completed on mapping the EMG gradient artifact depending on position within the bore and this information could be used to inform the artifact template generation and subsequent removal to improve upon the signal to noise ratio of the EMG signal. The extremely noisy environment of the MRI when recording EMG could benefit from this improved artifact template creation leading to improved SNR.

The last extension that will be discussed is to examine the differences in functional imaging with and without a SAT band more in depth. A preliminary analysis of the imaging with and without the SAT band, which is 50mm and proximal to the slice location, show decreased vessel noise and consequently differences in activation in the lower leg. Although these findings are unprecedented there are still numerous options to explore the benefit of using a SAT band in muscle BOLD imaging. One such analysis would be to examine the fractional Gaussian noise, through the use of the power spectral representation of the muscle BOLD signal, during rest with and without the SAT band to see if there is a reduction of said noise. In addition to this, SAT band placement and the affect on the resulting data needs to be explored more in depth. The SAT band was placed flush to the top imaging slice of the two slices. The relative spacing between the SAT band and the proximal imaging slice and its affect on noise suppression needs to be tested to find the optimal spacing to attain the best noise suppression. Finally, a SAT band was placed anterior to the imaging slices in the lower leg in an effort to reduce the inflow effects of the arteries, but no SAT band was placed below the leg to reduce the venous inflow affects. This was done as the venous blood is de-oxygenated will have a lower BOLD signal amplitude and should not be of primary concern. In saying this, it is still an assumption that needs to be tested and proven which could only be done by placing a SAT band posterior to the imaging slice to reduce venous inflow effects either in isolation or in combination with a SAT band anterior to the slices reducing arterial inflow affects.

12.3.1 Clinical Implications

Although the future directions listed above are important to further the understanding of muscle the most important future direction is translation to clinical use. What is most easily translated to having clinical utility is the non-invasive muscle fibre type representation. I believe the further exploration in confirming the non-invasive biopsy metric with the biopsy samples has the potential to yield the most clinical utility as it could improve muscular disorder diagnosis. The multi-state representation of the muscle could show clinical utility in more accurately describing muscle fatigue or grading its function when comparing healthy to diseased skeletal muscle. This means muscle activation could be more accurately and non-invasively assessed which would allow for the assessment of muscle function or dysfunction to grade muscle injury, quantify disease state or assess functional improvements in muscle activation over the course of rehabilitation plans. Thirdly, further exploration of SAT band placement and its noise suppression properties across all muscle groups in the lower leg could have an impact on how muscle BOLD imaging is performed clinically. Suppressing noise in functional data is advantageous to more accurately characterize behaviour and it is a simple modification to existing clinical functional scans. If the SAT noise suppression investigations proved robust it would not be difficult to promote adoption of using a SAT band due to its ease of use with the current scanning architecture.

Finally, the BOLD change in amplitude between contraction states over time could also be used as a fatigue metric to non-invasively investigate muscle wasting. The techniques and metrics explored in this thesis, although one step removed, with some additional exploration could show excellent clinical utility, which was the desired outlook of this work.

12.4 Conclusion

To provide a very brief overarching summary this thesis provided novel insight into the functional behaviour of muscle. Through using the BOLD imaging of the lower leg, at rest and during a variety of weighted plantar-flexion paradigms at 40% maximal voluntary contraction, a variety of novel analysis techniques provided insight on muscle. The first technique of examining muscle blood-flow complexity at rest using a bi-fractal dimension representation was able to determined differences between muscle fibre types, which means it could replace the currently invasive techniques that find muscle fibre type distribution to determine muscle disease state. The second exploratory technique of using the phase space to define the state of the BOLD signal over time provided two key findings. The first, that the amount of separation of the active and rest state in the phase space can be used to determine regions of muscle activation, without relying on a model which will introduce bias into the measure. The second, was that during exercise muscle blood flow appeared to change between two or more states, and that the fatigued muscle more closely approaches the active state. The third technique, of using a saturation band proximal to the imaging region to mitigate the arterial in-flow effects, was successful in doing so, as it improved the classification of muscle activation in the regions of highest uncertainty when the affects of arterial noise would be expected to be the largest. The final outlook on muscle behaviour involved using EMG measures of fatigue, collected through an in-house EMG acquisition and analysis framework, to develop novel metrics of fatigue based off of the BOLD signal. Concurrent BOLD and EMG of the anterior compartment of the lower leg during a plantar-flexion block design, demonstrated that the change in blood-flow between rest and contracted states is an excellent indicator of muscle fatigue. The bi-fractal analysis, phase space muscle outlook, proximal SAT band placement, and novel BOLD fatigue metric all warrant further investigation as they all serve to better improve clinical magnetic resonance imaging. Therefore, I was able to achieve my goal of performing medical imaging research that some day could have clinical implications, and I can be happy with the thesis put before you.

Bibliography

[1] L. Bherer, K. I. Erickson, and T. Liu-Ambrose, "A review of the effects of physical activity and exercise on cognitive and brain functions in older adults," *Journal of Aging Research*, vol. 2013, p. 657 508, 2013.

[2] C. Marras, J. C. Beck, J. H. Bower, E. Roberts, B. Ritz, G. W. Ross, R. D. Abbott, R. Savica, S. K. Van Den Eeden, A. W. Willis, and C. M. Tanner, "Prevalence of parkinson's disease across north america," *NPJ Parkison's Disease*, vol. 4, no. 21, pp. 1–7, 2018.

[3] R. L. Ernst and J. W. Hay, "The us economic and social costs of alzheimer's disease revisited," *American Journal of Public Health*, vol. 84, no. 8, pp. 1261–1264, 1994.

[4] J. L. Alberts, M. Phillips, M. J. Lowe, A. Frankemolle, A. Thota, E. B. Beall, M. Feldman, A. Ahmed, and A. L. Ridgel, "Cortical and motor responses to acute forced exercise in parkinson's disease," *Parkinsonism & Related Disorders*, vol. 24, pp. 56–62, 2016.

[5] S. R. Shrivastava, P. S. Shrivastava, and J. D. Ramasamy, "Reduction in global burden of stroke in underserved areas," *Journal of Neurosciences in Rural Practice*, vol. 4, no. 4, pp. 475–476, 2013.

[6] B. H. Dobkin, "Training and exercise to drive poststroke recovery," *Nature Clinical Practice Neurology*, vol. 4, no. 2, pp. 1035–1043, 2008.

[7] T. W. H. Organization. "Types of stroke." (2021), [Online]. Available: https://www.who.int/news-room/fact-sheets/detail/obesity-and-overweight (visited on 07/12/2022).

[8] H. H. Publishing. "The 4 most important types of exercise." (2022), [Online]. Available: https://www.health.harvard.edu/exercise-and-fitness/the-4-most-important-types-of-exercise (visited on 07/12/2022).

[9] R. T. Hurt, C. Kulisek, L. A. Buchanan, and S. A. McClave, "The obesity epidemic: Challenges, health initiatives, and implications for gastroenterologists," *Gastroenterology & Hepatology*, vol. 6, no. 12, pp. 780–792, 2010.

[10] C. Roehrig, "Mental disorders top the list of the most costly conditions in the united states: $201 billion," *Health Affairs*, vol. 35, no. 6, pp. 1130–1135, 2016.

[11] H. Ritchie and R. M. "Mental health - our world our data." (2018), [Online]. Available: https://ourworldindata.org/mental-health (visited on 07/12/2022).

[12] A. Institute. "Adhd epidemiology." (2021), [Online]. Available: https://adhd-institute.com/burden-of-adhd/epidemiology/ (visited on 07/12/2022).

[13] S. Waston. "Adult adhd and exercise." (2021), [Online]. Available: https://www.webmd.com/add-adhd/adult-adhd-and-exercise (visited on 07/12/2022).

[14] L. Mandolesi, A. Polverino, S. Montuori, F. Foti, G. Ferraioli, P. Sorrentino, and G. Sorrentino, "Effects of physical exercise on cognitive functioning and wellbeing: Biological and psychological benefits," *Frontiers in Psychology*, vol. 9, p. 509, 2018.

[15] C. for Disease Control and Prevention. "Benefits of physical activity." (2022), [Online]. Available: https://www.cdc.gov/physicalactivity/basics/pa-health/index.htm (visited on 07/12/2022).

[16] L. National Heart and B. Institute. "Physical activity and your heart." (2022), [Online]. Available: https://www.nhlbi.nih.gov/health/heart/physical-activity (visited on 07/12/2022).

[17] R. Rettner. "The 4 types of exercise you need to be healthy." (2016), [Online]. Available: https://www.livescience.com/55317-exercise-types.html (visited on 07/12/2022).

[18] N. I. of Aging. "Four types of exercise can improve your health and physical ability." (2021), [Online]. Available: https://www.nia.nih.gov/health/four-types-exercise-can-improve-your-health-and-physical-ability (visited on 07/12/2022).

[19] Q. Gu, L. Zou, P. D. Loprinzi, M. Quan, and T. Huang, "Effects of open versus closed skill exercise on cognitive function: A systematic review," *Frontiers in Psychology*, vol. 27, no. 10, p. 1707, 2019.

[20] Cedars-Sinai. "Neuromuscular disorders." (2021), [Online]. Available: https://www.cedars-sinai.org/health-library/diseases-and-conditions/n/neuromuscular-disorders.html (visited on 07/15/2022).

[21] J. Deenen, C. Horlings, and J. Verschuuren, "The epidemiology of neuromuscular disorders: A comprehensive overview of the literature," *Journal of neuromuscular diseases*, vol. 2, pp. 73–85, Jan. 2015. DOI: 10.3233/JND-140045.

[22] A. Theadom, M. Rodrigues, R. Roxburgh, S. Balalla, C. Higgins, R. Bhattacharjee, K. Jones, R. Krishnamurthi, and V. Feigin, "Prevalence of muscular dystrophies: A systematic literature review," *Neuroepidemiology*, vol. 2, pp. 259–268, Jan. 2014. DOI: 10.1159/000369343.

[23] Cedars-Sinai. "Muscular dystrophy." (2021), [Online]. Available: http://surl.li/cfkzi (visited on 07/15/2022).

[24] N. C. Joyce, B. Oskarsson, and L. W. Jin, "Muscle biopsy evaluation in neuromuscular disorders," *Physical Medicine and Rehabilitation Clinics of North America*, vol. 23, no. 2, pp. 609–631, 2012. DOI: 10.1016/j.pmr.2012.06.006.

[25] V. C. Constantinides, M. M. Papahatzaki, G. K. Papadimas, N. Karandreas, T. Zambelis, P. Kokotis, and P. Manda, "Diagnostic accuracy of muscle biopsy and electromyography in 123 patients with neuromuscular disorders," *In Vivo*, vol. 32, no. 6, pp. 1647–1652, Dec. 2018. DOI: 10.21873/invivo.11427.

[26] S. Hodsden. "Fiber optics may provide minimally invasive alternative to traditional muscle biopsy." (2017), [Online]. Available: https://www.meddeviceonline.com/doc/fiber-optics-may-provide-minimally-invasive-alternative-to-traditional-muscle-biopsy-0001 (visited on 07/15/2022).

[27] A. Baguet, I. Everaert, P. Hespel, M. Petrovic, E. Achten, and W. Derave, "A new method for non-invasive estimation of human muscle fiber type composition," *PLOS One*, vol. 6, no. 7, e21956, Jul. 2011. DOI: 10.1371/journal.pone.0021956.

[28] T. Winkler, F. Mersmann, P. von Roth, R. Dietrich, S. Bierbaum, and A. Arampatzis, "Development of a non-invasive methodology for the assessment of muscle fibre composition," *Frontiers in Physiology*, vol. 10, 2019. DOI: 10.3389/fphys.2019.00174.

[29] T. L. Fernandes, A. Pedrinelli, and A. J. Hernandez, "Muscle injury - physiopathology, diagnosis, treatment and clinical presentation," *Revista brasileira de ortopedia*, vol. 46, no. 3, pp. 247–255, Dec. 2015. DOI: 10.1016/S2255-4971(15)30190-7.

[30] B. A. Baker, "An old problem: Aging and skeletal-muscle-strain injury," *Journal of Sports Rehabilitation*, vol. 26, no. 2, pp. 180–188, Jan. 2017. DOI: 10.1123/jsr.2016-0075.

[31] G. V. Ostir, I. M. Berges, Y. F. Kuo, J. S. Goodwin, S. R. Fisher, and J. M. Guralnik, "Mobility activity and its value as a prognostic indicator of survival in hospitalized older adults," *Journal of the American Geriatrics Society*, vol. 61, no. 4, pp. 551–557, 2013. DOI: 10.1111/jgs.12170.

[32] S. Ogawa, T. M. Lee, A. R. Kay, and D. W. Tank, "Brain magnetic resonance imaging with contrast dependent on blood oxygenation," *Proceedings of the National Academy of Sciences of the United States of America*, vol. 87, no. 24, pp. 9868–9872, 1990. DOI: 10.1073/pnas.87.24.9868.

[33] S. Partovi, S. Karimi, B. Jacobi, A.-C. Schulte, M. Aschwanden, L. Zipp, J. K. Lyo, C. Karmonik, M. Müller-Eschner, R. W. Huegli, G. Bongartz, and D. Bilecen, "Clinical implications of skeletal muscle blood-oxygenation-level-dependent (bold) mri," *Magnetic Resonance and Material Physics*, vol. 25, pp. 251–261, 2012. DOI: 10.1007/s10334-012-0306-y.

[34] L. M. Biga, S. Dawson, A. Harwell, R. Hopkins, J. Kaufmann, M. LeMaster, P. Matern, K. Morrison-Graham, D. Quick, and J. Runyeon, "Anatomy & physiology - chapter 10 muscle," in 2013. DOI: http://cnx.org/content/col11496/latest/.

[35] D. A. Rosenbaum, "Chapter 3 - physiological foundations," in *Human Motor Control (Second Edition)*, D. A. Rosenbaum, Ed., Second Edition, San Diego: Academic Press, 2010, pp. 43–91. DOI: 10.1016/B978-0-12-374226-1.00003-6.

[36] W. Scott, J. Stevens, and S. A. Binder–Macleod, "Human Skeletal Muscle Fiber Type Classifications," *Physical Therapy*, vol. 81, no. 11, pp. 1810–1816, Nov. 2001, ISSN: 0031-9023. DOI: 10.1093/ptj/81.11.1810. eprint: https://academic.oup.com/ptj/article-pdf/81/11/1810/31661405/ptj1810.pdf. [Online]. Available: https://doi.org/10.1093/ptj/81.11.1810.

[37] V. Edgerton, J. Smith, and D. Simpson, "Muscle fibre type populations of human leg muscles," *The Histochemical journal*, vol. 7, pp. 259–66, Jun. 1975. DOI: 10.1007/BF01003594.

[38] R. N. Pittman, "The circulatory system and oxygen transport," in 2011.

[39] M. J. Joyner and D. P. Casey, "Regulation of increased blood flow (hyperemia) to muscles during exercise: A hierarchy of competing physiological needs," *Physiological Reviews*, vol. 95, no. 2, pp. 549–601, 2015.

[40] N. B. I. A. |. B. Columbia. "Brain structure and function." (2017), [Online]. Available: https://www.nbia.ca/brain-structure-function/ (visited on 07/15/2022).

[41] J. S. Querido and A. W. Sheel, "Regulation of cerebral blood flow during exercise," *Sports Medicine*, vol. 37, no. 9, pp. 765–782, 2007.

[42] G. Rash, "Electromyography fundamentals," in 1999.

[43] M. Chowdhury R andReaz, M. Ali, A. Bakar, K. Chellappan, and T. Chang, "Surface electromyography signal processing and classification techniques," *Senors*, vol. 13, no. 9, pp. 12 431–12 466, 2013.

[44] N. C. Joyce, B. Oskarsson, and L. W. Jin, "Muscle biopsy evaluation in neuromuscular disorders," *Physical medicine and rehabilitation clinics of North America*, vol. 23, no. 3, pp. 609–631, 2012. DOI: 10.1016/j.pmr.2012.06.006.

[45] J. Björn, G. Bongartz, S. Partovi, A.-C. Schulte, M. Aschwanden, A. Lumsden, M. Davies, M. Loebe, G. Noon, S. Karimi, J. Lyo, D. Staub, R. Huegli, and D. Bilecen, "Skeletal muscle bold mri: From underlying physiological concepts to its usefulness in clinical conditions," *Journal of magnetic resonance imaging : JMRI*, vol. 35, pp. 1253–65, Jun. 2012. DOI: 10.1002/jmri.23536.

[46] H.-P. Ledermann, A.-C. Schulte, H.-G. Heidecker, M. Aschwanden, K. Jäger, K. Scheffler, W. Steinbrich, and D. Bilecen, "Blood oxygenation level–dependent magnetic resonance imaging of the skeletal muscle in patients with peripheral arterial occlusive disease," *Circulation*, vol. 113, pp. 2929–35, Jun. 2006. DOI: 10.1161/CIRCULATIONAHA.105.605717.

[47] B. Behnke, R. Armstrong, and M. Delp, "Adrenergic control of vascular resistance varies in muscles composed of different fiber types: Influence of the vascular endothelium," *American journal of physiology. Regulatory, integrative and comparative physiology*, vol. 301, R783–90, Jun. 2011. DOI: 10.1152/ajpregu.00205.2011.

[48] E. Amaro and G. J. Barker, "Study design in fmri: Basic principles," *Brain and Cognition*, vol. 60, no. 3, pp. 220–232, 2006.

[49] C. for Nondestructive Evaluation | IOWA State University. "Magnetism." (2020), [Online]. Available: https://www.nde-ed.org/Physics/Magnetism/index.xhtml (visited on 07/15/2022).

[50] K. Schewzow, M. Andreas, E. Moser, M. Wolzt, and A. I. Schmid, "Automatic model-based analysis of skeletal muscle bold-mri in reactive hyperemia," *Journal of Magnetic Resonance Imaging*, vol. 38, no. 4, pp. 963–969, 2013. DOI: 10.1002/jmri.23919.

[51] J. Hennig, K. Scheffler, and A. Schreiber, "Time resolved observation of bold effect in muscle during isometric exercise," *Proc Int Soc Magn Reson Med*, vol. 8, Jan. 2000.

[52] I. Talos, A. Mian, K. Zou, L. Hsu, D. Goldberg-Zimring, S. Haker, J. Bhagwat, and R. Mulkern, "Magnetic resonance and the human brain: Anatomy, function and metabolism," *Cellular and molecular life sciences : CMLS*, vol. 63, pp. 1106–24, Jun. 2006. DOI: 10.1007/s00018-005-5522-4.

[53] M. R. Fisher, G. C. Dooms, H. Hricak, C. Reinhold, and C. B. Higgins, "Magnetic resonance imaging of the normal and pathologic muscular system," *Magnetic Resonance Imaging*, vol. 4, no. 6, pp. 491–496, 1986, ISSN: 0730-725X. DOI: https://doi.org/10.1016/0730-725X(86)90029-9.

[54] R. L. DeLaPaz, "Echo planar imaging," *Radiographics*, Sep. 1994.

[55] B. Poser and D. Norris, "Fast spin echo sequences for bold functional mri," *Magma (New York, N.Y.)*, vol. 20, pp. 11–7, Mar. 2007. DOI: 10.1007/s10334-006-0063-x.

[56] S. S. Cross, "Fractals in pathology," *The Journal of Pathology*, vol. 182, no. 1, pp. 1–8, 1997. DOI: 10.1002/(SICI)1096-9896(199705)182:1<1::AID-PATH808>3.0.CO;2-B.

[57] G. Bianciardi and F. Pontenani, "Fractals and pathology," *Journal of Biometrics and its Applications*, vol. J Biometrics App 1(1): 104, Oct. 2015. DOI: 10.15744/2455-765X.1.104.

[58] Vanerbilt. "Magnetism." (2012), [Online]. Available: https://www.vanderbilt.edu/AnS/psychology/cogsci/chaos/workshop/Fractals.html (visited on 07/15/2022).

[59] G. Reishofer, K. Koschutnig, C. Enzinger, F. Ebner, and H. Ahammer, "Fractal dimension and vessel complexity in patients with cerebral arteriovenous malformations," *PloS one*, vol. 7, e41148, Jul. 2012. DOI: 10.1371/journal.pone.0041148.

[60] L. Ming, "Fractal time series—a tutorial review," *Mathematical Problems in Engineering*, vol. 2010, 2010. DOI: 10.1155/2010/15726.

[61] R. L. Armentano, W. Legnani, and L. J. Cymberknop, "Fractal analysis of cardiovascular signals empowering the bioengineering knowledge," in *Fractal Analysis*, F. Brambila, Ed., IntechOpen, 2017, ch. 1. DOI: 10.5772/67784.

[62] M. Warsi, D. Molloy, and M. Noseworthy, "Correlating brain blood oxygenation level dependent (bold) fractal dimension mapping with magnetic resonance spectroscopy (mrs) in alzheimer's disease," *Magma (New York, N.Y.)*, vol. 25, pp. 335–44, Mar. 2012. DOI: 10.1007/s10334-012-0312-0.

[63] O. Dona, M. D. Noseworthy, C. DeMatteo, and J. F. Connolly, "Fractal analysis of brain blood oxygenation level dependent (bold) signals from children with mild traumatic brain injury (mtbi)," *PLoS One*, vol. 12, no. 1, e0169647, Jan. 2017. DOI: 10.1371/journal.pone.0169647.

[64] T. Varley, M. Craig, R. Adapa, P. Finoia, G. Williams, J. Allanson, J. Pickard, D. Menon, and E. Stamatakis, "Fractal dimension of cortical functional connectivity networks & severity of disorders of consciousness," *PLOS ONE*, vol. 15, e0223812, Feb. 2020. DOI: 10.1371/journal.pone.0223812.

[65] B. Chen and N. Wang, "Determining emg embedding and fractal dimensions and its application," *Proceedings of the Annual International Conference of the IEEE Engineering in Medicine and Biology Society*, vol. 2, pp. 1341–1344, 2000. DOI: 10.1109/IEMBS.2000.897986.

[66] L. Smith, T. Zhong, and P. Bawa, "Nonlinear behaviour of human motor neurons," *Canadian Journal of Physiology and Pharmacology*, vol. 73, no. 1, pp. 113–123, 1995. DOI: 10.1139/y95-0162.

[67] M. Matilla-García, I. Morales, J. M. Rodríguez, and M. M. Ruiz, "Selection of embedding dimension and delay time in phase space reconstruction via symbolic dynamics," *Entropy (Basel)*, vol. 23, no. 2, p. 221, Feb. 2021. DOI: 10.3390/e23020221.

[68] D. P. Bulte, J. Alfonsi, S. Bells, and M. D. Noseworthy, "Vasomodulation of skeletal muscle bold signal," *Journal of Magnetic Resonance Imaging*, vol. 24, no. 4, pp. 886–890, 2006. DOI: 10.1002/jmri.20690.

[69] S. Partovi, A.-C. Schulte, J. Björn, M. Klarhöfer, A. Lumsden, M. Loebe, M. Davies, G. Noon, C. Karmonik, L. Zipp, G. Bongartz, and D. Bilecen, "Blood oxygenation level-dependent (bold) mri of human skeletal muscle at 1.5 and 3 t," *Journal of magnetic resonance imaging : JMRI*, vol. 35, pp. 1227–32, May 2012. DOI: 10.1002/jmri.23583.

[70] O. A. Sanchez, E. A. Copenhaver, C. P. Elder, and B. M. Damon, "Absence of a significant extravascular contribution to the skeletal muscle bold effect at 3 t," *Magnetic Resonance in Medicine*, vol. 64, no. 2, pp. 527–535, 2010. DOI: 10.1002/mrm.22449.

[71] K. Schewzow, M. Andreas, E. Moser, M. Wolzt, and A. I. Schmid, "Automatic model-based analysis of skeletal muscle bold-mri in reactive hyperemia," *Journal of Magnetic Resonance Imaging*, vol. 38, no. 4, pp. 963–969, 2013. DOI: 10.1002/jmri.23919.

[72] T. F. Towse, B. T. Childs, S. A. Sabin, E. C. Bush, C. P. Elder, and B. M. Damon, "Comparison of muscle bold responses to arterial occlusion at 3 and 7 tesla," *Magnetic Resonance in Medicine*, vol. 75, no. 3, pp. 1333–1340, 2016. DOI: 10.1002/mrm.25562.

[73] T. F. Towse, C. P. Elder, E. C. Bush, S. W. Klockenkemper, J. T. Bullock, R. D. Dortch, and B. M. Damon, "Post-contractile bold contrast in skeletal muscle at 7t reveals inter-individual heterogeneity in the physiological responses to muscle contraction," *NMR in Biomedicine*, vol. 29, no. 12, pp. 1720–1728, 2016. DOI: 10.1002/nbm.3593.

[74] S. Partovi, A. C. Schulte, M. Aschwanden, D. Staub, D. Benz, S. Imfeld, B. Jacobi, P. Broz, K. A. Jäger, M. Takes, R. W. Huegli, D. Bilecen, and U. A. Walker, "Impaired skeletal muscle microcirculation in systemic sclerosis," *Arthritis Research and Therapy*, vol. 14, no. 5, R209, 2012. DOI: 10.1186/ar4047.

[75] S. Partovi, M. Aschwanden, B. Jacobi, A.-C. Schulte, U. A. Walker, D. Staub, S. Imfeld, P. Broz, D. Benz, L. Zipp, K. A. Jaeger, M. Takes, M. R. Robbin, R. W. Huegli, and D. Bilecen, "Correlation of muscle bold mri with transcutaneous oxygen pressure for assessing microcirculation in patients with systemic sclerosis," *Journal of Magnetic Resonance Imaging*, vol. 38, no. 4, pp. 845–851, 2013. DOI: 10.1002/jmri.24046.

[76] S. Partovi, A.-C. Schulte, D. Staub, B. Jacobi, M. Aschwanden, U. A. Walker, S. Imfeld, P. Broz, D. Benz, L. Zipp, M. Takes, K. A. Jäger, R. W. Huegli, and D. Bilecen, "Correlation of skeletal muscle blood oxygenation level-dependent mri and skin laser doppler flowmetry in patients with systemic sclerosis," *Journal of Magnetic Resonance Imaging*, vol. 40, no. 6, pp. 1408–1413, 2014. DOI: 10.1002/jmri.24503.

[77] R. Huegli, A.-C. Schulte, M. Aschwanden, C. Thalhammer, S. Kos, A. Jacob, and D. Bilecen, "Effects of percutaneous transluminal angioplasty on muscle bold-mri in patients with peripheral arterial occlusive disease: Preliminary results," *European radiology*, vol. 19, pp. 509–15, Oct. 2008. DOI: 10.1007/s00330-008-1168-6.

[78] S. Potthast, A.-C. Schulte, S. Kos, M. Aschwanden, and D. Bilecen, "Blood oxygenation level-dependent mri of the skeletal muscle during ischemia in patients with peripheral arterial occlusive disease," *RöFo : Fortschritte auf dem Gebiete der Röntgenstrahlen und der Nuklearmedizin*, vol. 181, pp. 1157–61, Oct. 2009. DOI: 10.1055/s-0028-1109786.

[79] A.-C. Schulte, M. Aschwanden, and D. Bilecen, "Calf muscles at blood oxygen level–dependent mr imaging: Aging effects at postocclusive reactive hyperemia," *Radiology*, vol. 247, no. 2, pp. 482–489, 2008. DOI: 10.1148/radiol.2472070828.

[80] J. Slade, T. F. Towse, V. V. Gossain, and R. A. Meyer, "Peripheral microvascular response to muscle contraction is unaltered by early diabetes but decreases with age," *Journal of Applied Physiology*, vol. 111, no. 5, pp. 1361–1371, 2011. DOI: 10.1152/japplphysiol.00009.2011.

[81] T. NISHII, A. K. KONO, M. NISHIO, K. KYOTANI, K. NISHIYAMA, and K. SUGIMURA, "Dynamic blood oxygen level-dependent mr imaging of muscle: Comparison of postocclusive reactive hyperemia in young smokers and nonsmokers," *Magnetic Resonance in Medical Sciences*, vol. 14, no. 4, pp. 275–283, 2015. DOI: 10.2463/mrms.2014-0105.

[82] A. J. Bakermans, C. H. Wessel, K. H. Zheng, P. F. Groot, E. S. Stroes, and A. J. Nederveen, "Dynamic magnetic resonance measurements of calf muscle oxygenation and energy metabolism in peripheral artery disease," *Journal of Magnetic Resonance Imaging*, vol. 51, no. 1, pp. 98–107, 2020. DOI: 10.1002/jmri.26841.

[83] A. Akbari, C. P. Rockel, D. A. Kumbhare, and M. D. Noseworthy, "Safe mri-compatible electrical muscle stimulation (ems) system," *Journal of Magnetic Resonance Imaging*, vol. 44, no. 6, pp. 1530–1538, 2016. DOI: 10.1002/jmri.25316.

[84] M. D. Muller, Z. Li, C. T. Sica, J. C. Luck, Z. Gao, C. A. Blaha, A. E. Cauffman, A. J. Ross, N. J. Winkler, M. D. Herr, K. Brandt, J. Wang, D. C. Gallagher, P. Karunanayaka, J. Vesek, U. A. Leuenberger, Q. X. Yang, and L. I. Sinoway, "Muscle oxygenation during dynamic plantar flexion exercise: Combining bold mri with traditional physiological measurements," *Physiological Reports*, vol. 4, no. 20, e13004, 2016. DOI: 10.14814/phy2.13004.

[85] X. Xie, Z. Cao, and X. Weng, "Spatiotemporal nonlinearity in resting-state fmri of the human brain," *Neuroimage*, vol. 40, no. 4, pp. 1672–1685, 2008. DOI: 10.1016/j.neuroimage.2008.01.007.

[86] E. Tagliazucchi, P. Balenzuela, D. Fraiman, and D. Chialvo, "Criticality in large-scale brain fmri dynamics unveiled by a novel point process analysis," *Frontiers in physiology*, vol. 3, p. 15, Feb. 2012. DOI: 10.3389/fphys.2012.00015.

[87] R. D., X. Hu, and G. Deshpande, "Phase synchronization in brain networks derived from correlation between probabilities of recurrences in functional mri data," *International journal of neural systems*, vol. 23, p. 1 350 003, Apr. 2013. DOI: 10.1142/S0129065713500032.

[88] Z. Wang, *Resting state fmri-based temporal coherence mapping*, Ithaca, NY 14850, United States, 2021.

[89] J. E. McGillivray, H. Debruin, and M. D. Noseworthy, "Book of abstracts esmrmb 2021 online 38th annual scientific meeting 7–9 october 2021," *Magnetic Resonance Materials in Physics, Biology and Medicine*, vol. 34, S148, Sep. 2021. DOI: 10.1007/s10334-021-00947-8.

[90] G. R. Adams, M. R. Duvoisin, and G. A. Dudley, "Magnetic resonance imaging and electromyography as indexes of muscle function," *Journal of Applied Physiology*, vol. 73, no. 4, pp. 1578–1583, 1992. DOI: 10.1152/jappl.1992.73.4.1578.

[91] E. Piovanelli, D. Piovesan, S. Shirafuji, B. Su, N. Yoshimura, Y. Ogata, and J. Ota, "Towards a simplified estimation of muscle activation pattern from mri and emg using electrical network and graph theory," *Sensors*, vol. 20, no. 3, 2020. DOI: 10.3390/s20030724.

[92] C. McDonald, G. Carter, R. Fritz, M. Anderson, R. Abresch, and D. Kilmer, "Magnetic resonance imaging of denervated muscle: Comparison to electromyography," *Muscle & nerve*, vol. 23, pp. 1431–4, Sep. 2000. DOI: 10.1002/1097-4598(200009)23:93.0.CO;2-P.

[93] R. A. Nardin, M. R. Patel, T. F. Gudas, S. B. Rutkove, and E. M. Raynor, "Electromyography and magnetic resonance imaging in the evaluation of radiculopathy," *Muscle & Nerve*, vol. 22, no. 2, pp. 151–155, 1999.

[94] D. Jonas, B. Conrad, H. G. Von Einsiedel, and C. Bischoff, "Correlation between quantitative emg and muscle mri in patients with axonal neuropathy," *Muscle & Nerve*, vol. 23, no. 8, pp. 1265–1269, 2000.

[95] S. Kamath, N. Venkatanarasimha, M. Walsh, and P. Hughes, "Mri appearance of muscle denervation," *Skeletal radiology*, vol. 37, pp. 397–404, Jun. 2008. DOI: 10.1007/s00256-007-0409-0.

[96] E. T. Tan, K. C. Serrano, P. Bhatti, F. Pishgar, A. M. Vanderbeek, C. J. Milani, and D. B. Sneag, "Quantitative mri differentiates electromyography severity grades of denervated muscle in neuropathy of the brachial plexus," *Journal of Magnetic Resonance Imaging*, DOI: https://doi.org/10.1002/jmri.28125.

[97] N. Dickx, R. D'hooge, B. Cagnie, E. Deschepper, K. Verstraete, and L. Danneels, "Magnetic resonance imaging and electromyography to measure lumbar back muscle activity," *Spine*, vol. 35, no. 17, E836–E842, 2010. DOI: 10.1097/BRS.0b013e3181d79f02.

[98] A. Rutkowska-Kucharska and A. Szpala, "The use of electromyography and magnetic resonance imaging to evaluate a core strengthening exercise programme," *Journal of Back and Musculoskeletal Rehabilitation*, vol. 31, pp. 1–8, Oct. 2017. DOI: 10.3233/BMR-169780.

[99] R. Kinugasa and H. Akima, "Neuromuscular activation of triceps surae using muscle functional mri and emg," *Medicine and science in sports and exercise*, vol. 37, pp. 593–8, Apr. 2005. DOI: 10.1249/01.MSS.0000159026.99792.76.

[100] T. Price, G. Kamen, B. Damon, C. Knight, B. Applegate, J. Gore, K. Eward, and J. Signorile, "Comparison of mri with emg to study muscle activity associated with dynamic plantar flexion," *Magnetic resonance imaging*, vol. 21, pp. 853–61, Oct. 2003. DOI: 10.1016/S0730-725X(03)00183-8.

[101] F. Hug, D. Bendahan, Y. Fur, P. Cozzone, and L. Grelot, "Heterogeneity of muscle recruitment pattern during pedaling in professional road cyclists: A magnetic resonance imaging and electromyography study," *European journal of applied physiology*, vol. 92, pp. 334–42, Aug. 2004. DOI: 10.1007/s00421-004-1096-3.

[102] T. Ono, A. Higashihara, and T. Fukubayashi, "Hamstring functions during hip-extension exercise assessed with electromyography and magnetic resonance imaging," *Research in sports medicine (Print)*, vol. 19, pp. 42–52, Jan. 2011. DOI: 10.1080/15438627.2011.535769.

[103] J. Kubota, T. Ono, M. Araki, N. Tawara, S. Torii, T. Okuwaki, and T. Fukubayashi, "Relationship between the mri and emg measurements," *International journal of sports medicine*, vol. 30, pp. 533–7, Apr. 2009. DOI: 10.1055/s-0029-1202352.

[104] M. Behr, *Simultaneous electromygraphy and functional magnetic resonance imaging of skeletal muscle*, Hamilton, ON, L8S 4L8, Canada, 2016.

[105] W. R. Frontera and J. Ochala, "Skeletal muscle: A brief review of structure and function," *Calcified Tissue International*, vol. 96, no. 3, pp. 183–195, 2015. DOI: 10.1007/s00223-014-9915-y.

[106] J. A. Hawley, L. M. Burke, S. M. Phillips, and L. L. Spriet, "Nutritional modulation of training-induced skeletal muscle adaptations," *Journal of Applied Physiology*, vol. 110, no. 3, pp. 834–845, 2011. DOI: 10.1152/japplphysiol.00949.2010.

[107] R. H. Fitts and J. J. Widrick, "Muscle mechanics: Adaptations with exercise-training," *Exercise and Sport Sciences Reviews*, vol. 24, no. 1, pp. 427–474, Jan. 1996.

[108] W. Derave, I. Everaert, S. Beeckman, and A. Baguet, "Muscle carnosine metabolism and beta-alanine supplementation in relation to exercise and training," *Sports medicine*, vol. 40, no. 3, pp. 247–263, 2010. DOI: 10.2165/11530310-000000000-00000.

[109] M. Krššák, L. Lindeboom, V. Schrauwen-Hinderling, L. S. Szczepaniak, W. Derave, J. Lundbom, D. Befroy, F. Schick, J. Machann, R. Kreis, and C. Boesch, "Proton magnetic resonance spectroscopy in skeletal muscle: Experts' consensus recommendations," *NMR in Biomedicine*, vol. 34, no. 5, e4266, 2021. DOI: 10.1002/nbm.4266.

[110] H. Degens, S. Arvydas, S. Albertas, B. Statkevičienė, and T. Venckunas, "Physiological comparison between non-athletes, endurance, power and team athletes," *European Journal of Applied Physiology*, vol. 119, Jun. 2019. DOI: 10.1007/s00421-019-04128-3.

[111] A. H. Elzibak and M. D. Noseworthy, "Assessment of diffusion tensor imaging indices in calf muscles following postural change from standing to supine position," *Magnetic Resonance Materials in Physics, Biology and Medicine*, vol. 27, pp. 387–395, 2014. DOI: 10.1007/s10334-013-0424-1.

[112] A. Boss, R. Kreis, P. Saillen, M. Zehnder, C. Boesch, and P. Vermathen, "Skeletal muscle 1h mrsi before and after prolonged exercise. ii. visibility of free carnitine," *Magnetic resonance in medicine : official journal of the Society of Magnetic Resonance in Medicine / Society of Magnetic Resonance in Medicine*, vol. 68, pp. 1368–75, Nov. 2012. DOI: 10.1002/mrm.24167.

[113] M. Wilson, G. Reynolds, R. Kauppinen, T. Arvanitis, and A. Peet, "A constrained least-squares approach to the automated quantitation of in vivo h-1 magnetic resonance spectroscopy data," *Magnetic resonance in medicine : official journal of the Society of Magnetic Resonance in Medicine / Society of Magnetic Resonance in Medicine*, vol. 65, pp. 1–12, Jan. 2011. DOI: 10.1002/mrm.22579.

[114] J. Near, "Spectral quantification and pitfalls in interpreting magnetic resonance spectroscopic data," in Dec. 2014, pp. 49–67, ISBN: 9780124016880. DOI: 10.1016/B978-0-12-401688-0.00005-7.

[115] E. Lievens, K. Van Vossel, F. Van de Casteele, M. Krssak, J. Murdoch, D. Befroy, and W. Derave, "Cores of reproducibility in physiology (corp): Quantification of human skeletal muscle carnosine concentration by proton magnetic resonance spectroscopy," *Journal of Applied Physiology*, vol. 131, May 2021. DOI: 10.1152/japplphysiol.00056.2021.

[116] J. Near, A. Harris, C. Juchem, R. Kreis, M. Marjańska, G. Öz, J. Slotboom, M. Wilson, and C. Gasparovic, "Preprocessing, analysis and quantification in single-voxel magnetic resonance spectroscopy: Experts' consensus recommendations," *NMR in Biomedicine*, vol. 34, e4257, Feb. 2020. DOI: 10.1002/nbm.4257.

[117] M. Jenkinson, C. F. Beckmann, T. E. Behrens, M. W. Woolrich, and S. M. Smith, "Fsl," *NeuroImage*, vol. 62, no. 2, pp. 782–790, 2012, ISSN: 1053-8119. DOI: 10.1016/j.neuroimage.2011.09.015.

[118] G. Helms, H. Dathe, N. Weiskopf, and P. Dechent, "Identification of signal bias in the variable flip angle method by linear display of the algebraic ernst equation," *Magnetic Resonance in Medicine*, vol. 66, no. 3, pp. 669–677, 2011. DOI: 10.1002/mrm.22849.

[119] M. J. Cannon, D. B. Percival, D. C. Caccia, G. M. Raymond, and J. B. Bassingthwaighte, "Evaluating scaled windowed variance methods for estimating the hurst coefficient of time series," *Physica A*, vol. 241, no. 3-4, pp. 606–626, 1997. DOI: 10.1016/S0378-4371(97)00252-5.

[120] H. W. Chung and H. J. Chung, "Correspondence re: J. w. baish and r. k. jain, fractals and cancer.," *Cancer Research*, vol. 61, no. 22, pp. 8347–8348, 2001.

[121] B. Barisch-Fritz and M. Mauch, "Foot development in childhood and adolescence," in Aug. 2013. DOI: 10.1533/9780857098795.1.49.

[122] J. Mehta, M. Verber, J. Wieser, B. Schmit, and S. Schindler-Ivens, "A novel technique for examining human brain activity associated with pedaling using fmri," *Journal of neuroscience methods*, vol. 179, pp. 230–9, Jun. 2009. DOI: 10.1016/j.jneumeth.2009.01.029.

[123] L. Friedman and G. Glover, "Report on a multicenter fmri quality assurance protocol," *Journal of magnetic resonance imaging : JMRI*, vol. 23, pp. 827–39, Jun. 2006. DOI: 10.1002/jmri.20583.

[124] H. van Duinen, I. Zijdewind, H. Hoogduin, and N. Maurits, "Surface emg measurements during fmri at 3t: Accurate emg recordings after artifact correction," *NeuroImage*, vol. 27, pp. 240–6, Sep. 2005. DOI: 10.1016/j.neuroimage.2005.04.003.

[125] B. MacIntosh, S. Baker, R. Mraz, J. Ives, A. Martel, W. McILROY, and S. Graham, "Improving functional magnetic resonance imaging motor studies through simultaneous electromyography recordings," *Human brain mapping*, vol. 28, pp. 835–45, Sep. 2007. DOI: 10.1002/hbm.20308.

[126] Conmed. "Adult ecg electrodes." (2020), [Online]. Available: https://www.conmed.com/-/media/conmed/documents/literature/adult_ecg_electrodes_productbrochure.ashx (visited on 07/15/2022).

[127] F. Esposito, G. Pignataro, G. Renzo, A. Spinali, A. Paccone, G. Tedeschi, and L. Annunziato, "Alcohol increases spontaneous bold signal fluctuations in the visual network," *NeuroImage*, vol. 53, pp. 534–43, Nov. 2010. DOI: 10.1016/j.neuroimage.2010.06.061.

[128] H.-C. Yang, Z. Liang, J. Yao, X. Shen, B. Frederick, and Y. Tong, "Vascular effects of caffeine found in bold fmri," *Journal of Neuroscience Research*, vol. 97, Nov. 2018. DOI: 10.1002/jnr.24360.

[129] R. Cox and J. Hyde, "Software tools for analysis and visualization of fmri data," *NMR in biomedicine*, vol. 10, no. 4-5, pp. 171–178, 1997, ISSN: 0952-3480. DOI: 10.1002/(sici)1099-1492(199706/08)10:4/5<171::aid-nbm453>3.0.co;2-l.

[130] A. Delorme and S. Makeig, "Eeglab: An open source toolbox for analysis of single-trial eeg dynamics," *Journal of Neuroscience Methods*, vol. 134, pp. 9–12, Jan. 2004.

[131] S. Thurner, C. Windischberger, E. Moser, P. Walla, and M. Barth, "Scaling laws and persistence in human brain activity," *Physica A-statistical Mechanics and Its Applications - PHYSICA A*, vol. 326, pp. 511–521, Aug. 2003. DOI: 10.1016/S0378-4371(03)00279-6.

[132] A. D. Davies and M. D. Noseworthy, "Fourier analysis of muscle bold data after exercise," *Proceedings of the International Society for Magnetic Resonance in Medicine*, vol. 19, 2011.

[133] B. Maus, G. Breukelen, R. Goebel, and M. Berger, "Optimization of blocked designs in fmri studies," *Psychometrika*, vol. 75, pp. 373–390, Jun. 2010. DOI: 10.1007/s11336-010-9159-3.

[134] E. Arnold and S. Delp, "Fibre operating lengths of human lower limb muscles during walking," *Philosophical transactions of the Royal Society of London. Series B, Biological sciences*, vol. 366, pp. 1530–9, May 2011. DOI: 10.1098/rstb.2010.0345.